TRANSFORMATION OF BIOMASS AND SHALE GAS CARBON

TO FUELS AND CHEMICALS

A Dissertation

Submitted to the Faculty

of

Purdue University

by

Taufik Ridha

In Partial Fulfillment of the

Requirements for the Degree

of

Doctor of Philosophy

December 2018

Purdue University

West Lafayette, Indiana

THE PURDUE UNIVERSITY GRADUATE SCHOOL
STATEMENT OF DISSERTATION APPROVAL

Dr. Rakesh Agrawal

   Charles D. Davidson School of Chemical Engineering

Dr. Fabio H. Ribeiro

   Charles D. Davidson School of Chemical Engineering

Dr. Gintaras Reklaitis

   Charles D. Davidson School of Chemical Engineering

Dr. Mohit Tawarmalani

   Krannert School of Management

Approved by:

   Dr. John A. Morgan

      Head of Graduate Program

To my late close and best friend, Jessica Lin Marrs.

ACKNOWLEDGMENTS

Firstly, I would like to thank my advisor, Prof. Rakesh Agrawal, for his endless support, insightful feedback, impactful research guidance, and belief in me as a graduate student. I was truly inspired to work with such a great visionary. Working on papers, lectures, patents, and proposals were truly invaluable and impactful on my overall development. His considerate thoughts go beyond the academic environment and have provided me support during struggles in my personal life. I hope that I have learned to continuously ask the right questions, check my results, employ structured thinking, and always look for gaps for potential improvements. I cannot express enough how appreciative I am for his never ending support and encouragement throughout my PhD career.

In addition, I would like to thank my committee members, Prof. Mohit Tawarmalani, Prof. Fabio H. Ribeiro, and Prof. Gintaras Reklaitis for their constructive comments and insights during the course of my Ph.D. program. Also, I would like to thank Prof. W. Nicholas Delgass for his insights in catalysis and reaction engineering. Also, I would like to acknowledge Prof. Tawarmalani for his assistance on mathematical modeling and optimization theory and striving toward structured thinking.

I would like to thank Prof. Hilkka Kenttamaa for her continuous feedback in organic chemistry synthesis and constructive support. I would like to thank Prof. Jeffrey J. Siirola for his support in providing knowledge and additional research directions. Also, I enjoyed my time as his teaching assistant for the senior design course.

Besides my academic committee, I would like to thank all other graduate students that I worked closely with and had deep discussion regarding our research topics, particularly members in the modeling and biomass group, Dr. Emre Gençer, Dr. John Degenstein, Dr. Harshavardhan Choudhary, Yiru Li, Zheyu Jiang, Dr. Gautham

Ramapriya, Abhijit Talpade, Richard Caulkins, and Radhakrishna T. Gooty. Also, the recent members, Tony Matthew, Jose Adrian Valsco, Zewei Chen, and Peter W. Oladipopu, thank you for your words of encouragement and inputs. I would like to again extend my gratitude to Richard Caulkins and Abhijit Talpade for having critical discussions on combining experimental and modeling effort. In addition, I would like to thank my collaborators and friends in the chemistry department, Dr. Yuan Jiang, Dr. McKay Easton, Zuang Chen, Yan Lu, and Duan Cheng for their inputs and discussions on organic chemistry synthesis.

I would like to thank many great professors whom I got to know and learned from during my undergraduate studies at Texas A&M University. Special thanks for Prof. M. Sam Mannan, Dr. Ray Mentzer, Prof. Mahmoud El-Halwagi, and Prof. Arul Jayaraman, for their encouragement and support for me in pursuing graduate studies. I would like to specially thank Prof. M. Sam Mannan for providing ample opportunities for undergraduate research in process safety, which established my foundation to pursue further research opportunities.

Finally, I would to thank my parents and siblings for their endless support during my PhD program. My father, Syukri Abdullah, is always passionate about education and moved the mountains to ensure that I had endless opportunities in education. My mother, Bara Chatun, is extremely patient throughout my entire life. I am extremely lucky to have the best parents I could have ever asked for. They taught me how to

listen and connect with people through selflessness, genuine kindness, and patience. My sister, Mahdiyati, is unconditionally supportive, always expressed her love, and is a gold sponsor for my PhD journey. She has always been a beacon during both good and bad moments. My sister and brother, Fina Mutqina and Aviscenna, have always expressed their support and love.

I would to thank my wonderful friends for their support and encouragement. Hashilla A. Rivai, Todd Zhen, Shaunak Ray, Santiago Rodriguez, Ghazi Binarandi, Praditya Ajidarma, and Listiawan Hadi Waskito, and Edwin Rodriguez, they all treated me well and I would like to thank them for their friendships. I would like to extend a special thank you to Hashilla A. Rivai for her unconditional support through several difficult moments and instantaneous impulses.

Last, but not least, I would like to express my sincere gratitude to my late close and best friend, Jessica L. Marrs, and my best friend, Melisa Alanis, for their constant support throughout my Ph.D. program. Jessica always showed me that there is always more to life than from what I endured. In addition, she always gave me a glimmering perspective, when things get tough, and reasons to move forward. She was a cheerful, supportive, and thoughtful individual. I will never forget her as she made such a big impact in my life. To Melisa, she was always there for me to handle graduate school. They both were always there for me when I needed them. I am thankful to have them by my side during my PhD journey.

TABLE OF CONTENTS

LIST OF TABLES

LIST OF FIGURES

ABSTRACT

Taufik Ridha Ph.D., Purdue University, December 2018. Transformation of Biomass and Shale Gas Carbon to Fuels and Chemicals. Major Professor: Rakesh Agrawal.

Currently, fossil resources dominate fuel and chemical production landscape. Besides concerns related to the ever-increasing greenhouse gas emission, fossil resources are also limited. In a petroleum-deprived future, sustainably available biomass can serve as a renewable carbon source. Due to its limited availability, however, this biomass resource must be utilized and converted efficiently to minimize carbon losses to undesirable by-products. A modeling and optimization approach that can identify optimal process configurations for chemical and fuel production from biomass using stoichiometric and thermodynamic knowledge of the underlying biomass reaction system is proposed in this dissertation. Several case studies were performed with this approach, and the outcomes found agreement with reported experimental results. In particular, a case study on fast-hydropyrolysis vapor of cellulose led to the discovery of new reaction route and provided insights in comprehending the formation of experimentally observed molecules. The modeling and optimization approach consists of two main steps. The first step is the generation of the search space and the second step is the identification of all optimal reaction routes.

For the first step, literature review and automated reaction network generator are employed to identify all possible processes for biomass conversion. Through literature review, yield data on processes that generate biomass-derived molecules are collected. As these biomass-derived molecules often possess multiple functional groups, utilization of automated reaction network generator, which considers a set of biomass-derived molecules and reaction rules, enables generation of all possible reactions. In this work, an automated reaction network generator tool called Rule

Input Network Generator is utilized. Using this generated search space, a mathematical optimization problem, which identifies the optimal reaction network, is constructed. For the second step, the optimization problem identifies all reaction routes with the minimum number of reactions for a given set of biomass and target products. This formulation constructs a process superstructure that contains processes that generate biomass-derived molecules and all possible reactions from biomass-derived molecules. In this optimization problem, the main constraint for the reaction is its thermodynamic favorability within a certain temperature range. Using optimization solver, optimal solutions for this problem are obtained.

Using this developed approach, a case study on upgrading fast-hydropyrolysis vapor of cellulose to higher molecular weight products was investigated. Levoglucosan and glycolaldehyde are major components from fast-hydropyrolysis of cellulose. This approach identified a reaction route that can upgrade these molecules to hydrocarbons with carbon number ranging from eight to 12 and this route has not been reported in the literature. The coupling of levoglucosan and glycolaldehyde requires a key intermediate, levoglucosenone, which is identified by this approach. Preliminary experimental results suggest that the proposed reactions are feasible and this serves as another validation for this approach. Other potential pathways to not only branched alkanes, but also substituted cycloalkanes and aromatics, were also identified. Molecules with those structures have been observed experimentally, and potential pathways to those molecules can provide insights for experimentalists as to how these products can form and which intermediates may lead to their formations. This approach has not only revealed unknown reaction routes, but also provided insights for experimentalists for analyzing complex systems.

Toward reduction of carbon losses toward char during fast pyrolysis, potential pathways toward char formation during fast pyrolysis were proposed. Investigating proposed char precursors identified using mass spectroscopy, several potential pathways toward the formation of these char precursors were obtained, which include initial

insights to the potential driving force for the formation of these char precursors and, ultimately, char itself.

Going beyond fast pyrolysis, primary processes that have been developed in C3Bio along with several existing primary processes were considered in order to identify optimal biorefinery configurations. This approach identified biorefinery configurations with carbon efficiencies from 60-64%. These configurations generate not only fuel type molecules, but also commodity chemicals that are being produced in a traditional refinery. In addition, it is capable of providing these products at their current relative production rates in the United States. Other studies on biorefinery reported only 25-59% carbon efficiency and generated mostly fuel-type molecules. Therefore, this approach not only indicates the appropriate reaction sequences, but also optimal utilization of carbon in biomass-derived molecules. This dissertation provides an initial roadmap toward sustainable production of fuels and chemicals from lignocellulosic biomass.

Considering that the transition to renewable energy is gradual and shale resource is an abundant fossil resource in the United States, opportunities to valorize shale gas condensate are explored. Recent shale gas boom has transformed the United States energy landscape. Most of the major shale basins are located in remote locations and historically non-gas producing regions. Therefore, many major shale basins regions are lacking the infrastructure to distribute the extracted gas into the rest of the US and particularly the Gulf Coast region. In this dissertation, shale gas catalytic upgrading processes were synthesized, designed, and simulated using Aspen Plus Simulation. Using Aspen Economic Analyzer, preliminary techno-economic analysis and evaluation of its economic potential were assessed at varying scales to assess its impact on the United States chemical industry landscape.

1. INTRODUCTION

1.1 Motivation

After one hundred years since Pechlbrenn Oil constructed the first modern oil refinery in 1857, petroleum refineries emerged and began producing a variety of transportation fuels. In the effort to utilize all components of crude oil, the product slate from petroleum refineries has been extended to feedstock for many other chemical processes. In 2006, it was reported that 90% of the organic chemicals produced annually in the US are derived from petroleum [1,2]. Considering a petroleum-deprived future, there is a need for a substitute for fossil resources in fuel and chemical production.

The overall impact of fossil resources as both an energy source and petrochemical source has been clearly recorded by many agencies. In 2010, 83% of the world energy demand was satisfied using fossil resources [3]. Even with the recent shale gas boom, the optimistic estimates about the remaining fossil resources suggest that we have at most 162 years remaining. The details of the numbers are more critical. The remaining crude oil reserves, which supply 95% of the transportation fuel, will be consumed within 40 years and the natural gas resources, which provide 25% of the electricity generation, will be exhausted within 55 years (excluding oil shale, tar sand reserves, and shale reserves) [4]. Although many studies have given varied projections to the end of fossil sources, they all concur on the fact that fossil sources are limited. Global warming resulting from an ever-increasing greenhouse gas emissions from the utilization of fossil resources causes changes in climate patterns, which are more frequently and more severely experienced around the globe in the form of melting of glaciers, changes in rainfall, records of high and low temperatures. There is an urgent necessity to find a substitute for fossil fuel.

Solar energy has offered a promising potential as the energy source of the future. The amount of solar energy that hits Earth in a single hour can provide enough energy to fulfill the energy consumption of the world in 2013 [5]. Solar energy alone, however, is not sufficient for sustainable production of chemicals and fuels. Fuel is mostly compromised of hydrogen and carbons while commodity chemicals mainly consist of the following four elements: hydrogen, carbon, oxygen, and nitrogen. Solar energy can only serve as the source of energy that is required during the production of fuels and chemicals. There must be sustainable sources for carbon, oxygen, nitrogen, and hydrogen to use solar energy in producing fuels and chemicals.

1.2   Biomass

Biomass has the potential as a renewable carbon source in converting solar energy into fuels and chemicals. Land availability and competition with other critical utilization of biomass must be carefully considered while using biomass as a feedstock. Generally, biomass can be categorized into two kinds: sustainably available waste (SAW) and dedicated fuel (DF) [6]. SAW biomass is usually grown from readily available space with minimal energy input while DF biomass is grown in a constrained land and managed by energy use [7].To sustainably meet the demand for fuels and commodity chemicals, every carbon molecule in the biomass must be completely recovered as end-use products. Therefore, a careful selection of the processes and reactions for the biomass conversion process is required.

Production of liquid fuel alone from biomass has mainly captured the attention of research groups [8–10]. In this endeavor, the objectives have been to increase the energy content of the biomass-derived molecules and to reduce the oxygen content of the products. Also, the product specifications are pushed to mimic that of gasoline or diesel. However, to effectively produce chemicals from biomass, the oxygen content of the biomass must not necessarily be removed since oxygen-based functionalities offer numerous reaction options [11]. Exploiting the features that already exist in biomass for conversion to chemicals calls for analysis at a molecular level.

1.3 Biorefinery Concept: Chemical and Fuel Production

As a result of these extensive studies and advances in biomass conversion processes, the concept of "biorefinery" has been established. In a general sense, a biorefinery is a processing facility or a cluster of processing facilities that transforms biomass into any value-added products [12]. It is conceived that a biorefinery will partition the complex structure of biomass into biomass-derived substrates which are then further converted to fuels and chemicals. Currently, there are more than 200 biorefineries in the United States that are concentrated into producing corn-ethanol and biodiesel [13]. Unlike a traditional refinery, the outputs from these existing plants do not compromise many commodity chemicals such as aromatics and plastic precursors. Despite receiving significant research focus on biofuels by both academia and industry, it is important to note that the dominant players in traditional refinery economics are the commodity chemicals [12]. Daoutidis et al. and Maravelias et al. have extensively worked on biorefinery designs [14–16]. Maravelias et al. mostly focused on laboratory proposed routes by Dumesic and Huber et al., which both focus on liquid phase reactions [10]. Daoutidis et al. have also worked on process superstructure problems using well known primary processes [15] You et al. worked on generating superstructure for biorefinery and claimed to have the most complete literature on biomass conversion [17].

Due to the numerous commodity chemicals that are desirable and a plethora of functional groups in biomass, there is a need for a systematic method to assess all the relevant chemistry and processes and determining the best process configuration. El Halwagi et al. proposed this hierarchical approach, but he has not implemented or created a working framework [18,19]. His most recent work on the symbiotic network of C-H-O is more related to mass integration, but it can be applied to biomass processing plants [20]. Daoutidis et al. and Marquardt et al. have worked using reaction network for optimization of synthetic routes [14, 21]. Daoutidis et al. have only focused on the optimizing the product slate instead of the reaction route [22]. Marquardt et al. on the other hand focuses on the reaction route by using Reaction Network Flux

Analysis (RNFA) and Process Network Flux Analysis (PNFA) [21, 23–25]. Besides this, Marquardt et al. and Daoutidis et al. have only focused on the subsequent processes, as shown in Figure 1.1, instead of the entire biomass conversion system.
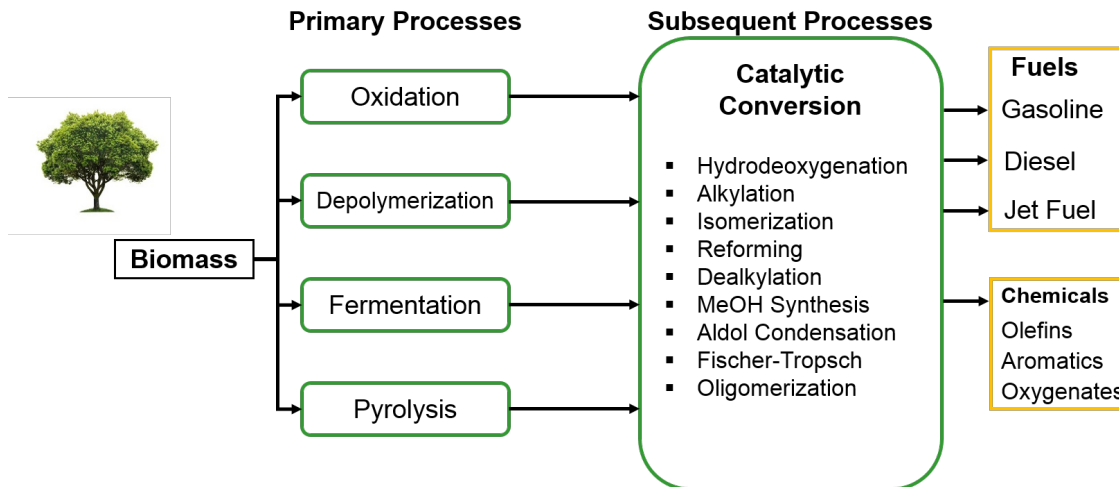
Figure 1.1.: Overall Biorefinery Concept

In this dissertation, we proposed a systematic approach to screen many process routes and configurations based on the fundamental knowledge of biomass conversion reaction system. It is worth noting that, unlike existing methods which have only focused on experimentally-proven chemistry, this method considers all the relevant chemistry to biomass. In addition, using the fundamental knowledge of the biomass conversion reaction system creates numerous opportunities for synergism because there could be unidentified intermediates that exist in producing the slate of target products.

1.4   Transition to Renewable Fuels: Shale Gas as Bridge Fuel

The transition from fossil resources to renewable energy is likely to be gradual as extensive infrastructure and policy changes are required. During this transition period, it is imperative that fossil resources be employed efficiently in order to mitigate the greenhouse gas emission. In addition, among the available fossil resources, it is

well-known that natural gas can be utilized for end-use energy needs, such as electricity, at higher efficiencies and lower carbon emission compared to coal power plants [26]. Figure 1.2 illustrates this concept. Therefore, it is crucial to employ natural gas and other fossil resources in a manner that mitigates greenhouse gas emission and maximizes energy efficiencies for various end-uses.
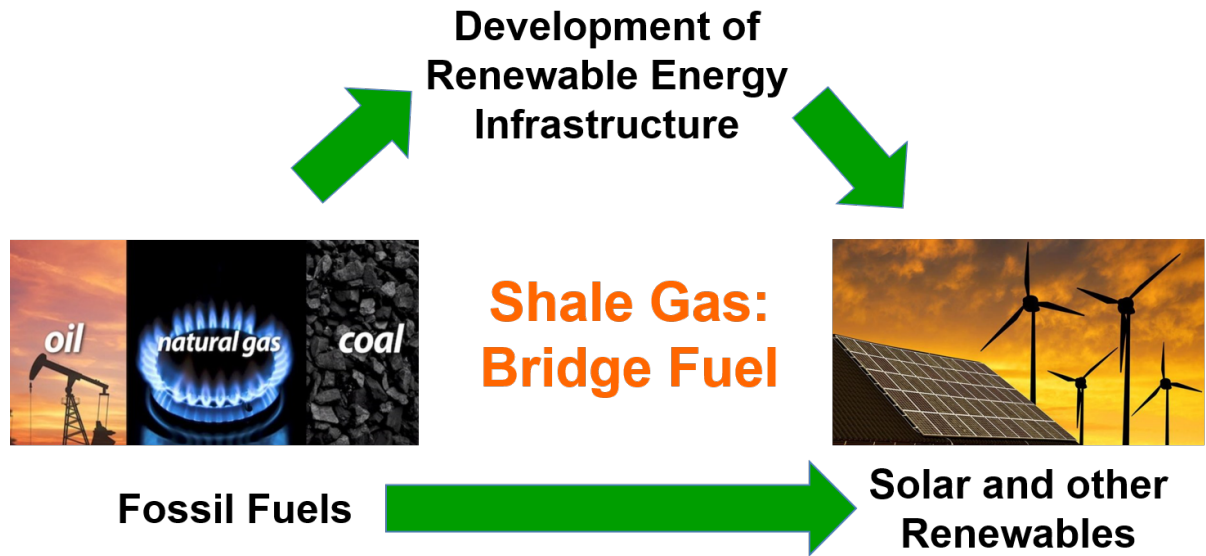
Figure 1.2.: Shale gas has the potential to serve as a bridge fuel during the transition toward a complete sustainable solar economy.

In order to meet the energy demands of the twenty-first century, engineers and scientists are working to develop new methods to discover, extract, and refine fossil resources including oil, coal, natural gas, shale oil, and shale gas. Recent advances in hydraulic fracturing and horizontal drilling have led to a surge in shale resource production. Similar to natural gas, methane concentration in shale gas ranges from 50% to 90%, which sets it as the major component [27, 28]. Unlike natural gas, shale gas contains higher concentrations of hydrocarbons other than methane, such as ethane, propane, butane, isobutane, and pentane. These hydrocarbons are known as

condensate or natural gas liquids (NGLs), and their concentrations vary from 0% to 50% [29].

It has been shown that the ethane and propane field productions in the United States exceeded their respective domestic consumptions. In addition, many shale gas resources are located in historically non-gas producing or processing regions. Existing pipeline infrastructure reached their capacities and resulted in discounted local prices for these shale resources. These circumstances led to an opportunity to locally convert shale gas hydrocarbons into easily transportable and marketable products.

1.5   Thesis Overview

1.5.1   Production of Hydrocarbons from Biomass

In chapter 2, process design and analysis of H2Bioil and catalytic depolymerization of lignin are presented. These thermochemical processes convert lignocellulosic biomass, such as poplar, to hydrocarbons. Agrawal et al. suggested a sustainable H2Bioil process for conversion of biomass to liquid fuel where biomass is co-fed to a fast-hydropyrolysis and hydrodeoxygenation (HDO) reactor system along with hydrogen produced from a carbon-free energy source such as solar, to produce liquid fuels in a single step process [7]. This H2Bioil process is based on continuous-flow biomass fast-hydropyrolysis, which is the rapid heating of biomass at rates of $1000°C \ s^{-1}$ in the presence of up to 50 bar hydrogen, to produce hydropyrolysis vapors which are upgraded in the vapor phase by catalytic HDO and quenched to form a high-energy density, deoxygenated liquid product that can supplement petroleum-based liquid fuels or potentially be used directly as a fuel [30]. Using available experimental data, this process was synthesized and designed to assess its thermal efficiency and process parameters, such as hydrogen consumption.

In fast pyrolysis, lignin and its aromatic structures are generally lost or converted into its deoxygenated forms. As stated earlier, lignin per se is a very lucrative target. In many fermentation processes and pulp processing, lignin is extracted and used as

fuel for other unit operations. Using lignin as fuel only wastes the carbon that could instead be allocated to chemical production. Klein et al. developed a novel catalytic process that extracts and hydrodeoxygenates lignin-derived products while leaving a carbohydrate residue from biomass. Using on available experimental data, this process was synthesized and designed to assess its thermal efficiency and process parameters, such as hydrogen and methanol consumption.

1.5.2 Upgrading Fast Pyrolysis Vapor of Cellulose

Toward developing an integrated biorefinery, in chapter 3, we present a holistic and systematic approach to biorefinery design by fully considering the underlying biomass conversion reaction systems. Our approach examines the biomass-to-fuels-and-chemicals landscape, which mainly consists of primary and subsequent processes. Using an automated reaction network generator (RING), we exhaustively define the possible search space of the reaction system. We then construct an ideal reaction-separator superstructure and determine the optimal reaction route described by the minimum number of allowed reaction steps through optimization. To select a thermodynamically feasible reaction route, we also consider thermodynamic parameters in our approach.

To illustrate the approach, we present a case study on upgrading fast-hydropyrolysis of cellulose to higher molecular weight molecules. Levoglucosan and glycolaldehyde are the primary products of the fast-hydropyrolysis of cellulose. Identifying the optimal reaction route to convert these molecules is crucial to reach fuel range molecules. In this study, we identified several promising reaction routes to transform the vapor to higher molecular weight compounds and showed that key intermediates are required in order to allow carbon coupling between glycolaldehyde and levoglucosan. The proposed reaction routes from this approach have been validated by the identification of several of the predict products in the accompanying experimental results.

1.5.3   Biorefinery: Fuels and Chemicals from Biomass

In Chapter 4, we conceptualize a biorefinery that is based on major primary processes through mathematical modeling and optimization. The ultimate objective of this study is to establish a roadmap which can be used to identify various biorefinery configurations that can convert lignocellulosic biomass, such as poplar, to fuels and chemicals. To establish this roadmap, we consider several scenarios for biorefinery design. More importantly, the study is aimed to maximize the carbon yield of the biorefinery while minimizing the number of reactions and satisfying various target demands for fuels and chemicals. Through this work, several potential biorefinery configurations were identified for fuels and chemical production in tandem. Also, their reported carbon efficiencies are relatively higher than those of reported studies.

1.5.4   Elucidation of Char Formation in Fast Pyrolysis

In chapter 5, potential pathways that lead to the formation of char precursors during fast pyrolysis of cellulose are identified using systems-level molecular mapping. Char accounts for almost 30% of carbon loss during fast pyrolysis of intact lignocellulosic biomass [30–32]. Therefore, it is imperative to understand as to how char forms during pyrolysis. Advances in mass spectroscopy enable identification of primary products during fast pyrolysis of carbon-containing moieties, such as cellulose and char. Jiang et al. used mass spectroscopy to identify several proposed char-derived molecules formed during fast pyrolysis of char from fast pyrolysis of cellulose. Based on these proposed molecules, we identified potential pathways for their formations from primary products during fast pyrolysis of cellulose. These pathways offer insights into the key driving forces and reaction steps that lead toward char formation during fast pyrolysis of cellulose.

1.5.5 Valorization of Shale Gas Condensate

The energy landscape of the United States has been impacted tremendously by the recent shale gas boom. Shale resources contain a substantial amount of condensate and natural gas liquids (NGLs). Many regions containing shale resources are located in remote areas and are deficient of the needed infrastructure to distribute the extracted NGLs to other areas, such as the Gulf Coast. In chapter 6, we propose a shale gas transformation process that converts NGLs in shale resources into liquid hydrocarbons, which are easier to transport than NGL or its constituents. This process entails catalytic dehydrogenation followed by catalytic oligomerization. Preliminary Thermodynamic process analysis indicates that this process has the potential to be more energy efficient than existing NGL-to-liquid fuel (NTL) technologies. Besides, the estimated payback period for this process is within the average lifetime of shale gas wells. Based on these preliminary evaluation and conceptualization, the proposed process holds the promise to be an energy efficient and economically attractive step to utilize condensate in remote regions containing shale resources.

1.5.6 Conclusions and Outlook

Chapter 7 presents key findings from this dissertation along with recommendations and directions for future work.

2. PROCESS DESIGN OF NOVEL THERMOCHEMICAL PROCESSES: H2BIOIL AND CATALYTIC DEPOLYMERIZATION OF LIGNIN

2.1 Introduction

The increasing world population, limited fossil resources, and rising environmental concerns continue to push the interest in the sustainable design of chemical processes. Fossil resources dominate the energy production landscape. With 93% of the energy demand in the transportation sector derived from petroleum resources [33]. Energy production is expected to double globally by 2040, accentuating interest in biomass as a potential renewable carbon resource. Langholtz et al. reported that the United States has the potential to generate enough lignocellulosic biomass to replace 27-47% of the United States liquid fuel demand [34]. Therefore, converting biomass to fuels would mitigate the heavy reliance on fossil resources, while at the same time helping to reduce CO_2 emission. Transitioning to biomass, however, calls for a need to efficiently convert lignocellulosic biomass to fuel while utilizing every carbon available in biomass.

Agrawal et al. proposed a process called H2Bioil, which is a fast-hydropyrolysis process followed by a catalytic hydrodeoxygenation reactor to produce liquid fuel [6, 35, 36]. Shown through experimental results, this process liquid fuel yield is approximately 16 MJ/kg of biomass. Mallapragada et al. modeled this process using certain process assumptions based on similar tandem fast pyrolysis and downstream catalytic system [37]. However, these assumptions are not based on the process data reported by Venkatakrishan et al., which reported lower carbon efficiency and distinct carbon distribution for the final hydrocarbon products [30]. In addition, it has been reported that this process is operated at excess hydrogen condition, which has significant implications on the downstream product recovery. Therefore, it is imperative to properly synthesize and design the H2Bioil process that accounts for its

process conditions. With poplar feed, H2Bioil still results in high char yield, which has been suggested to be due to lignin.

In fast pyrolysis, lignin and its aromatic structure are generally lost or converted into its hydrogenated products [30, 38]. Lignin itself contains aromatic ring structures and composes of 40-35% of carbon in lignocellulosic biomass [39, 40]. In many fermentation processes, once lignin is extracted, it is used as fuel to supply heat and power [41]. Using lignin as fuel only wastes the carbon that could instead be converted into chemical products [42]. Klein et al. developed a novel catalytic process that extracts and hydrodeoxygenates lignin derived molecules while leaving a carbohydrate residue from biomass and this process occurs in a single step [39]. In this process, the lignocellulosic biomass, such as poplar, is placed in a methanol solution under a hydrogen atmosphere at 35 bar and 498K. The catalyst they used is a Pd/Zn on a carbon support. The products from this process are mainly carbohydrate residue and lignin-derived chemicals, such as dihydroeugenol and propylsyringyol. To understand the overall process performance, we synthesize and simulate this catalytic process while appropriately accounting for its process conditions.

2.2   H2Bioil: Process Description and Modeling

Gençer and Mallapragadra et al. simulated this process for an augmented biomass conversion process and integrated Biomass-Natural Gas process to liquid fuel [37, 43]. In both works, the process was simulated using data from reported studies on fast pyrolysis system [37, 43, 44]. Recent studies by Venkatakrishnan et al. provided more accurate H2Bioil process and, using this experimental data, the process modeling and design are based on this study. [30].

A stoichiometric H2 consumption was also assumed while in actuality the H2Bioil process runs at significantly excess hydrogen flow. The H2Bioil process was simulated using Aspen Plus. First, the biomass undergoes fast-pyrolysis with hydrogen at 753 K and 25 bar [30]. There are two types of biomass feed considered for this model, cellulose and wild type-poplar [30]. Modeling biomass in Aspen Plus calls for the coal
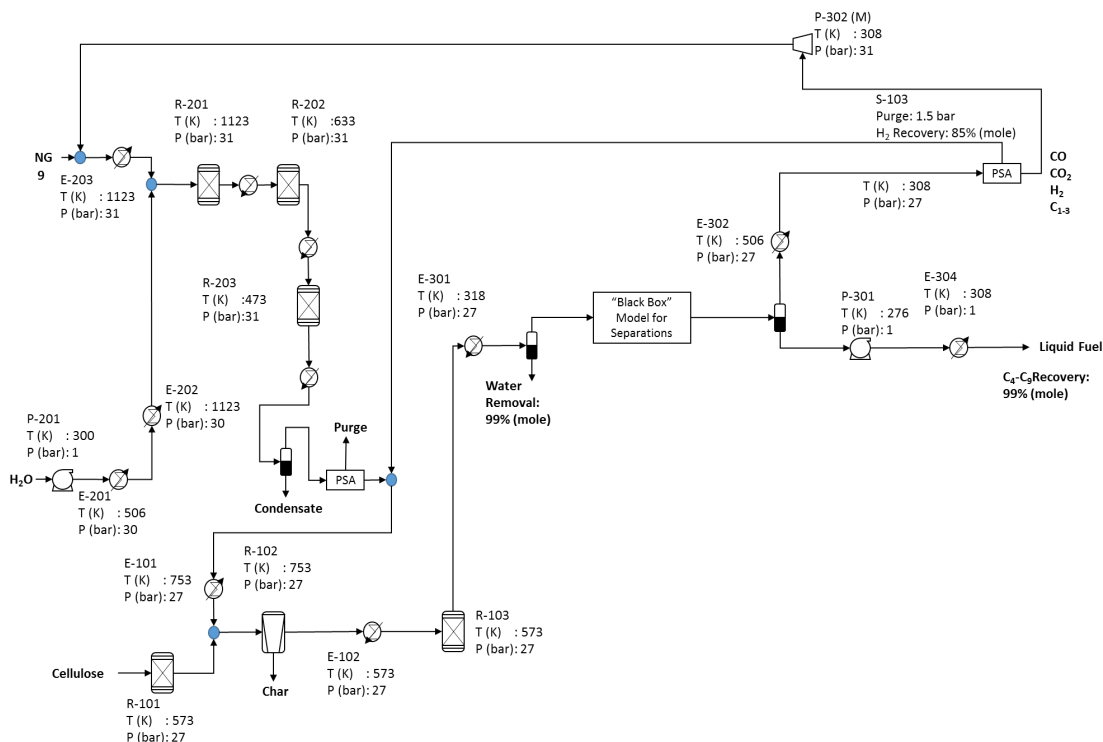
Figure 2.1.: Process flow sheet for H2Bioil of cellulose with excess hydrogen.

thermodynamic model. For this model, the hydrogen is produced by Steam-Methane Reforming (SMR). Data from the literature are used for the operating conditions of SMR. In this model, the process runs at excess hydrogen, and the amount of excess hydrogen is determined by minimum fluidization velocity. Data from literature and an empirical equation for minimum fluidization velocity were both used to determine the amount of excess hydrogen [9, 45].

The product from the fast-pyrolysis reactor is then adjusted to the appropriate temperature before entering the hydrodeoxygenation (HDO) reactor, which operates at 573 K. Finally, the products are then cooled, and excess hydrogen along with permanent gases are separated. For this separation step, a black box model is used since determining the optimum separation step can be a tremendous task. To calculate the heat duty for this separation step, the minimum work for separation is calculated, and then an efficiency from literature is assumed [46]. Figure 2.1 shows the Aspen

Plus flowsheet for this process with cellulose as the feed. In Table 2.1, the process summary for H2Bioil at excess hydrogen with cellulose as the feedstock is shown.

2.3 Catalytic Depolymerization of Lignin: Process Description and Modeling

The experimental procedure of this process serves as the basis for the process modeling. The procedure involves placing the biomass in a methanol solution along with a Pd/Zn catalyst under a hydrogen atmosphere. Then, the mixture is heated up to 498K. After it is heated, the catalyst and the carbohydrate residue are filtered. The methanol solution contains dissolved C5 sugars along with dihydroeugenol and syringylphenol, which are derived from lignin. There are experimental results from wild-type poplar and genetically modified poplars [39].

Experimental results for this process have no more than 80% mass balance closure and the experiments were performed using batch reactors. Modeling this process in Aspen Plus calls for several assumptions. For the mass balance closure, it is assumed that the unknown mass from the lignin is consisted of the unreacted monolignols. For the unidentified mass from hemicellulose, humins are selected to account for the unidentified mass. Humins are not included in the Aspen Plus library and literature suggests dibenzofuran can be used to model humins in Aspen Plus as it mimics the monomer of humins [47]. Hydrogen required for this process is also produced using natural gas through SMR. First, the biomass, hydrogen, and methanol enter the reactor operating at 523K and 90 bar. The solid products are then separated from the liquid products. Similarly to H2Bioil, a black box model is assumed for the separation of the liquid phase products. The minimum work of separation and efficiency from the literature are again used to determine the heat duty of the separation process [46]. The recovered methanol is then recycled back into the reactor. No evidence has shown that methanol is consumed in this process and equilibrium analysis of methanol reforming at the process operation condition has also supported the assumption of no methanol consumption. The C5 sugars are also recovered and recrystallized. Finally,

the lignin-derived products are recovered [48]. The monolignols are assumed as waste in this model. Figure 2.2 is the Aspen Plus Flowsheet for this process.

Figure 2.2.: Process flowsheet for catalytic depolymerization of lignin with wild-type poplar.

2.4 Results and Discussions

Table 2.1 summarizes the result of the model based on WT-Poplar experimental data. Gasification is used as a reference for conventional biomass transformation process toward fuels.

Table 2.1.: Summary of H2Bioil and CDL Process Parameters.

	H2Bioil - Cellulose	CDL - WT - Poplar	Gasification - Wood Chips
Efficiency	0.43	0.55	0.41
LHV Ratio	0.88	0.78	0.47

All the Aspen Plus models for the mentioned processes are approximate since model compounds and black box unit operations are used. In addition, none of the processes is heat integrated in this work. Therefore, there is ample opportunity for improvement on the thermal efficiency. Also, the efficiencies between the processes shown in Table 2.1 are not directly comparable because different assumptions were made in each process. In H2bioil, the process operates at excess hydrogen condition while, in CDL, the process uses only stoichiometric amount of hydrogen, which is significantly less than that of H2Bioil. In Table 2.1 above, the overall efficiency is defined:

$$\eta_{OverallEfficiency} = \frac{\sum_i \dot{m}_{product,i} LHV_i}{\dot{m}_{feed,i} LHV_i + \frac{\dot{Q}_{HeatDuty}}{\eta_{HeaterEfficiency}} + \frac{\dot{W}_{NetPowerConsumption}}{\eta_{PowerGenerationEfficiency}}} \quad (2.1)$$

where, $\dot{m}_i$ is the mass flowrate of species i and LHV_i is the lower heating value of species i. $\eta_{PowerGenerationEfficiency}$ and $\eta_{HeaterEfficiency}$ are generally assumed to be 0.4 and 0.6, respectively. The LHV ratio is defined by the equation below:

$$LHV\ Ratio = \frac{\sum_i \dot{m}_{product,i} LHV_i}{\sum_i \dot{m}_{feed,i} LHV_i} \quad (2.2)$$

2.5   Conclusions

Bench-scale demonstrations of H2Bioil and catalytic depolymerization of lignin offer insights into the process conditions necessary to obtain hydrocarbons from lignocellulosic biomass. Using experimental data and conditions, these processes are simulated in Aspen Plus and hydrogen generation and downstream separations are also considered. These two processes generate two distinct product slates. On the one hand, H2Bioil generates mostly hydrocarbon products, a mixture of permanent gases, such as CO, CO_2, and CH_4, and solid char. On the other hand, catalytic

depolymerization of lignin produces propylbenzene and a solid residue containing mostly cellulose.

In both processes, SMR is employed to provide hydrogen derived from natural gas. Blackbox separation models are also utilized in both overall processes. Their estimated thermal efficiencies are higher than that of gasification processes. These, however, are only preliminary estimates as many downstream alternatives can upgrade their products further.

Potential integration between these two processes must also be properly assessed. Solid residue from catalytic depolymerization of lignin can be subjected to H2Bioil. The resulting permanent gas from H2Bioil can be used for methanol production and sent to the catalytic depolymerization process as a make-up stream. Similarly, the permanent gas can be used toward hydrogen production to supply both processes and also downstream hydrodeoxygenation process. These thermochemical processes have the potential to convert lignocellulosic biomass into liquid fuels and chemicals efficiently.

3. UPGRADING FAST-HYDROPYROLYSIS VAPOR PRODUCTS OF CELLULOSE TO HIGHER MOLECULAR WEIGHT PRODUCTS USING SYSTEMS-LEVEL MOLECULAR MAPPING OF BIOMASS-DERIVED MOLECULES

3.1   Introduction

As mentioned in Chapter 2, Agrawal et al. proposed a process called H2Bioil, which converts biomass to liquid fuel. In this process, biomass is co-fed to a fast-hydropyrolysis and catalytic hydrodeoxygenation (HDO) reactor system with hydrogen produced from a carbon-free energy source, such as solar, to produce liquid fuels in a single step process [7]. This H2Bioil process is a continuous-flow biomass fast-hydropyrolysis, which is the rapid heating of biomass at rates of $1000°C$ s^{-1} under the presence of up to 50 bar hydrogen, to produce vapors which are upgraded in the gas phase by catalytic HDO and rapidly quenched to form a high-energy density, deoxygenated liquid product that can be blended petroleum-based fuels or potentially be used directly as a fuel [30]. Venkatakrishnan et al. have demonstrated H2Bioil using PtMo on multi-walled carbon nanotubes (MWCNTs) as the hydrodeoxygenation catalyst [30,31]. Although the products are indeed deoxygenated, their carbon numbers, which range from four to six, are lower than those of hydrocarbon molecules found in gasoline and diesel, indicating their unsuitability as a drop-in fuel. For cellulose and poplar as feeds into H2Bioil process, the yields of hydrocarbons with carbon number greater than or equal to four are 30% and 23%, respectively, while 65.3% and 38.8% of the carbon product has carbon chain length of less than or equal to six, respectively. Clearly, hydrodeoxygenation alone is insufficient for drop-in fuel production.

To our knowledge, the literature shows no systematic studies to understand the optimal catalytic system for upgrading vapors obtained from fast pyrolysis of biomass

using thermodynamic and stoichiometric models of the biomass conversion system. Molecules from fast-hydropyrolysis and other processes, such as depolymerization, contain many functional groups which can be subjected to numerous catalytic reactions. In addition, biomass constituent polymers such as, cellulose, hemicellulose, and lignin, contain structures that can produce existing commodity chemicals, such as aromatics, ethylene glycol, and hydroxymethylfurfural. Therefore, it is pertinent to identify process configurations that retain and exploit functional groups that exist in biomass while maximizing the carbon efficiency toward the production of fuels and chemicals.

Numerous functional groups in biomass-derived molecules, which are those obtained from primary processes, present opportunities for catalytic transformations. There is a need for a systematic method to assess all pertinent chemistry and determining the best process configuration for transforming the biomass-derived molecules to the intended target products. El-Halwagi et al. proposed this hierarchical approach, but a functioning framework has not been demonstrated yet [18]. The research study by Noureldin et al. proposed a mass integration approach to synthesize a symbiotic network of C-H-O [20]. In this approach, an atom targeting approach is used to identify the atomic gaps in a set of processes being studied. Based on these gaps, additional processes are considered in order to improve the overall atom efficiency. Through a case study, the approach can identify an integrated complex with the potential of saving 47% of the cost of an unintegrated complex. Marvin et al. used an automated reaction network generator called Rule Input Network Generator (RING), and formulated a mathematical optimization problem to find the optimal oxygenates and hydrocarbons for bio-gasoline blend and determine their synthetic routes [49]. This research study focused on selecting the optimal target products for a gasoline blend from a candidate set of platform chemicals proposed by the United States Department of Energy as the top 10 most promising platform chemicals from biomass. In this work, Marvin et al. proposed several sets of optimal molecules for bio-gasoline blend and their reaction routes. Rangarajan et al. also employed RING to identify routes for the production of fatty alcohols from platform chemicals [50]. The focus of that

study is on the identification and analysis of a synthesis route. They identified several routes starting with hydroxymethylfurfural and ethanol to produce lauryl alcohol. In these works, however, Marvin et al. and Rangarajan et al. did not consider the processes required to generate the platform chemicals they considered. These processes, called primary processes, play a crucial role as each process has an associated carbon efficiency and produces a distinct set of biomass-derived molecules and by-products. In addition, the abundances of biomass-derived molecules produced by the primary process impact the selection of optimal process configurations. Voll et al., on the other hand, focus on the selection of reaction routes by constructing a Reaction Network Flux Analysis (RNFA) [21]. Through RNFA, Voll et al. identified the optimal reaction route to produce 3-methyltetrahydrofuran, claimed as a promising molecule for biofuel, from itaconic acid. In this study, however, the reactions were collected from literature, primarily through reaction databases such as Reaxys. Ulonksa et al.extended RNFA by accounting for process parameters such as operating conditions, energy consumptions, and capital and operating expenses, in order to determine the most economically profitable reaction configuration [24]. This approach is termed Process Network Flux Analysis (PNFA) and, similar to RNFA, PNFA utilizes reactions collected from the literature. These approaches limit the possibility of combining and utilizing biomass-derived molecules to only previously reported reactions.

Here, we present a systematic approach to generate and screen process routes and configurations based on thermodynamic and stoichiometric knowledge of biomass conversion systems. Unlike existing methods, which only focus on experimentally-proven chemistry and start with platform chemicals, this method considers all chemistry relevant to biomass-derived molecules and the primary processes which generate those biomass-derived molecules. Also, using stoichiometric models of biomass conversion systems create numerous opportunities for overall process synergy because key reaction intermediates and effective utilization of biomass-derived molecules toward the production of target products can be identified. There are two main steps in this approach. First, the search space is defined using process yield data from the

literature and an automated reaction network generator tool (RING) [51]. Second, an optimization problem is formulated in order to identify thermodynamically favorable and carbon efficient networks for the biomass conversion. In this chapter, a case study entailing upgrading of fast-hydropyrolysis vapors of cellulose to higher molecular weight hydrocarbons is presented to illustrate the use of this approach. In this study, experiments are also included to compare with the model predictions.

First, the problem statement entailing this approach is introduced along with the problem structure. Then, the methodology is described in detail.

3.2   Problem Statement

The problem of identifying a biomass processing configuration may be stated as the following: given is a set of primary processes (p | p = 1,2,...,$N_{process}$). A primary process disassembles biomass into a distinct set of biomass-derived molecules at specific abundances. These biomass-derived molecules then become the feed for subsequent processes such as catalytic reactions (j | j = 1,2,....,$M_{process}$). Each subsequent process is represented as a reactor-separator block, configured as a reactor followed by a separator that performs a complete split separation for each component.

To allocate biomass-derived molecules from the primary process to the reactor-separator blocks, a distributor block is created for each biomass-derived molecule. The distributor block consists of three unit operations, one mixer and two splitters. The mixer combines the fresh feed stream, $n_i^{in,fresh}$, of molecule i, which comes from primary processes with outlet streams, $n_{i,j,FEED}$, of molecule i coming from reactor-separator block j. The outlet of this mixer enters the first splitter which only has two outlet streams, $n_{i,Reactors}$ and $n_{i,Outlet}$. The first outlet stream, $n_{i,Outlet}$, serves an exit for molecule i, and the second stream, $n_{i,Reactors}$, is sent to the second splitter. Finally, the second splitter distributes its inlet, $n_{i,Reactors}$, to reactor-separator blocks. As with the separators, the splitters are also assumed to be 100% efficient. This construct is illustrated in Figure 3.1. It is worth noting that the construct considered in this work represents an ideal reactor network in which any participating molecule can react

liberally with other molecules in order to identify potential process synergies and key intermediates while neglecting any penalty from separation.
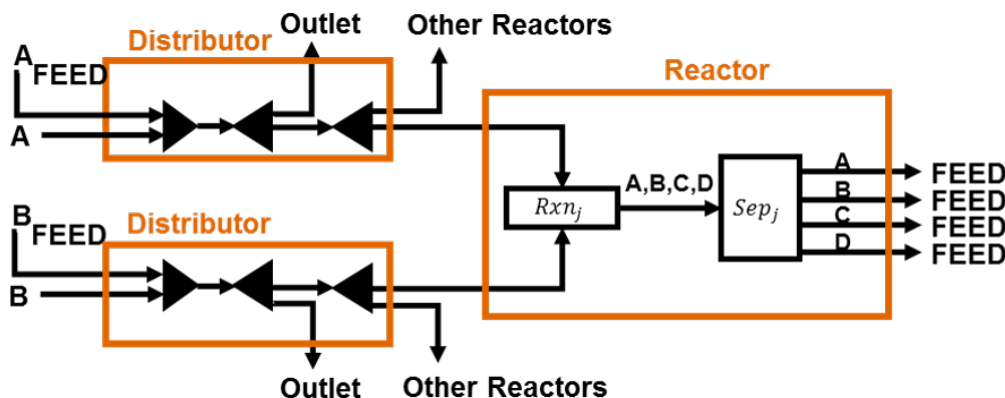
Figure 3.1.: Distributor and Reactor-Separator structures used in this work

As stated earlier, each subsequent process is configured as reactor-separator block. There are diverse configurations for reactor-separator blocks based on the type of reaction and physical properties of the molecules. In this work, the reactor-separator block is stoichiometry-based and assumed to have 100% selectivity towards the product of the reaction represented by this block. The details of separation are not considered and there is no penalty associated with the separator. Selection of the appropriate reactor-separator configuration would require detailed knowledge of the properties of the wide variety of reactions and mixtures considered here. Instead, all reactor outlet streams are separated into individual component streams that have 100% purity.

A set of primary processes and subsequent processes (i.e., reactions) is given. The aim is to synthesize a process network that is capable of managing the production, transformation, and distribution of biomass into target products while achieving a desired objective or a combination of objectives and satisfying process constraints. We are interested in finding a set of primary processes and reactions that satisfies thermodynamic constraints within a specified operating range while constituting the minimum number of reactions and achieving target carbon efficiency for transforming

biomass to desired products. Because of the assumptions of 100% selectivity and separator, the optimal solution found represents an ideal best case.

3.3 Modeling and Optimization Approach

Figure 3.2 describes the overall approach proposed in this work. Given a biomass feed, a set of target molecules, and an objective function, first, the search space is defined using experimental data for primary processes from literature and an automated reaction network generator tool, specifically RING [14, 51, 52]. Primary processes and reaction libraries, defined in later sections, also contain the relevant parameters related to the primary and subsequent processes. A reaction-to-process module then constructs a superstructure that contains the connectivities in the primary process and reaction set. An optimization problem is then formulated in order to identify thermodynamically favorable and carbon efficient networks for biomass conversion.

3.3.1 Primary Process Library

Many primary processes for biomass conversion have been proposed in the literature, including thermochemical and enzymatic routes. Through analysis of that literature, a library is populated with process yields of several primary processes, such as pyrolysis. The primary processes are modeled based on reported yields. The molecules generated by these primary process are the inputs into the subsequent processes.

3.3.2 Reaction Library

The reaction library contains the search space for the subsequent processes. Since biomass-derived molecules possess many functional groups, it is critical to exhaustively identify all known reactions pertinent to biomass-derived molecules and their derivatives. There are two methods to populate the reaction library: performing literature review and employing an automated reaction network generator tool. For example, Marquardt et al. and Mitsos et al. performed a literature review to collect
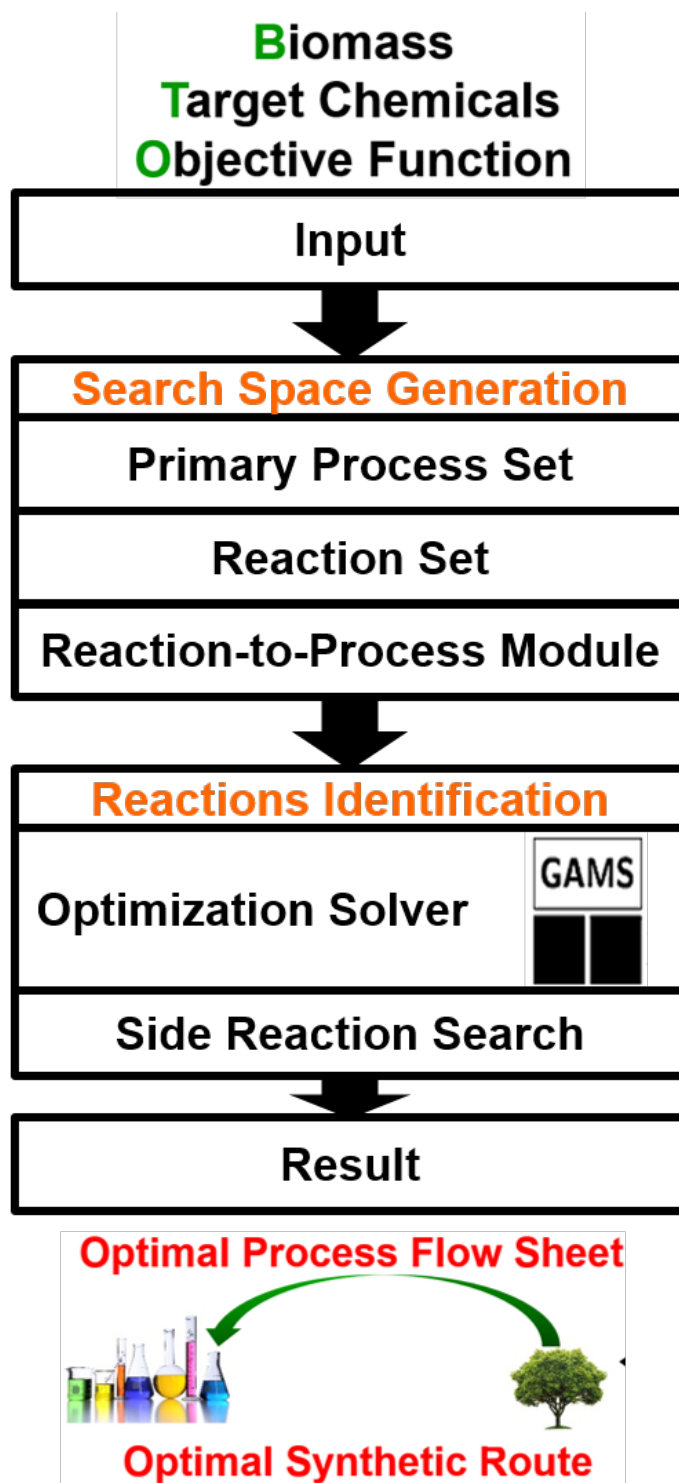
Figure 3.2.: Systems-Level Molecular Mapping Modeling and Optimization Approach

all relevant reactions related to their studies [21, 24, 25]. There have been extensive works on automated reaction network generator tools [52]. These tools exhaustively and iteratively generate reactions based on a set of initial molecules and reaction rules. In this work, the Rule Input Network Generator (RING) tool is selected. [52].

3.3.2.1   Rule Input Network Generator

The algorithms behind RING have been described in the literature [51–53]. The inputs to this tool are the initial molecules and a set of reaction rules. The initial reactants, here, are defined as the biomass-derived molecules. Reaction rules are a set of logical statements that identify the appropriate reactants and modify the bonds between the reactants to generate the products. Marvin et al. have compiled a set of reaction rules for oxygenates-to-gasoline chemistry [22]. In this work, we modified five reaction rules for that set and also added ten additional reaction rules. The search space is defined by the reaction rules included. We strove to include rules for all reactions that are relevant to biomass chemistry. The details of those reaction rules can be found in the Supplementary Information. For the case study, the maximum rule rank, i.e., the number of sequential rule applications, is limited to four in order to mitigate a combinatorial explosion from this tool.

3.3.2.2   Thermodynamic Properties Estimator

One of the main challenges for modeling biomass is the lack of published thermochemical property data for relevant molecules. Accurate thermochemical properties are necessary for calculating the thermodynamic viability of reaction pathways generated by this tool's algorithms. In this work, we utilized the Benson Group Additivity group contribution method to obtain a first approximation of thermochemical properties of molecules and reactions of interest. This method is implemented using the Reaction Mechanism Generator tool developed by Green et al. [54]. This method was also employed by other studies concerning biomass-derived molecules and indicated acceptable

errors for the estimated values [22]. The prediction accuracy of this group additivity method for biomass-related molecules is described in several works [22, 54, 55].

3.3.3 Identification of the Optimal Reaction Sequence

This problem is represented by a network of distributor and reactor-separator blocks. This representation is sufficient to embed potential synergistic configurations. An optimization problem is formulated in order to identify thermodynamically favorable and carbon efficient networks for the biomass conversion. Here we describe the constraints for the construction of the network and determine the optimal reaction network.

3.3.3.1 Optimization Model Formulation

The following constraints are implemented for the mixers, splitters, and the reactor-separator block shown in Figure 3.1:

Mixer and Splitter Material Balance. Each mixer and splitter in the distributor block has several inlet and outlet streams. There is a total of one mixer and two splitters. The mixer is used to combine biomass-derived molecules from primary processes with streams coming in as the outlet products of other reactor-separator blocks. Therefore the material balance for each mixer for molecule i with outlet streams directed from reactor-separator block j is given by Equation (3.1).

$$\dot{n}_i^{in,fresh} + \sum_{j}^{M_{process}} \dot{n}_{i,j}^{out} = \dot{n}_i^{in} \,, \ \ \forall \, i \tag{3.1}$$

The first splitter enables removal of a molecule before further distribution. Direct removal may occur when the product of the primary process is desirable. There

are two outlet streams from the first splitter, $\dot{n}_{i,outlet}$ and $\dot{n}_{i,reactors}$. Therefore, the material balance for the first splitter is given by Equation (3.2).

$$\dot{n}_i^{in} = \dot{n}_{i,reactors}^{splt1} + \dot{n}_{i,outlet}^{splt1} , \ \forall \, i \tag{3.2}$$

The second splitter acts as a distributor for all reactor-separator blocks. The outlets of the second splitter are only for reactors where the molecule, i, is a reactant. Therefore, the material balance is given by Equation (3.3).

$$\dot{n}_{i,reactors}^{split1} = \sum_{j \in I_i^{Reactant}} \dot{n}_{i,j}^{in} , \ \forall \, i \tag{3.3}$$

$I_i^{Reactant}$ is a set of reactions where molecule i is a reactant. Each component outlet stream from the reactor-separator block is then sent to its corresponding distributor block next in sequence, as shown in Figure 3.3.
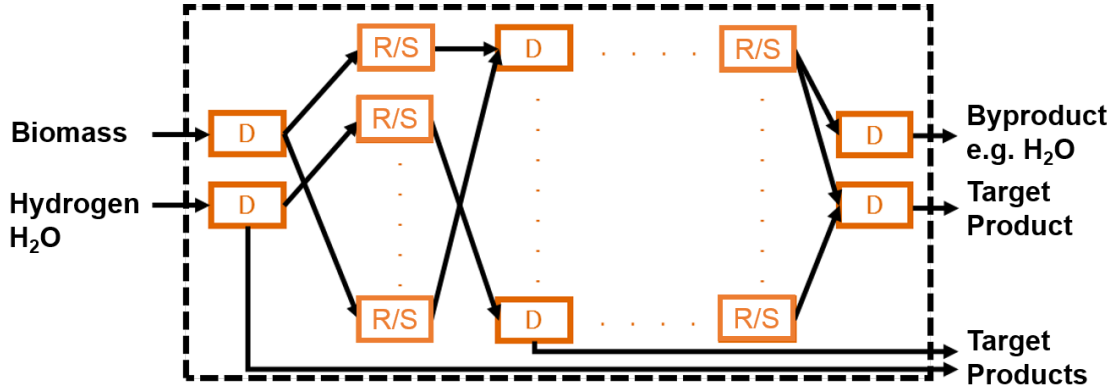
Figure 3.3.: Reactor-Separator and distributors superstructure constructed by the optimization formulation. "D" and "R/S" blocks represent distributors and reactor-separator, respectively.

Reactor Model. As mentioned earlier, the reactor is modeled as stoichiometric reactor model with unrestricted conversion and 100% selectivity toward the product. Extent of the reaction, $\dot{n}_j^{rxn}$, is used to control conversion on each reactor and $A_{i,j}$

is the stoichiometric coefficient of molecule i in reaction j. Therefore, the material balance around the reactor is given by Equations (3.4-3.6).

$$\dot{n}_{i,j}^{out} = \dot{n}_{i,j}^{in} + A_{i,j}\dot{n}_j^{rxn}, \ \forall i, j \ s.t. \ A_{i,j} < 0 \tag{3.4}$$

$$\dot{n}_{i,j}^{out} = A_{i,j}\dot{n}_j^{rxn}, \ \forall i, j \ s.t. \ A_{i,j} > 0 \tag{3.5}$$

$$\dot{n}_{i,j}^{in} \leq M\dot{n}_j^{rxn} \ \forall i, j \ s.t. \ A_{i,j} < 0 \tag{3.6}$$

The third constraint above is a Big-M constraint that relates extent of reaction to the presence of inlet and outlet streams. We are also interested in determining the activity of each reactor. Therefore, we introduce $a_j \in 0, 1$ which is a binary variable where 0 and 1 indicate inactive and active reactor, respectively. Using the Big-M constraint, the presence of active outlet streams is related to the activity of that reactor. Therefore, the reactor activity constraint is given by Equation (3.7).

$$\sum_{j \in I_i^{Products}} \dot{n}_{i,j}^{out} \leq U a_j, \ \forall j \tag{3.7}$$

where U is an arbitrary big-M constant.

Product Separator. In the reactor-separator block considered in this work, the separator partitions the product stream into its component streams. Here, we assume that separations are perfect with no penalties. Separation of biomass-derived molecules and their derivatives is an on-going research field, and it is challenging to incorporate analysis of these separations on a general basis due to the lack of thermochemical and physical properties of these molecules.

In order to ensure overall material balance closure, the mole balance constraint is imposed using Equation (3.8).

$$\dot{n}_i^{in,o} + \sum_j A_{i,j}\dot{n}_j^{rxn} - \dot{n}_{i,outlet}^{split1} = 0, \ \forall i \tag{3.8}$$

Thermodynamic Restriction. Since we assume there is no penalty associated with the separation and the reaction in terms of conversion and selectivity; we must use a parameter to refine the identification of the reaction routes. Calculating thermodynamic properties of molecules using the Benson Group additivity method as previously discussed, the Gibbs free energies of reaction at 298 K and 1073 K are estimated for each reaction. Each reaction is required to be thermodynamically favorable at some temperature between 298 - 1073 K in order to satisfy typical operating conditions for well-known industrial chemical reactions. [56]. Therefore, we impose this restriction by Equation (3.9).

$$a_j = 0 \ , \ \ \forall \, j \, s.t. \, \Delta G_j^{rxn}(1073K) > 0 \ and \ \Delta G_j^{rxn}(298K) > 0 \tag{3.9}$$

Objective Function. Subject to the assumptions we considered here, we are interested in determining a thermodynamically favorable route with the minimum number of reactions. The number of reactions may impact overall carbon loss and total capital cost in the real system. However, the number of reactions in a pathway does not determine whether that pathway would be kinetically favorable. Nevertheless, this objective function will not select thermodynamically feasible pathways with a higher number of reactions than the set limit. In order to address this gap, competing reaction pathways, particularly those with more reactions, are identified and the approach for their identification is described in a later section. In each application of the method, the objective function to minimize the total number of reactions is given by Equation (3.10).

$$min \sum_j a_j \tag{3.10}$$

where a_j is a binary variable that takes a value of 0 if reaction j is not active and a value of 1 if it is otherwise. It is clear, however, that the reaction network with the minimum number of reactions is not guaranteed to be kinetically favorable.

Target Carbon Efficiency. As described, the objective function is the number of active reactions. Therefore, a constraint must be placed in order to induce production of target molecules. Here, a carbon efficiency constraint is written as Equation (3.11).

$$\eta_{carbon} = \frac{\sum_{i \in I^{product}} C_i \dot{n}_i^{out}}{C_{biomass}} \geq \eta_{targetcarbon} \tag{3.11}$$

where $C_{biomass}$ and C_i are the numbers of moles of carbon in the biomass and the carbon number of molecule i, respectively. $\eta_{targetcarbon}$ is a scalar variable that is specified and the upper bound for this variable can be determined by calculating the number of unusable carbons (e.g. Char, humins, CO2, and CO) that are present in exhaust streams from the primary processes. Note that all the secondary processes are assumed to have unrestricted conversion and 100% selectivity. Therefore, only the primary processes are needed to calculate the upper bound for $\eta_{targetcarbon}$.

Determining Alternative Optimal Solutions. Considering that the constraint of the thermodynamic feasibility is not tight and the problem formulated above is MILP, alternative optimal solutions could exist. Hence, there could be many routes with the same number of reactions to reach a particular molecule. Since the thermodynamic criteria are considered between 298 to 1073 K, it is not necessarily strict. Therefore, we want to obtain all alternative optimal solutions so that those interested in this tool can choose the option that works best for them. We utilize the Solution Pool from CPLEX to obtain all alternative optimal solutions and its implementation is described in the Supplementary Information.

3.3.4   Identification of Other Potential Side Reactions

Based on the optimal reaction sequence, the catalysts required for each reaction can be selected using their corresponding reaction rules. For example, acid catalysts promote dehydration. Using this information, breadth-first network traversal using a set of filters can be performed to determine other side reactions and their corresponding products. These filters are the following: 1) Only reactions belonging to reaction

rules that require the same catalytic function can be traversed 2) The reaction is thermodynamically feasible at the temperature of interest.

The breadth-first traversal algorithm uses a first-in-first-out queue list. At each node traversal, the filters are applied to the corresponding edge properties, which, in this case, include the Gibbs free energy of reaction and the reaction rule. All these criteria must be simultaneously satisfied in order to traverse an edge. Otherwise, the edge is not traversed. The resulting network of traversed edges and nodes contains both reactions from the optimal solutions and competing reactions, along with all generated intermediates. In particular, the terminal nodes from this traversed network indicate other potential molecules that may form under certain catalytic and operating conditions. Further description of this approach can be found in the Supplementary Information.

3.4   Comparison of the Optimal Solution To Experimental Data

The primary function of our approach is to determine potential reaction sequence candidates for transforming biomass-derived molecules to target products. In order to both employ and validate our approach, its output must be tested by experiment. As this approach is a screening technique, the experiment setup is envisioned to provide a preliminary validation step. This step allows verification of the presence of any intermediates and target products identified by our modeling approach. In addition, the experimentalist can gain insights as to how any starting molecules or intermediates may evolve to their corresponding final products.

In the case study that is described in the next section, experiments guided by results obtained from our approach were conducted and the results both validated this approach and its insights.

3.5   Transformation of Fast Hydropyrolysis Vapor of Cellulose to Shippable Liquid
      Products

Here, a case study is illustrated to highlight the application of our approach. The
current H2bioil process only has 7% yield toward hydrocarbons with carbon number
greater than seven, which we called as C7+, while 65.3% of the carbon is transformed to
C1-C6 hydrocarbon molecules, which are not suitable as drop-in fuels [30]. Therefore, in
order to produce appropriate higher molecular weight hydrocarbons, we are interested
in increasing the C7+ hydrocarbon fraction in the final product. The objective is
to design a process configuration that transforms biomass into target products in
the minimum number of reaction steps while exploiting the functional groups in the
biomass-derived molecules and maximizing carbon efficiency. The current focus is on
liquid fuel products due to their ease of transport and tremendous demand.

The product compositions and distributions following cellulose fast hydro-pyrolysis
were obtained from studies conducted by Venkatakrishnan et al. and are shown in
Table 3.1 [31].

Table 3.1.: Product distribution of fast-hydropyrolysis of cellulose at 753 K and 26
bar of hydrogen.

Molecule	10^{-3} Mole/Carbon Mole of Cellulose	Carbon Distribution Based on Cellulose (%)
Levoglucosan (LVG)	79	47.7
Hydroxymethylfurfural (5-HMF)	1	0.63
Furfural	16	8.21
Glycolaldehyde (GA)	46	9.19
Formic Acid	35	3.52
Acetic Acid	12	2.40
Methanol	5	0.54
CO	22	2.19
CO_2	21	2.06
CH_4	3	0.34
Char	200	19.9
Water	80	-

A reaction set was then generated from the molecules listed above using RING. The maximum number of steps for each molecule is limited to four in order to avoid combinatorial explosion. The resulting reaction set contains 48,061 reactions and 15,000 molecules. Note that this set of reactions generates not only C7+ molecules, but also other sets of molecules. In this network, 9,200 molecules have a carbon number greater than seven. Using the experimental setup and the reaction set, the optimization problem described previously was executed in order to determine the optimal reaction network to produce liquid products.

3.5.1   Results and Discussion

The solution to the optimization gave two alternative solutions. Each of which contains several reaction sequences that produce sets of the molecules which fall under the criteria of liquid products.

As shown in Figure 3.4, the optimal route to C7+ hydrocarbons is through aldol condensation reactions involving levoglucosan-derived molecules, glycolaldehyde and furfural. Prior to undergoing aldol condensation, levoglucosan undergoes double dehydration in order to generate a carbonyl group. Also, a double bonded carbon is formed on the alpha carbon of the carbonyl group, which must be hydrogenated. This carbonyl group with hydrogen on its adjacent alpha-carbon serves as the aldol reaction site. Furfural also undergoes a coupling reaction with a levoglucosan-derived molecule. Self-aldol condensations of HMF and furfural are not observed here or in the solution [57] as these molecules do not do direct coupling because of structural restrictions and they require molecular structure transformations that are contradictory. In addition, self-aldol reaction of the hydrogenated levoglucosenone is not selected because of its unfavorable Gibbs free energy of reaction in the required temperature range we selected. Transformation of levoglucosan to levoglucosenone by using $SO_4/TiO_2Fe_3O_4$, an acid catalyst known to perform dehydration reactions, has been reported by Lu et al.
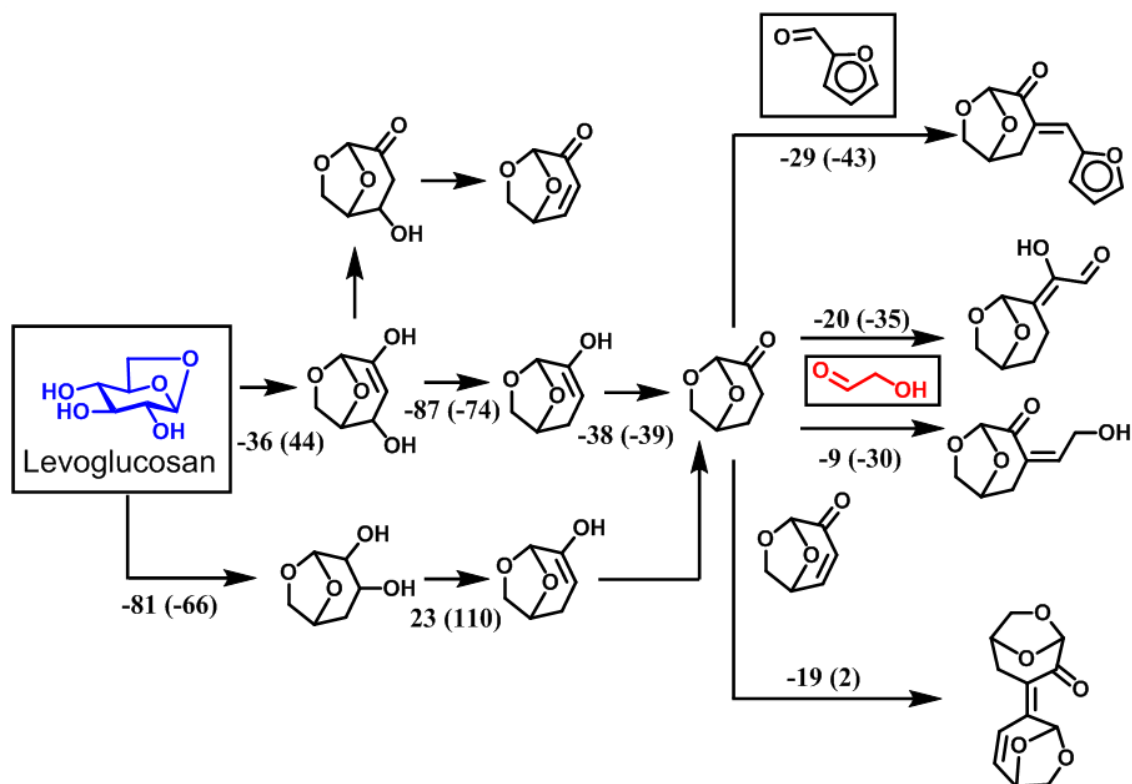
Figure 3.4.: Optimal reaction network for transforming cellulose fast pyrolysis vapor to C7+ molecules. The label represents Gibbs free energy of reaction at 573K and heat of reaction in the parentheses, both in kJ/mol.
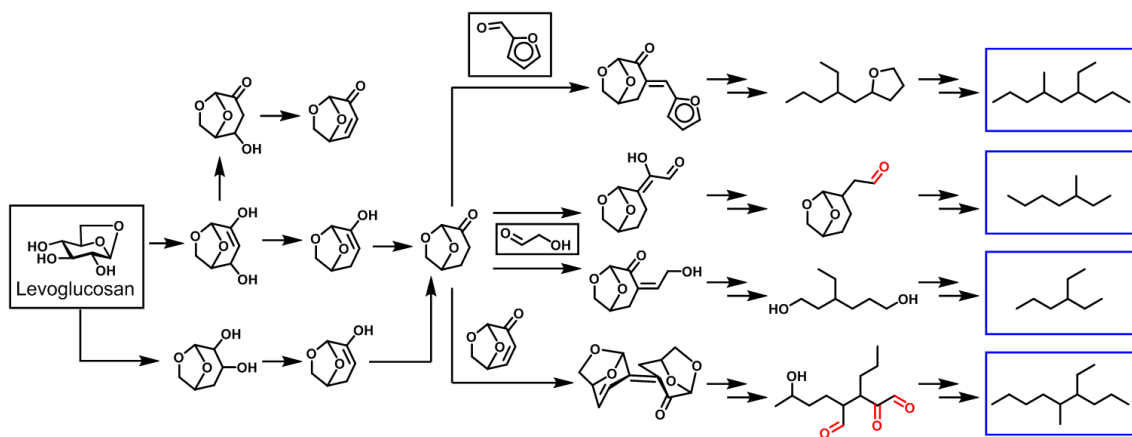
Figure 3.5.: Optimal reaction network mapped to hydrocarbon molecules. Highlighted carbonyl groups indicate possible sites for decarbonylation in hydrodeoxygenation catalyst.

[58]. In addition, Pt-catalyzed hydrogenation of the carbon double bond on levoglucosenone has been reported by Keinan et al. [59]. None of the aldol condensation reactions shown in Figure 3.4 are found in Reaxys database. This approach therefore reveals reaction sequences that are thermodynamically feasible but not previously recorded in reaction databases.

Figure 3.6.: Glycolaldehyde self-coupling and cross coupling with other molecules except levoglucosan. The label represents Gibbs free energy of reaction at 573K and heat of reaction in the parentheses, both in kJ/mol.

Many molecules present in the fast pyrolysis system including methane, methanol, formic acid, and acetic acid are not active for aldol condensation. Therefore, the upper bound for the carbon efficiency is calculated to be 63%, and the optimization solutions are obtained at this upper bound.

The remaining light oxygenates, which are not active for aldol condensation, are valuable and are usually generated from petroleum which contains no oxygen atoms. In the current H2Bioil process, these light oxygenates are ultimately reduced to light alkanes, which are hydrocarbons with carbon number less than three and are neither suitable for drop-in fuels nor valuable as commodity chemicals.

It is important to note that this approach does not require that the optimal reaction sequence be the dominant reaction sequence. Instead, the optimal reaction sequence shows the ideal distribution and reaction routes of the biomass-derived molecules in order to achieve the potential carbon yield. It should also be noted that the selected C7+ molecules still possess oxygen atoms because full hydrodeoxygenation would exceed the maximum rule rank is four. As there are at most six oxygen atoms in this set of biomass-derived molecules, at least six additional reactions are needed to remove these oxygen atoms. In order to map the selected C7+ molecules to their resulting hydrocarbons, we employed a second iteration starting with those C7+ molecules and a maximum rule rank of eight. The solution for that optimization problem is shown below in Figure 3.5.

Due to the numerous reaction steps required to reach saturated hydrocarbons, the complete reaction pathways are listed in the Supplementary Information. As shown above, several proposed intermediates during hydrodeoxygenation possess carbonyl groups, and this is important because the decarbonylation side reaction has been observed on several HDO catalysts [30]. This approach can provide insights as to which intermediates can undergo side reactions such as decarbonylation or formation of cyclic hydrocarbons. The feasibility of hydrodeoxygenation of pyrolysis vapor has been demonstrated by Ventakakrishnan et al. using PtMo supported on multiwalled carbon nanotubes (MWCNTs), which possesses both metal and acidic functions [30].

In addition to cross-coupling reactions, glycolaldehyde may also undergo self-couplings that are not presented in the optimal reaction network described previously. If we remove levoglucosan from the analysis, the optimization routine generates another optimal reaction network that demonstrates coupling of glycolaldehyde with itself and with other pyrolysis products, as shown in Figure 3.6, which reveals two main reaction routes that glycolaldehyde can take to form higher molecular weight molecules: aldol condensation and oligomerization. To our knowledge, glycolaldehyde self-aldol condensation and transformation of glycolaldehyde to ethylene have not been demonstrated in the literature. Oligomerization of ethylene, however, has been

demonstrated [60]. Since glycolaldehyde can undergo self-aldol condensation, the competition between self-aldol and cross-aldol condensation must be investigated further as their relative rates can determine whether the potential carbon yield can be achieved.

Our approach indicates that aldol condensation is the most suitable carbon coupling reaction for this chemical system. As shown in the Supplementary Information, we also considered other carbon coupling reactions, such as Diels-Alder, ketonization, and oligomerization of alkenes. Our approach suggests that these other coupling reactions require more reactions steps and other reactants, such as oxygen. Several of them require an oxidation environment followed by reducing environment, which can add complexity and cost in practice. However, these reaction routes can be obtained from our approach using additional constraints in the optimization problem formulation. The details of these other reaction routes can be found in Supplementary Information.

The optimal reaction sequence can be partitioned into three sections: dehydration, aldol condensation, and hydrodeoxygenation. These reactions require acid, base-acid, and metal catalysts, respectively. It is likely that other reactions, such as decarbonylation, may occur under each environment and identifying these competing reactions is crucial for both process design and catalyst development. The breadth-first network search is employed in order to determine these competing reactions. The following two cases, acid sites for dehydration and metal sites for hydrodeoxygenation, are considered in the table below for the identification of competing reactions:

Note that a majority of these side reactions also require a reducing environment to transform those oxygenated intermediates to their corresponding hydrocarbons. Several reactions, such as cyclization, can lead to the formation of five- and six-membered rings shown in Figure 3.7. Potential products from all identified side reactions are shown in Figure 3.8. As the final products of these side reactions are also hydrocarbons, the sheer number of these possible side reactions suggests that numerous sequences can accomplish the same task of removing oxygen atoms from the C7+ intermediates.
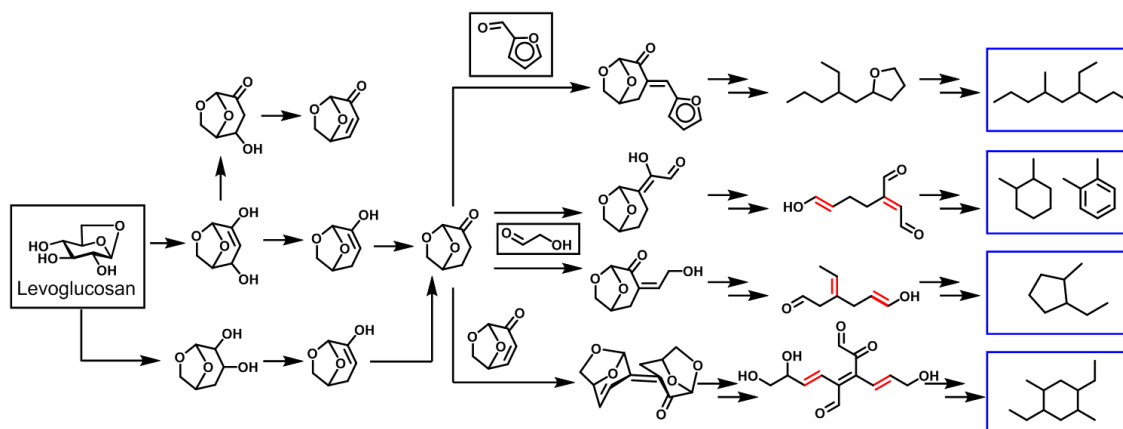
Figure 3.7.: Optimal reaction network mapped to cyclic hydrocarbon molecules. Highlighted double-bonded carbon indicate sites for cyclization
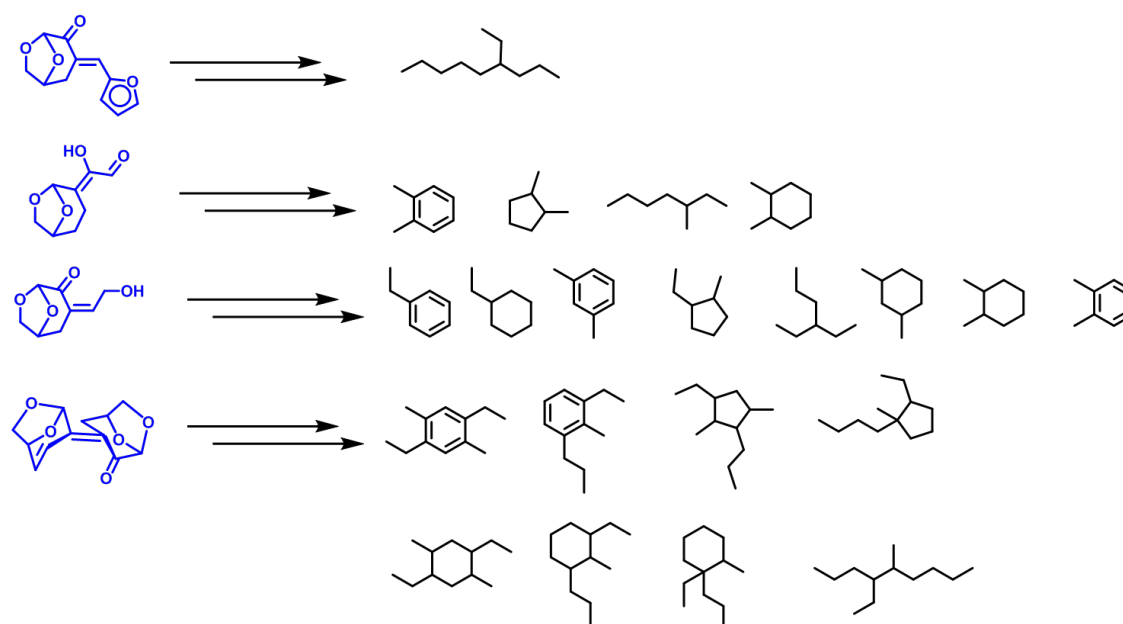
Figure 3.8.: Potential hydrocarbons products from C7+ intermediates under metal-acid catalysis.

Similarly, the acid catalyst used to dehydrate levoglucosan also catalyzes side reactions, such as ring opening as shown in Figure 3.9. Other hydroxyl groups in levoglucosan are also susceptible to dehydration. The estimated Gibbs free energies of these various dehydration reaction products are slightly different, but it alone cannot

indicate which hydroxyl group is most susceptible to dehydration. Halpern et al. proposed a mechanism for acid-catalyzed dehydration of levoglucosan to levoglucosenone, and carbon-3 on levoglucosan is claimed as the site for first dehydration to form a carbocation [61]. This is in agreement with the reaction sequence that is proposed and this dehydration step has the lowest Gibbs free energy of reaction compared to the other dehydration reactions as shown in Figure 3.9. Levoglucosenone formed from carbon-3 and carbon-4 dehydration, however, requires hydrogenation of the double bonded carbon on the alpha carbon before undergoing aldol condensation. This hydrogenation step is not identified in the optimal reaction network as the hydroxyl group on carbon-4 is removed through alcohol hydrogenolysis. This hydrogenation reaction can be introduced by adding a metal site on the acid catalyst for dehydration or the catalyst bed for aldol condensation. Hydrogenation of the double bonded carbon on the alpha carbon using metal catalyst has been demonstrated [62].

Table 3.2.: Identification of Competing Reaction Scenarios

	Seed Molecules	Catalyst Functionality	Number of Side Reactions
Dehydration	Levoglucosan	Acid	140
Hydrodeoxygenation	C7+ Intermediates	Metal - Acid	2,332

Aldol condensation takes places in the second catalyst bed and it is an auto-site regenerating reaction. This leads to many sequential aldol condensation reactions of the initial pyrolysis products and their derivatives, which ultimately lead to the formation of molecules with a larger number of carbons. Figure 3.4 and 3.6 highlight the initial aldol condensation reactions. The potential side reactions and their corresponding products in the aldol condensation catalyst bed are not discussed here as there are numerous potential side reactions. Nevertheless, aldol condensation catalyst generates a distribution of higher molecular weight oxygenates, which would be hydrodeoxygenated to hydrocarbons. Therefore, those reactions ultimately result in desirable products, but are beyond the scope of this analysis.
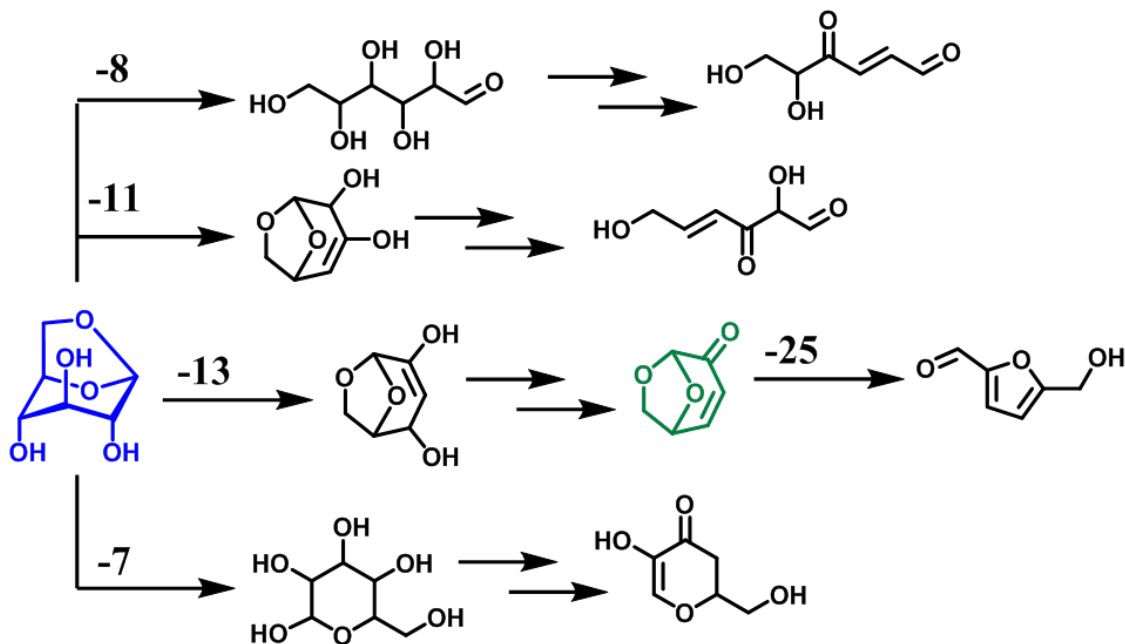
Figure 3.9.: Potential reactions from Levoglucosan under an acid condition with Gibbs free energy of reaction in each initial reaction in kcal/mol.

For the third catalyst bed involving hydrodeoxygenation, Figure 3.8 shows potential hydrocarbon products from C7+ intermediates. In addition to the branched alkanes, branched cycloalkanes, and aromatics can also be formed under these conditions. As will be discussed further below, several molecules identified in our approach have been observed experimentally.

It is also worth noting that the large boiling point gap between light and heavy oxygenates presents an opportunity to recover light oxygenates. As the boiling points of levoglucosan, HMF, formic acid, and methanol are 658 K, 564 K, 374 K, and 338 K, respectively, the separation between light and heavy oxygenates may not be difficult. In the current H2Bioil process, these light oxygenates are ultimately reduced into light alkanes which are neither suitable for drop-in fuels nor valuable as commodity chemicals. An optimal reaction network may allow co-production of chemicals and drop-in fuels from fast pyrolysis of cellulose. This proposed co-production of chemicals

and liquid fuel from fast pyrolysis vapor of cellulose is shown in Figure 3.10. Light oxygenates can be intercepted prior to HDO and valorized as commodity chemicals.
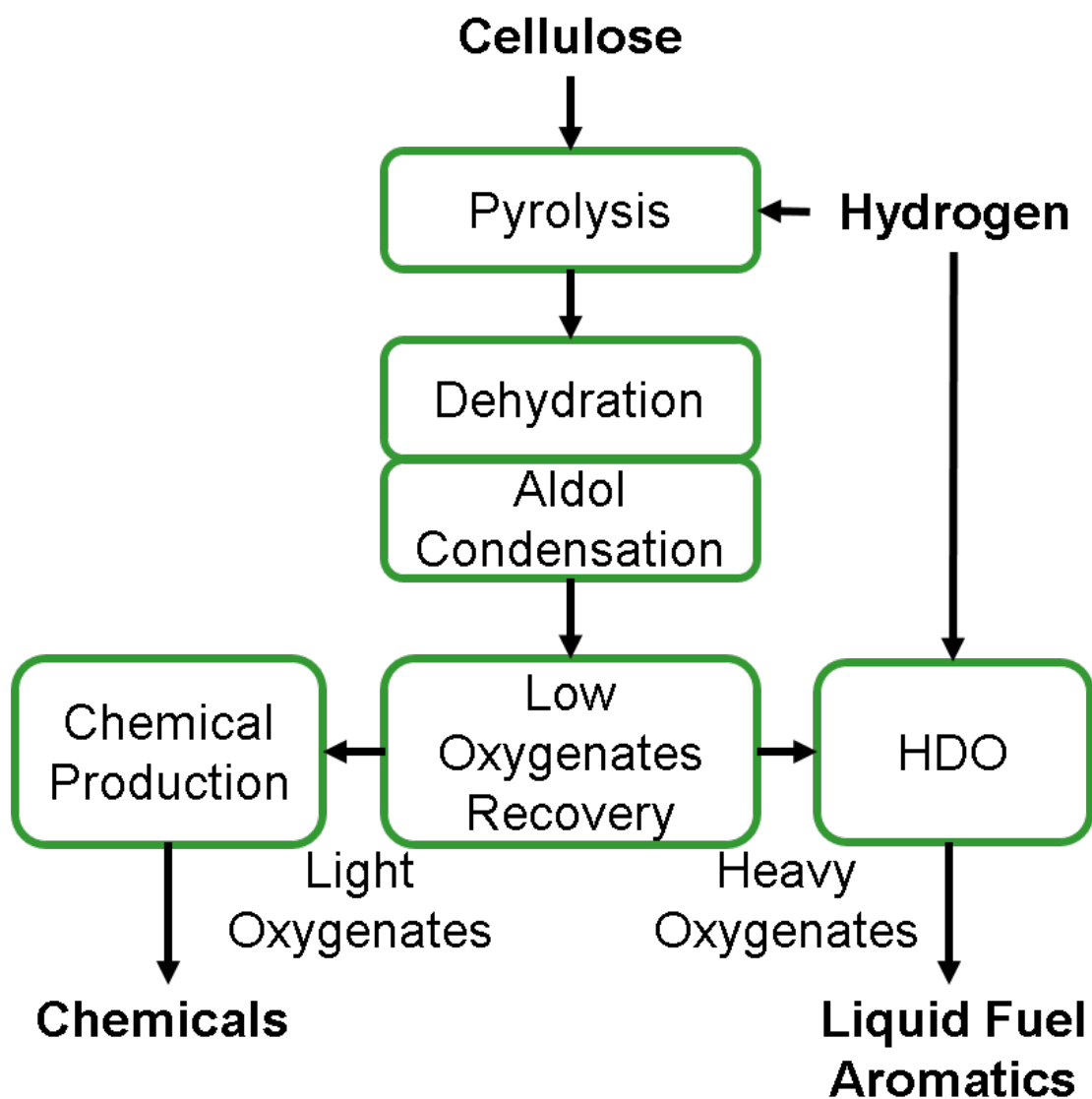
Figure 3.10.: Co-production of chemicals and fuels from Fast Pyrolysis Vapor of Cellulose

3.5.2   Catalytic Upgrading of Levoglucosenone and Glycolaldehyde

We have conducted experiments to validate several pathways of the proposed reaction sequences discussed above. The experimental setup used consists of a fixed bed reactor that operates as a pulse reactor, by using a pryoprobe to rapidly vaporize aqueous solutions of reactants which are carried over the catalyst beds. The outlet product is analyzed using GC/MS. Further details of the experimental setup can be found in the Supplementary Information.

As mentioned earlier, to our knowledge only dehydration of levoglucosan to levoglucosenone has been demonstrated previously in the literature. Therefore, an aqueous solution of levoglucosenone, an aqueous solution of glycolaldehyde, and an aqueous solution of levoglucosenone and glycolaldehyde in a 1.9:1 molar ratio were vaporized and reacted independently in the presence of hydrogen over sequential catalyst beds of Cu/TiO_2 and PtMo/MWCNT at 573 K and 3 bar H_2, yielding hydrocarbons with carbon number ranging from eight to nine. TiO_2 is a well-known aldol condensation catalyst, and Cu/SiO_2 has previously been used in combination with TiO_2 in a hydrogen environment to limit known carbon losses to coke formation over heterogeneous aldol condensation catalysts such as TiO_2 [63–68]. As shown in Figure 3.12, some of the major products from our dual bed experiment are branched cycloalkanes with six to eight carbon atoms. Our modeling approach predicted pathways leading to the formation of several of these products including ethylcyclohexane, dimethylcyclohexane, methylcyclohexane, ethylcyclopentane, and dimethylcyclopentane. A summary of the modeling prediction and experimental result is illustrated in Figure 3.11.

When aqueous levoglucosenone was vaporized and reacted in the presence of hydrogen over the same reactor system under identical conditions, hydrocarbons with carbon number ranging from eight to ten were obtained. As shown in Figure 3.13, formation of hydrocarbons with carbon number larger than six confirms that levoglucosenone can undergo condensation either with itself or its fragments. Cu/TiO_2, however, has not been observed to produce cracked products and PtMo/MWCNT
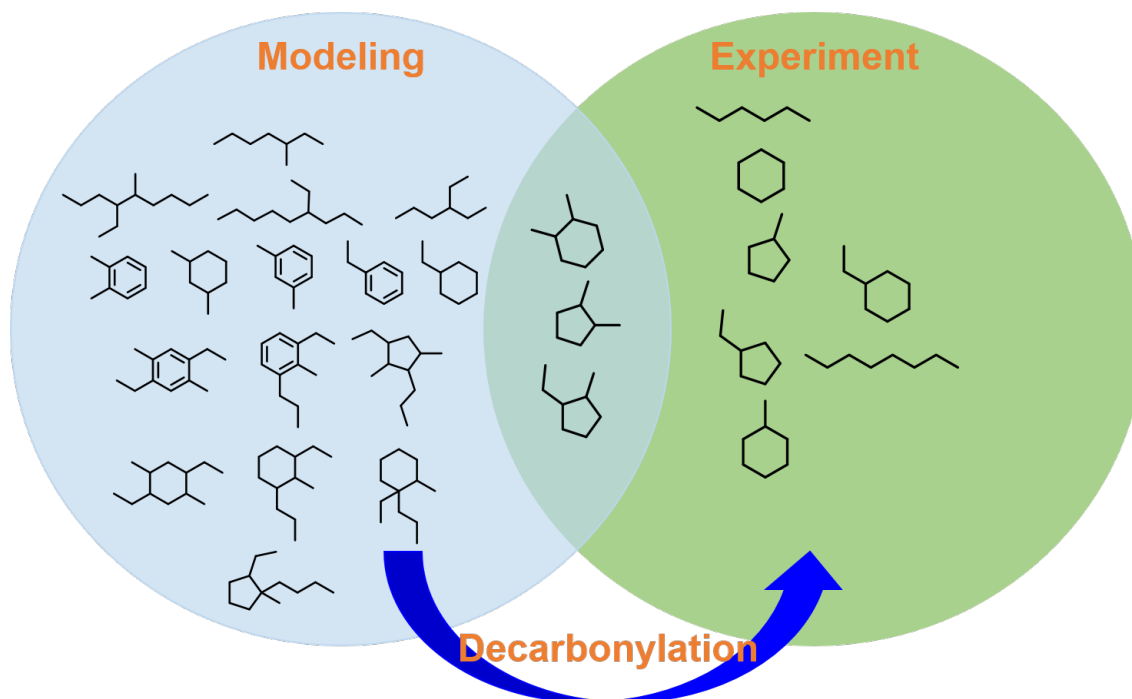
Figure 3.11.: Summary of modeling and experimental results from the case study.

does not exhibit aldol condensation functionality. Furthermore, the levoglucosenone solution was vaporized and analyzed directly with GC/MS and found to contain levoglucosenone and hydrated forms of levoglucosenone as major species, with no evidence of substantial cracking to lighter oxygenates capable of undergoing aldol condensation. Therefore, it is likely that levoglucosenone underwent self-condensation in the experiment presented here.

Our modeling approach proposed the formation of hydrocarbons with carbon number of 12, but such products were not observed experimentally, a result which we hypothesize can be attributed to the PtMo/MWCNT catalyst. Aldol condensation and tautomerization reactions result in a large number of structurally similar products that form in any system which contains glycolaldehyde. The mixture of oxygenated aldol condensation products proved extremely difficult to quantify directly via GC. Therefore, a PtMo/MWCNT catalyst was necessary to hydrodeoxygenate aldol condensation products to enable GC analysis. However, PtMo/MWCNT catalyst has been reported
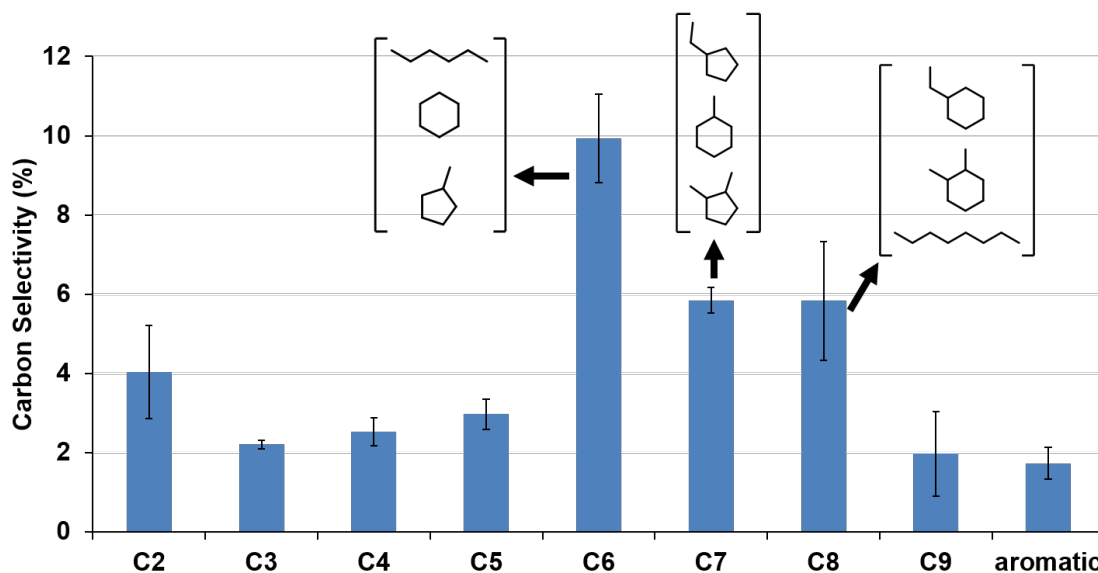
Figure 3.12.: Carbon selectivity of hydrocarbons based on their carbon numbers obtained from passing an equimolar mixture of levoglucosenone and glycolaldehyde at 573K under 40 psig of hydrogen through a dual catalyst bed of Cu-TiO_2 and Pt-Mo/MWCNT.

to exhibit a strong decarbonylation function, as seen in Figure S-4 in the Supplementary Information. Our modeling approach shows that aldol condensation can result in the formation of oxygenates with carbon number 12 that possess multiple carbonyl groups in series, terminating in an aldehyde group, which might all be removed via decarbonylation resulting in a final hydrocarbon molecule with carbon number less than 12.

It should be noted that there is a substantial amount of carbon in these experiments (e.g. 60%) that is unaccounted for, but is hypothesized to remain on the catalyst surface as adsorbed aldol condensation products or their derivatives based on literature reports of extensive coke formation over TiO_2, mainly when operating under high conversion as is the case in this work [65]. These experimental results nevertheless demonstrate the capability to couple glycolaldehyde and levoglucosenone as proposed by our modeling and optimization approach. Additional experimental work is required
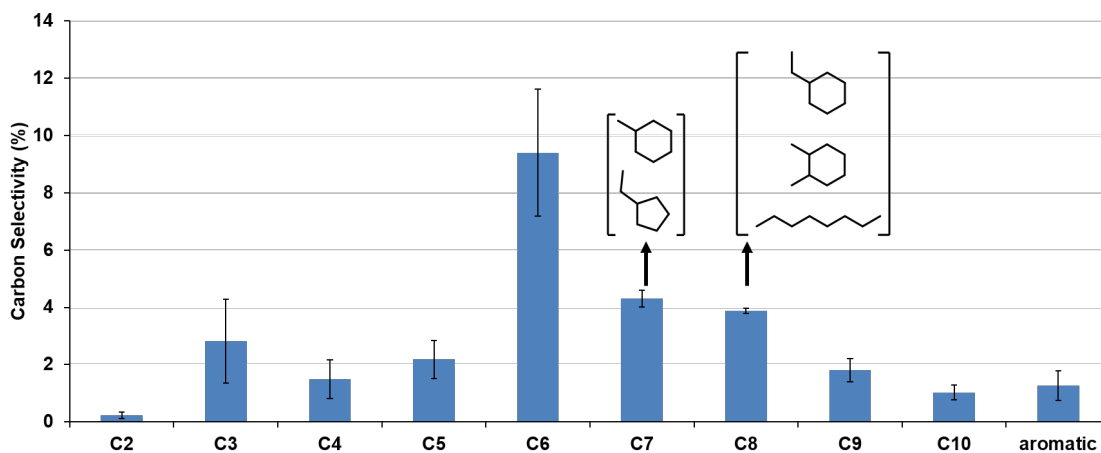
Figure 3.13.: Carbon selectivity of hydrocarbons based on their carbon numbers obtained from passing only levoglucosenone at 573K under 40 psig of hydrogen through a dual catalyst bed of Cu-TiO$_2$ and Pt-Mo/MWCNT.

to refine the catalyst and the reaction environment to achieve the selectivity necessary for the proposed optimum process carbon efficiency of 63%.

3.5.3 Comparison with Existing Fast-Hydropyrolysis Upgrading Systems

As shown previously, the optimal overall reaction sequence for upgrading cellulose fast-hydropyrolysis vapor starts with dehydration followed by aldol condensation. Finally, the resulting intermediates undergo hydrodeoxygenation to form hydrocarbon molecules. The final hydrocarbon molecules range from C8-C12 hydrocarbons and the overall process can achieve up to 63% carbon efficiency (assuming 100% selectivity of individual reactions predicted by the network). Currently, existing cellulose-to-fuel processes reported by Liu , Zhang , Deneyer, and Nolte, have mainly produced C6 molecules and report no formation of higher molecular weight hydrocarbons [69–74]. Their catalytic systems consist of only a hydrodeoxygenation catalyst, which is only a part of the proposed optimal reaction network. Our proposed reaction sequence has the potential to yield up to 63% of carbon in C7+ hydrocarbons.

To our knowledge, the catalytic system that we propose here has not been implemented in the literature yet. The key intermediate in this scheme is levoglucosenone

produced from levoglucosan. Levoglucosan itself is not susceptible to carbon coupling as it does not possess any functional group for forming carbon bonds and no carbon coupling reaction involving levoglucosan has not been reported in Reaxys. Therefore, this tool described here delineates the optimal reaction network from the plethora of reactions while revealing unconventional reaction sequences.

3.6   Conclusion

Biomass-derived molecules from primary processes are susceptible to many reactions, and determining the optimal biorefinery designs demands systematic screening of these primary processes and their relevant molecules. Our approach systematically determines all reactions that these biomass-derived molecules can undergo. By formulating an optimization problem, the optimal reaction network is identified while achieving the target carbon efficiency.

This approach can delineate the optimal reaction network for upgrading fast pyrolysis of cellulose to higher molecular weights and reveal previously unknown sequences for this transformation. Dehydration of levoglucosan is identified as a key reaction and levoglucosenone is the crucial resulting intermediate. Self-coupling of glycolaldehyde through oligomerization or aldol condensation is also indicated as another potential reaction sequence. In order to achieve the potential drop-in fuel yield, the catalyst must facilitate cross-coupling between glycolaldehyde and levoglucosenone as well as self coupling of levoglucosenone.

Using a micropulse, fixed bed reactor, the optimal reaction sequence obtained from our approach were tested using a dual catalyst-bed with Cu/TiO_2 followed by PtMo/MWCNT and the results indicate the occurrence of carbon-coupling between levoglucosenone and glycolaldehyde. Several molecules that were experimentally observed were indeed predicted by our modeling approach. These theory-guided experiments illustrate the potential of our approach and its ability to provide insights and potential reaction candidates for transforming biomass to a set of target molecules.

This approach can be extended to consider multiple primary processes besides fast-hydropyrolysis and also other target molecules, such as commodity chemicals or platform molecules. In this case, potential integrations and synergies between primary processes and their corresponding biomass-derived molecules can be identified by assessing the optimal reaction sequence. Thus this can provide a roadmap to guide the sustainable production of chemicals and fuels from biomass.

4. A SYSTEMS-LEVEL ROADMAP TOWARD SUSTAINABLE PRODUCTION OF DIESEL AND COMMODITY CHEMICALS FROM LIGNOCELLULOSIC BIOMASS

4.1 Introduction

Fossil resources dominate not only the energy landscape, but also chemical production landscape. More than 90% of the chemicals produced in the United States annually derived from petroleum resources [33]. Similar to energy production, commodity chemical production is expected to double globally by 2040, accentuating interest in biomass as a potential renewable carbon resource. Therefore, converting biomass to fuels and chemicals would mitigate the heavy reliance on fossil resources, while at the same time helping to mitigate CO_2 emission. This co-production of chemicals and fuels can be conceptualized as a biorefinery [12].

Biorefinery consists of two processing blocks, primary processes and subsequent processes. These primary processes can range from thermochemical to enzymatic processes. There are many research studies focused on developing new primary processes and improving existing primary processes in order to remove certain biomass constituents selectively [30,31,39]. Many biomass-derived molecules from existing primary processes are still highly oxygenated, unsuitable for liquid fuels and commodity chemicals, and therefore of limited utility. Subsequent processes, such as hydrodeoxygenation and other catalytic reactions, are employed in order to convert those biomass-derived molecules to fuel-type and commodity chemicals-type molecules [30,65]. There are a wide variety of chemistries available to perform subsequent processes [49,75]. In addition to the chemistries, the reaction sequence must also be configured to optimize the overall process.

In this work, we conceptualize a biorefinery that is based on major primary processes through mathematical modeling and optimization. The ultimate objective of this study is to establish a roadmap that can be used to identify various biorefinery configurations that can convert lignocellulosic biomass, such as poplar, to fuels and chemicals. More importantly, the study is aimed to maximize the carbon yield of the biorefinery while minimizing the number of reactions and satisfying various target demands for fuels and chemicals. We begin with a general overview of the transformation of lignocellulosic biomass to fuels and chemicals.

4.2 Meeting the United States Fuel and Commodity Chemical Demands using Sustainably Available Biomass

Considering that petroleum resources are used mainly for gasoline production, e.g., 47% of petroleum resource goes toward gasoline, and biomass itself cannot sustain the entire fuel demand in the US, it is difficult to consider chemical production altogether [76]. With rising interest in electric vehicles, many energy outlook studies have suggested that gasoline-based vehicles will be phased out by electric vehicles [76]. Therefore, it is reasonable to consider a scenario where biomass resources are only needed to sustain other liquid fuels other than gasoline such as jet fuel and diesel.

Current potential sustainably available biomass production is estimated to be between 505 - 709 million ton per year [34]. Assuming low biomass production potential and 100% carbon efficiency for biomass transformation process, 73% of sustainably available biomass can be used to sustain the entire diesel and jet fuel consumption in the US alone. The remaining biomass carbon can go toward commodity chemicals and ammonia production. This, however, only fulfills 69% of the current commodity chemical demands. The distribution of carbon toward commodity chemicals and fuels must be considered and accounted for carefully. Note that market demands play a significant role in the production and demands of commodity chemicals. Despite this, their relative production rates are generally similar and constant as these chemicals play specific roles in today's society.

Table 4.1.: United States petroleum usage in 2016 [77].

Product	Fraction of Total Petroleum Consumption
Gasoline	0.47
Diesel	0.20
Jet Fuel	0.08
Petrochemical Feedstock	0.15

To design biorefinery systems capable of sustaining the commodity chemical demands in the United States, we need to understand the production rates of these chemicals. Figure 4.1 shows the distribution of commodity chemicals production in the US-based on the latest available data from 2014. These chemicals can be categorized into two groups based on their carbon numbers, <C6 chemicals and C6+ chemicals, and their respective carbon distributions are 62% and 38%. This distribution is not surprising as polyethylene and polypropylene dominate a significant volume of commodity chemical market. With the recent shale gas boom, however, one can consider a case where polyethylene and polypropylene can be neglected as it is difficult to compete with this natural resource. In this case, <C6 and C6+ chemical distributions are 17% and 82%, respectively. Nevertheless, in a petroleum-deprived future, the entire commodity chemical landscape must be considered as sustainably available biomass serves a main renewable carbon source.

The minimum target for carbon efficiency can also be determined considering the best case scenario for biomass conversion to diesel and chemicals. At the high sustainably available biomass potential production of 709 million tons per day, the minimum carbon efficiency needed is 79.5% in order to sustain diesel, jet fuel, and commodity chemical production. Therefore, the biomass system that is being considered here should be able to meet this target carbon efficiency.

Here, the objective is to co-produce chemicals and diesel at their respective demands while using the minimum number of reactions. A set of demand and target carbon
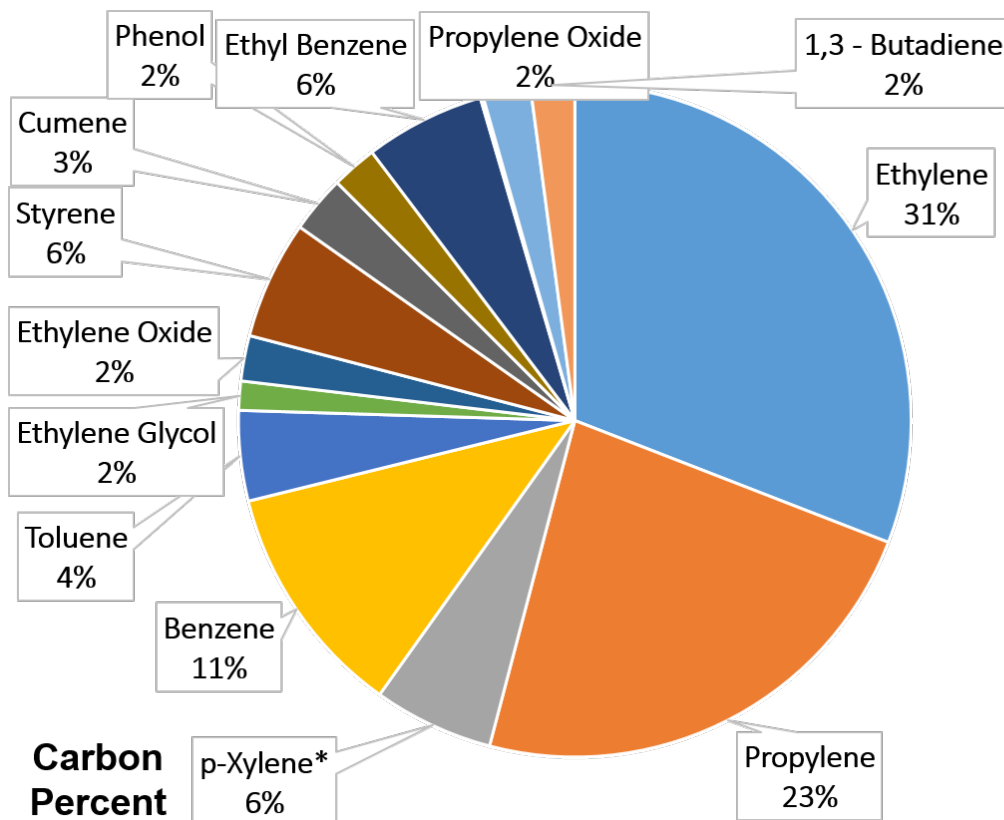
Figure 4.1.: US commodity chemical production distribution on carbon percentage based on adjusted 2010 data [78].

efficiency constraints must be imposed in order to sustain the existing chemical and diesel landscape.

One underlying assumption in this study is the availability of hydrogen, heat, and power source from renewable energy. As sustainably available biomass itself is limited, it is ineffective to utilize its carbon as a source of hydrogen, heat, and power. Therefore, here, we focus solely on maximizing the carbon efficiency and disregard the energy efficiency of the entire process as the energy input for this biorefinery can be obtained through other renewable sources.

4.3   Review of Systems-Level Molecular Mapping

Here, we employ systems-level molecular mapping for the identification of optimal biorefinery configurations. Systems-level molecular mapping is an optimization-based approach that identifies reaction sequences converting lignocellulosic biomass to target molecules by exhaustively defining all potential reaction sequences based on the biomass-derived molecules and a set of reaction rules and posing an optimization problem that includes thermodynamic constraints and stoichiometric models.

The problem of identifying a biomass processing configuration may be stated as the following: given is a set of primary processes(j | j = 1, 2, ..,$P_{process}$). A primary process disassembles biomass into a distinct set of biomass-derived molecules at specific abundances. These biomass-derived molecules then become the feed for subsequent processes such as catalytic reactions (j | j = P + 1, P + 2, ...,$M_{process}$). Each subsequent process is represented as a reactor-separator block, configured as a reactor followed by a separator that performs a complete split separation for each component. It is worth noting that the construct considered in this work represents an ideal reactor network in which any participating molecule can react liberally with other molecules in order to identify potential process synergies and key intermediates while neglecting any penalty from separation.

To allocate biomass-derived molecules from the primary process to the reactor-separator blocks, a distributor block is created for each biomass-derived molecule. The distributor block consists of three unit operations, one mixer, and two splitters. The mixer combines the fresh feed stream, $n_i^{in,fresh}$, of molecule i, which comes from primary processes with outlet streams, $n_{i,j,FEED}$, of molecule i coming from reactor-separator block j. The outlet of this mixer enters the first splitter which only has two outlet streams, $n_{i,Reactors}$ and $n_{i,Outlet}$. The first outlet stream, $n_{i,Outlet}$, serves an exit for molecule i, and the second stream, $n_{i,Reactors}$, is sent to the second splitter. Finally, the second splitter distributes its inlet, $n_{i,Reactors}$, to reactor-separator blocks. As with the separators, the splitters are also assumed to be 100% efficient.

As stated earlier, each subsequent process is configured as reactor-separator block. There are diverse configurations for reactor-separator blocks based on the type of reaction and physical properties of the molecules. In this work, the reactor-separator block is stoichiometry-based and assumed to have 100% selectivity towards the product of the reaction represented by this block. The details of separation are not considered, and there is no penalty associated with it. Selection of the appropriate reactor-separator configuration would require detailed knowledge of the properties of the wide variety of reactions and mixtures considered here. Instead, all reactor outlet streams are separated into individual component streams that have 100% purity.

A set of primary processes and subsequent processes (i.e., reactions) is given. The aim is to synthesize a process network that is capable of managing the production, transformation, and distribution of biomass into target products while achieving a desired objective or a combination of objectives and satisfying process constraints. We are interested in finding a set of primary processes and reactions that satisfies thermodynamic constraints within a specified operating range while constituting the minimum number of reactions and achieving target carbon efficiency for transforming biomass to desired products. Because of the assumptions of 100% selectivity and separator, the optimal solution found represents an ideal best case.

Details on all constraints related to this optimization problem have been shown previously in chapter 3. The set of primary processes considered in this work is now described.

4.4   Primary Processes

As shown in Figure 4.2, the primary processes network compromises of a total of 15 processes that belong to six process groups. These six process groups are the following: 1) Fast Pyrolysis 2) Catalytic Depolymerization of Lignin 3) Fermentation 4) Enzymatic Hydrolysis 5) Acid Catalyzed Dehydration 6) Maleic Acid Pretreatment. As several of these processes can convert not only intact lignocellulosic biomass, but also other biomass-derived residues, there is a total of 15 processes accounts for both

intact lignocellulosic biomass and lignocellulosic-derived residues. The process groups are described below. The yield data from these processes can be found in Appendix C.

In this work, gasification is not included as this process converts biomass into a mixture of carbon monoxide, hydrogen, water, and carbon dioxide. Although this process route is viable, it does not allow utilization of biomass natural structure for its transformation toward fuels and chemicals.
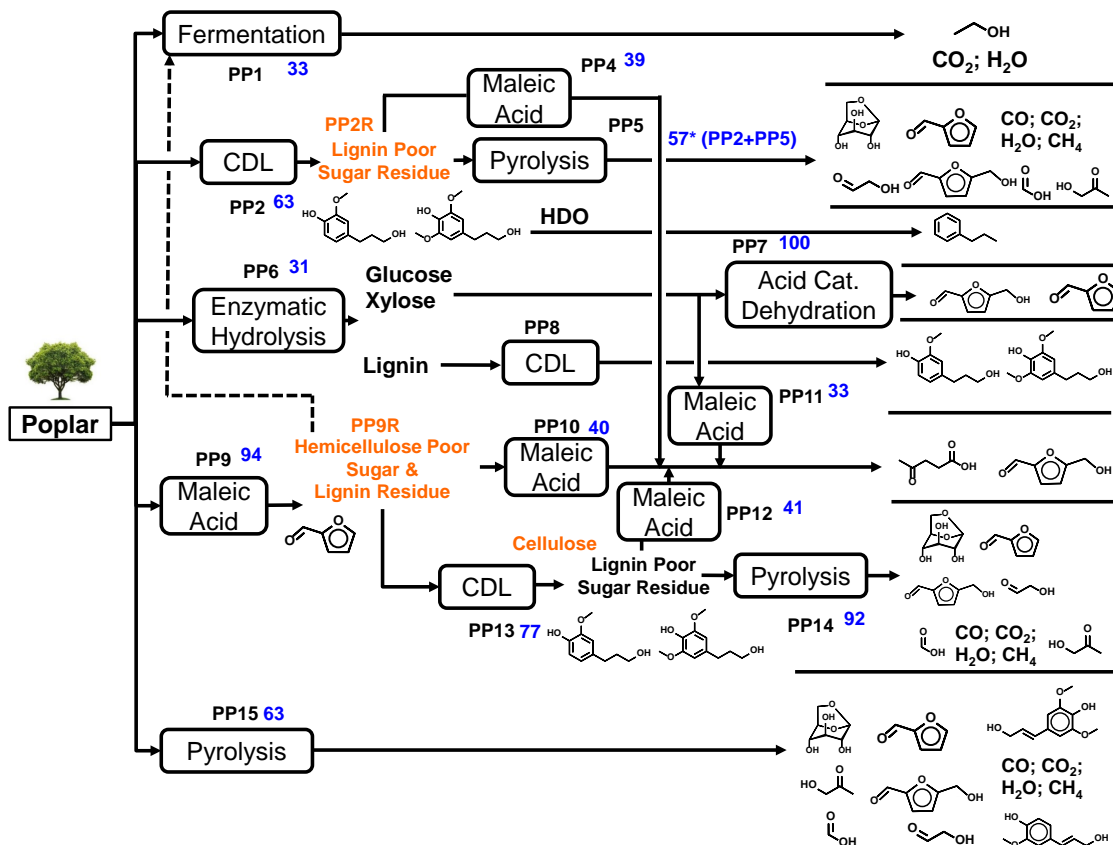
Figure 4.2.: Overall C3Bio primary processes network. The blue highlighted number indicates the carbon efficiency of the process. This efficiency is defined as the ratio between the total carbon in the active molecules (i.e., excluding char, methane, carbon monoxide, carbon dioxide, and humins) and the total carbon in the feed.

4.4.1 Fast Pyrolysis

Fast pyrolysis involves rapid heating of biomass in the absence of oxidants. It usually proceeds at a temperature below 600°C [42]. The products of pyrolysis are permanent gases, a mixture of oxygenated molecules, and char. Various pyrolysis studies on poplar and biomass constituents, such as cellulose, hemicellulose, and lignin, suggested the composition of the pyrolysis vapor. In this study, based on several studies on the literature, we considered the product distribution described in Table **??** for poplar. Note that the overall carbon efficiency of this process is 63% for poplar feed. 35% of carbon ends up as char.

Similarly, fast pyrolysis of cellulose has been reported by Venkatankrishan et al. [31]. It is evident that char formation in pyrolysis of cellulose is significantly lower compared to that of poplar and other studies confirmed this finding [31, 38, 79].

Processes 5 and 15 in Figure 4.2 belong to the fast pyrolysis process group.

4.4.2 Catalytic Depolymerization of Lignin

Parsell et al. proposed a catalytic process that converts lignin in intact lignocellulosic biomass into two methoxypropylphenol molecules while leaving a carbohydrate-rich residue [39]. In this process, lignocellulosic biomass is placed in a methanol solution with a Zn/Pd/C catalyst at 225°C and 500 psig of H_2. In this batch process, methoxypropylphenols are dissolved in the methanol solution and the carbohydrate residue is immiscible in the methanol phase.

The overall yield of methoxypropylphenols in this process is 54% with 69% and 31% selectivity toward dihydroeugenol and 2,5-dimethoxy-4-propyl phenol, respectively. Overall mass balance indicates that 6.2% and 8.3% of carbon in lignin and hemicellulose, respectively, are lost as fragments of oxygenate dissolved in methanol. The carbohydrate residue contains mostly cellulose and hemicellulose. Figure 4.3 summarizes the overall mass balance of this processes.

Processes 2, 8, and 13 in Figure 4.2 belong to the catalytic depolymerization of lignin process group.
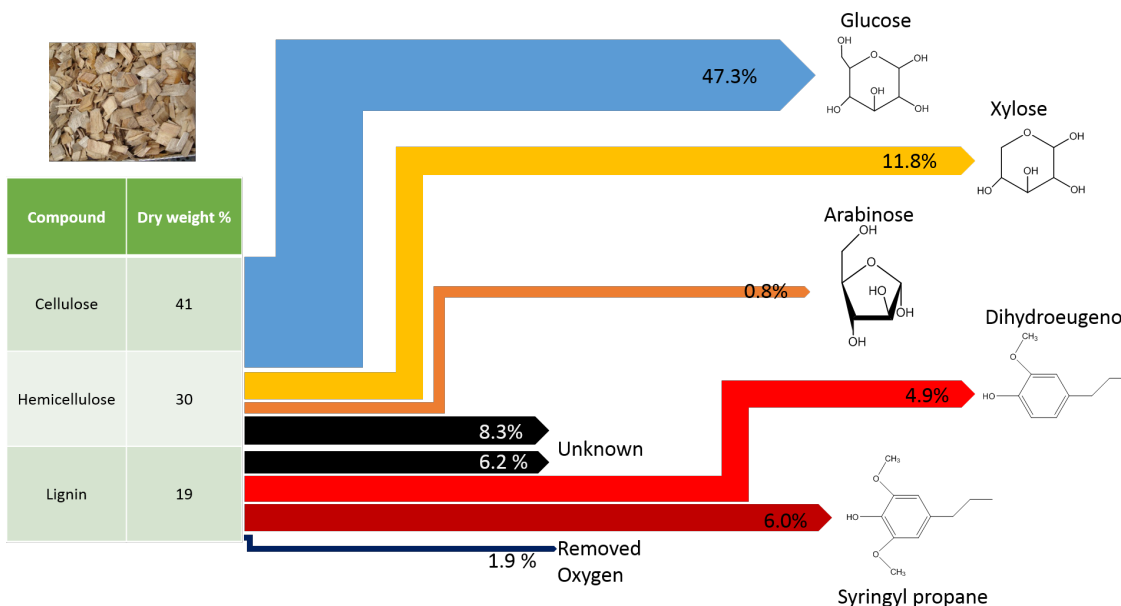
Figure 4.3.: Overall mass balance of CDL with wild-type poplar feed.

In addition to lignocellulosic biomass, theoretically, this process can extract lignin from other biomass-derived residues, such as residue obtained from other pretreatments that do not interfere with the physical structure of lignin.

The main advantage of this process is the extraction of lignin as methoxypropy-lphenol molecules that can be further upgraded into both fuel-type hydrocarbons and commodity chemicals such as aromatics. Besides, separation of methanol and methoxypropylphenols is feasible due to the large boiling point gap between these two components. It remains unclear as to how dissolved sugars in the methanol phase can be efficiently extracted. This process, however, has been observed to result in significant loss of hemicellulose as humins with wild-type poplar as the feedstock.

4.4.3 Fermentation of Lignocellulosic Biomass

Fermentation refers to anaerobic decomposition of carbohydrates to alcohols in the presence of enzymes. The main product of this process is ethanol with carbon dioxide as a by-product [42]. This process is strongly exothermic and the operating temperature must be maintained below 30°C. Therefore, the heat released is unavailable for recovery by means of co-generation.

Most existing biorefineries today produce ethanol as their major product with cellulosic feedstock such as corn grains. Lignocellulosic biomass can also be used as a feedstock for the fermentation process. The carbon efficiency of the lignocellulosic-based fermentation process is approximately 25% [41,80]. Lignin is generally recovered as a solid residue and used for power and heat generation.

Process 1 in figure 4.2 represents fermentation of poplar.

4.4.4 Maleic Acid Catalyzed Pretreatment

Kim et al. have demonstrated the use of maleic acid as a catalyst in biomass conversion, particularly efficient conversion of xylan to xylose and glucan to glucose at high yields [81, 82]. This catalytic process has been demonstrated with intact lignocellulosic biomass and it converts cellulose and hemicellulose in the solid biomass residue to 5-hydroxymethylfurfural and furfural, respectively, at two different operating temperature [83].

In this process, the feed, such as intact biomass, is placed in an aqueous solution of maleic acid and heated to a temperature between 100^{circle} - 200^{circle}C. Selectivity of 67% is reported for xylose derived from lignocellulosic biomass such as corn stover and poplar. Xylose conversion of 81% from poplar is also reported, which provides an overall conversion of 54% for hemicellulose to furfural. Similarly, at an elevated temperature of 200 C, this process converts cellulose to 5-HMF and it is reported that the overall conversion of cellulose from poplar to 5-HMF is 81%.

In addition to intact biomass, Maleic acid-catalyzed pretreatment has been demonstrated with glucose and xylose feed. Therefore, this process can transform sugar-containing residues obtained from other process groups to furfural or 5-HMF. Processes 4, 10, 11, and 12 represents maleic acid-catalyzed pretreatment of residues obtained from other primary processes.

4.4.5 Acid-Catalyzed Dehydration of Glucose and Xylose

Dilute acid solution is often used to dehydrate glucose and xylose into 5-Hydroxymethylfurfural and furfural, respectively. It has been reported that high conversions of glucose and xylose to 5-HMF and furfural, respectively, are achievable [84, 85].

Process 7 in figure 4.2 represents acid catalyzed dehydration of glucose and xylose.

4.4.6 Enzymatic Hydrolysis of Lignocellulosic Biomass

Enzymes are generally used to break down cellulose, hemicellulose, or starch into sugar monomers such as glucose and xylose. The enzymatic hydrolysis is generally carried out at 50°-60°C [86, 87]. In this process, lignin is not converted and usually recovered as an unusable solid residue [41].

Glucose and xylose are obtained from cellulose and hemicellulose contained in lignocellulosic biomass, respectively. Yields for this process are obtained from reported studies in the literature and shown in Appendix C [87].

Process 6 in figure 4.2 represent this process.

4.5 Subsequent Catalytic Processes

The biomass-derived molecules obtained from primary processes are then further processed in the subsequent processes. Generally, these processes consist of catalytic reaction systems. A reaction set was then generated from the molecules listed above using RING [14]. The maximum number of steps for each molecule is limited to four

in order to avoid combinatorial explosion. The resulting reaction set contains 69,067 reactions and $\tilde{3}$2,774 molecules.

Also, a set of 18 reactions is added as the catalytic network for converting propyl-benzene to various aromatic based commodity chemicals [88]. Unlike the reactions generated by RING, this set of reactions are well-established in literature and the aromatic commodity chemical network is commercialized and exists as a working chemical production infrastructure. This network is shown in Appendix C.

4.6 Optimization Problem

Utilizing the reactor-separator superstructure considered in systems-level molecular mapping, optimal biorefinery configuration is determined by possessing the maximum potential overall carbon efficiency and the minimum number of reactions. As each primary process has an associated carbon efficiency, we must first address its impact on the overall biorefinery system. Therefore, first, the maximum potential overall carbon efficiency is targeted and, second, using the obtained target carbon efficiency, a configuration with the minimum number of reactions is identified. Now, the targeting approach for the maximum carbon efficiency is described.

4.6.1 Targeting Maximum Carbon Efficiency

Most primary processes do not recover all carbon in intact biomass as usable biomass-derived molecules. For example, pyrolysis generates char which contains mostly carbon and liquid acid pretreatment generates humins as a by-product. Therefore, an indicator of an optimal biorefinery is the overall carbon efficiency. Using the optimization framework that was established early, carbon efficiency can now be used an objective function.

$$max \quad \eta_{Carbon} = \frac{\sum_{i \in I^{Products}} \dot{n}_i^{out} C_i}{C_{Poplar}} \tag{4.1}$$

This objective function, however, is likely to lead to solutions with number of reactions as the optimization problem does not have any constraints or penalties associated with utilizing many reactions.

Note that it is not sufficient to only consider the primary process network for targeting the carbon efficiency as the presence of limiting reagents and versatility of the biomass-derived molecules can potentially reduce the target carbon efficiency. Once the value of this target is determined, now, we employ it to determine biorefinery configuration with the minimum number of reactions.

4.6.2 Minimizing Number of Reactions subject to Target Carbon Efficiency

Maximizing the carbon efficiency provides the target on the achievable target carbon efficiency. In order to determine the optimal process configuration for this integrated biorefinery system, we need to determine the minimum number of reactions needed to achieve the achievable target carbon efficiency. Thus, the objective function is the following:

$$min \ \sum_j a_j \tag{4.2}$$

In addition, we add the following constraint:

$$\eta_{carbon} \geq \eta_{TargetCarbon} \tag{4.3}$$

This constraint ensures that the optimal solution achieves the achievable target carbon efficiency.

4.6.3 Incorporating Target Demands Constraints based on US Production of Fuel and Commodity Chemicals

As biorefineries are envisioned to substitute existing refineries and chemical processes that produce today's fuels and commodity chemicals, it is also pertinent to determine optimal process configuration for a biorefinery system that can produce

those same products at their current relative abundances. Therefore, we can impose additional constraints that ensure the desired fuel-type and commodity chemical molecules are generated at the appropriate abundances.

As mentioned previously, the target carbon efficiency for fuel type molecules is defined by the following:

$$\frac{\sum_{i \in I^{FuelProducts}} C_i \dot{n}_{out,i}}{C_{Biomass}} \geq \eta_{TargetCarbonFuels} \tag{4.4}$$

Second, the target carbon efficiency for chemical type molecules is defined by the following:

$$\frac{\sum_{i \in I^{ChemicalProducts}} C_i \dot{n}_{out,i}}{C_{Biomass}} \geq \eta_{TargetCarbonChemical} \tag{4.5}$$

Based on the assumption that only jet fuel, diesel, and commodity chemical are set as the target molecules, then $\eta_{TargetCarbonFuels}$ should be 0.72 of $\eta_{TargetCarbon}$ and $\eta_{TargetCarbonFuels}$ should be 0.28 of $\eta_{TargetCarbon}$. Target fuel molecules can be generalized as hydrocarbon molecules with carbon number greater than a value. For gasoline, it is generally above eight and for diesel, it is generally above twelve. Target chemical molecules are more well-defined than target fuel molecules.

Target chemical molecules can be categorized into two sets: C6< molecules and C6+ molecules. The first set consists of ethylene, propylene, 1,3-butadiene, light oxygenates (e.g., ethylene oxide, propylene oxide, methylformate, acetylformate), and polyols. The second set compromises of aromatics, cycloalkanes (e.g., cyclohexane), and plastic monomers (e.g., adipic acid and terephthalic acid).

Here, we define $I^{Products}$ as a set containing all molecules that are considered as target products. Now, I^{Fuels} and $I^{Chemicals}$ are sets of product molecules that are fuel type and chemical type molecules, respectively. Therefore, $I^{Fuels}, I^{Chemicals} \in I^{Products}$. Now, in $I^{Chemicals}$, there are $I^{LightChemicals}, I^{C9Arom}, I^{C8Arom}, I^{C7Arom}$, and I^{C6Arom}. Based on the chemical and fuel production landscape in the United States, we construct a set of demand constraints for each of these sets of target products.

Table 4.2.: Target carbon distribution for commodity chemicals based on US national production.

Target Products (k)	Target Carbon Efficiency - θ_k (%)
Ethylene	6.57
Ethylene Glycol	0.32
Ethylene Oxide	0.49
Propylene	5.23
Propylene Oxide	0.51
1,3-Butadiene	0.48
C6 Aromatics	2.84
C7 Aromatics	0.94
C8 Aromatics	3.63
C9 Aromatics	0.58
Diesel & Jet Fuel	73

$$\frac{\sum_{i \in I^k} C_i \dot{n}_{out,i}}{C_{Poplar}} \geq \eta_k^{TargetCarbon} \theta_k \quad \forall \ k \tag{4.6}$$

where k is the index for the target molecules Based on our analysis of the latest chemical and fuel production landscape, the target carbon efficiency of the aromatics and light oxygenates are determined. These targets are listed in Table 4.2.

Using these new set of constraints, we can identify which primary processes are needed and how much poplar should be sent to each one in order to fulfill the latest chemical and fuel production in the United States.

Using the targeting approach followed by minimization of the number of reactions, we now identify optimal biorefinery configurations. Five scenarios are considered:

1. Optimal biorefinery configuration without any demand constraints

2. Optimal biorefinery configuration for production of fuel

3. Optimal biorefinery configuration for production of chemicals

4. Optimal biorefinery configuration subject to US production demands

Evaluation and analysis of these four cases are described in the Results and Discussion section.

4.7 Results and Discussion

4.7.1 Scenario I: Optimal Biorefinery Configuration with no US Product Demands

For the case of biorefinery subject to no US product demands, the optimal process configuration has the potential to achieve 66% carbon recovery and a total of 22 subsequent reactions and four primary processes are required. Figures 4.5 and 4.4 show the 22 subsequent reactions and the four primary process network utilized, respectively.
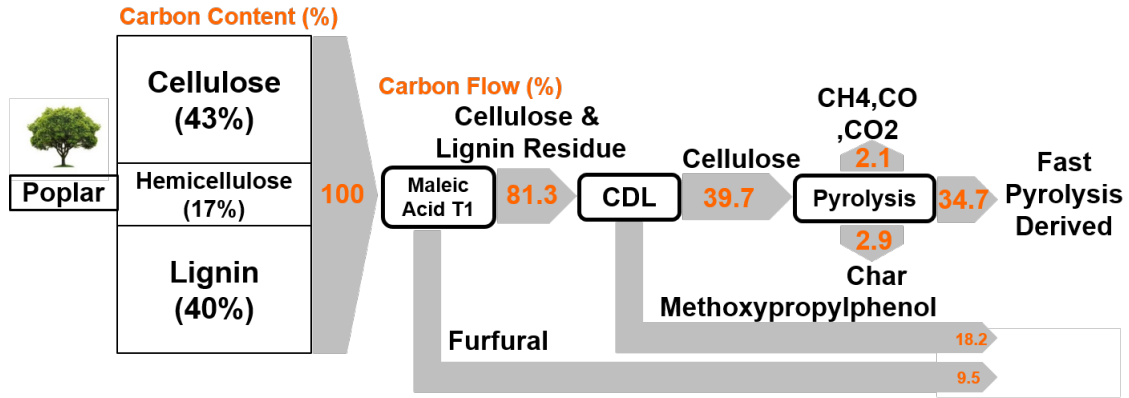
Figure 4.4.: Primary process configuration for biorefinery with the maximum target carbon efficiency and the minimum number of reactions.

Table 4.3.: Scenario I: Minimization of the number of active reaction subject to target carbon efficiency constraint.

Cases	η_{Carbon}	Number of Reactions
Biorefinery with Only Fast Pyrolysis	59.9	18
Biorefinery with Only Lignocellulosic Fermentation	33	2
Optimal Biorefinery	62.4	26
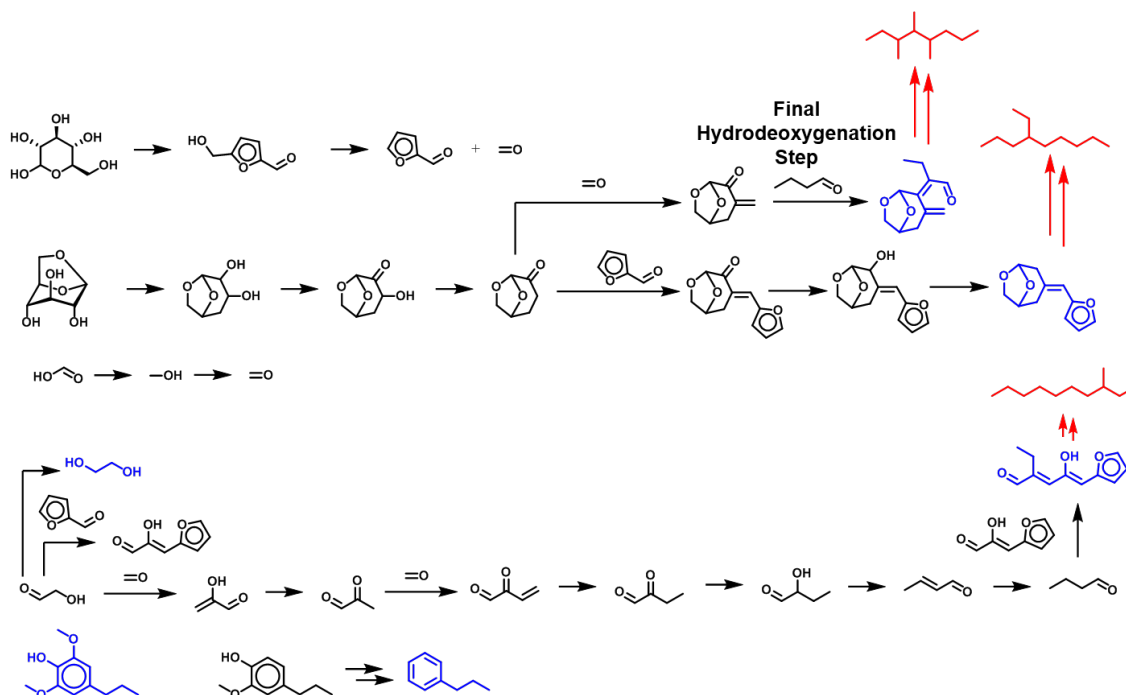
Figure 4.5.: Subsequent Processing for Integrated Biorefinery with Maximum Carbon Efficiency & Minimum Number of Reactions.

As shown in Table 4.3, standalone pyrolysis and lignocellulosic fermentation only achieve 59.9% and 33% carbon efficiency. For standalone pyrolysis, the main carbon loss is due to char which accounts up to 34%. In lignocellulosic biomass fermentation process, the main contributors for carbon loss are underutilization of lignin and CO_2 formation.

It is worth noting that other reported biorefinery systems achieve 25 - 60% carbon recovery toward fuel-type molecules [41, 89]. The main distinction between these biorefinery systems and the one presented here is the selective removal of lignocellulosic biomass constituents. It is evident that this approach results in higher carbon recovery than direct employment of any of the six process groups considered in this study.
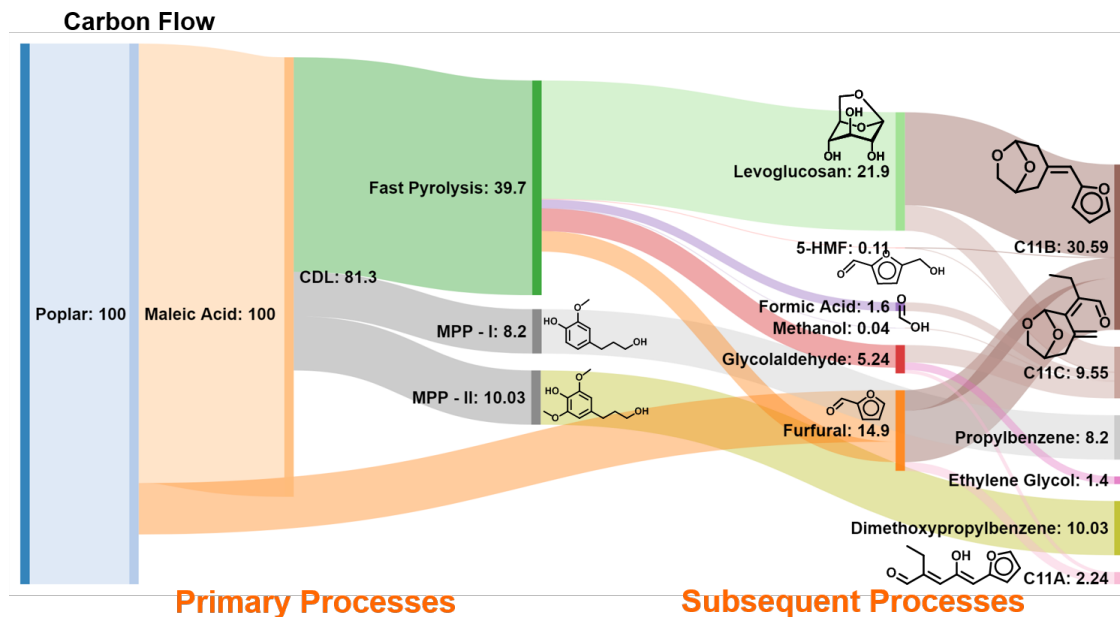
Figure 4.6.: Biomass-derived molecules allocations toward target products in biorefinery with maximum achievable carbon efficiency.

4.7.2 Scenario II: Biorefinery for production of fuel

For the case of biorefinery for production of fuel only, the target molecules are C11+ oxygenates only. The results are shown in Table 4.4.

Table 4.4.: Scenario II: Minimization of the number of active reactions for production of fuel.

Cases	η_{Carbon}	Number of Reactions
Biorefinery with Only Fast Pyrolysis	48.4	24
Biorefinery with Only Lignocellulosic Fermentation	33	5
Optimal Biorefinery	55	22

Compared to fast pyrolysis- and fermentation-based biorefinery, it is evident that the optimal biorefinery can achieve higher carbon efficiency. Compared to scenario I

carbon efficiency for optimal biorefinery, a 7.4% difference exists and this suggests that there are biomass-derived molecules that are more suited toward chemical productions.

4.7.3 Scenario III: Biorefinery toward Production of Chemical

For the case of biorefinery for production of fuel only, the target molecules are commodity chemicals only. The results are shown in Table 4.5.

Table 4.5.: Scenario III: Minimization of the number of active reactions for production of chemical.

Cases	η_{Carbon}	Number of Reactions
Biorefinery with Only Fast Pyrolysis	39.8	11
Biorefinery with Only Lignocellulosic Fermentation	33	2
Optimal Biorefinery	54.5	19

Compared to fast pyrolysis and fermentation based biorefinery, it is evident that the optimal biorefinery can achieve higher carbon efficiency. Again, a 8% difference in carbon efficiencies between the optimal biorefinery in this scenario and that of scenario I suggests that there are biomass-derived molecules that are more suited toward the production of fuel.

4.7.4 Scenario IV: Biorefinery subject to US Product Demands

For the case of biorefinery subject to US product demands, the optimal process configuration has the potential to achieve 60% carbon recovery and a total of 35 subsequent reactions and five primary processes are employed. Figures 4.8 and 4.7 shows these subsequent reactions and selected primary processes, respectively.

As shown in Table 4.4, standalone pyrolysis only achieves 37% carbon efficiency. There is no feasible solution for the lignocellulosic biomass fermentation biorefinery system. Although ethanol can be oxidized to acetaldehyde, which is a building block
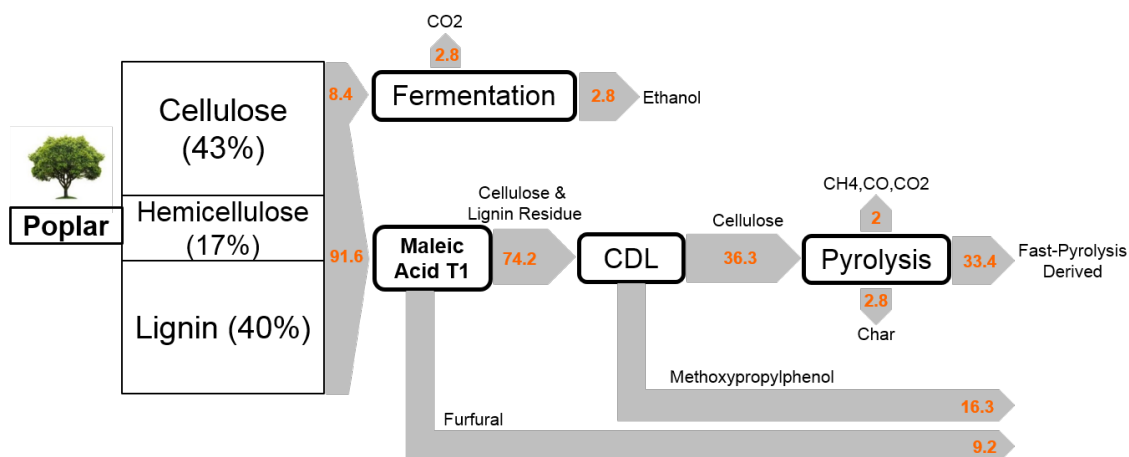
Figure 4.7.: Primary process configuration for Biorefinery with maximum target carbon efficiency, minimum number of reactions, and US product demands constraints.

molecule, specific target odd-carbon number products cannot be generated from acetaldehyde.

Table 4.6.: Scenario IV: Minimization of number of active reactions subject to target product demands.

Cases	η_{Carbon}	Number of Reactions
Biorefinery with Only Fast Pyrolysis	37	22
Biorefinery with Only Lignocellulosic Fermentation	-	-
Optimal Biorefinery	57.6	40

Shown in Figure 4.8, the use of lignin as pre-cursor to commodity chemicals has been demonstrated as propylbenzene serves as a platform toward all major aromatic-based commodity chemicals. Following dealkylation of propylbenzene, which involves commercially known technologies, such as Detol, Hydeal, and HDO, benzene can be further alkylated with methanol [88]. This alkylation process has been reported using AlCl$_3$ [88].
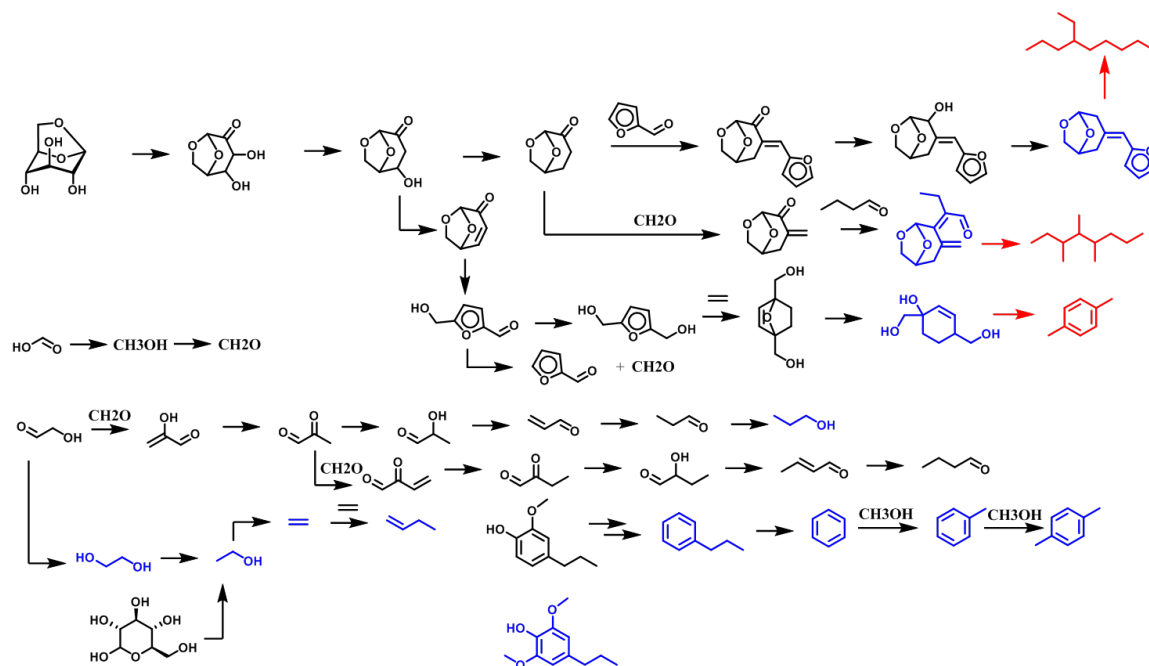
Figure 4.8.: Corresponding subsequent Processing for Integrated Biorefinery with the minimum number of reactions at the maximum carbon efficiency subject to the United States product demands.

In addition, there is sufficient carbon in lignin to sustain the current and future production of chemicals. As can be seen in Figure 4.9 2,6 - dihydromethoxypropylphenol is utilized mostly toward benzene, toluene, and xylene production. Methanol and formic acid from fast-pyrolysis of cellulose are employed as alkylating agents for the production of these aromatics. While methanol and formic acid can be transformed to formaldehyde for fuel production through aldol condensation, they are more readily available as an alkylating agent.

It is also evident that the use of cellulose and hemicellulose-derived sugars for commodity chemical production may not be necessary as there are sufficient aromatic-type biomass-derived molecules to generate relevant commodity chemicals. Light oxygenates generated in the primary processes, except glycolaldehyde, are utilized as precursors toward commodity chemicals and ligands for chemical productions.
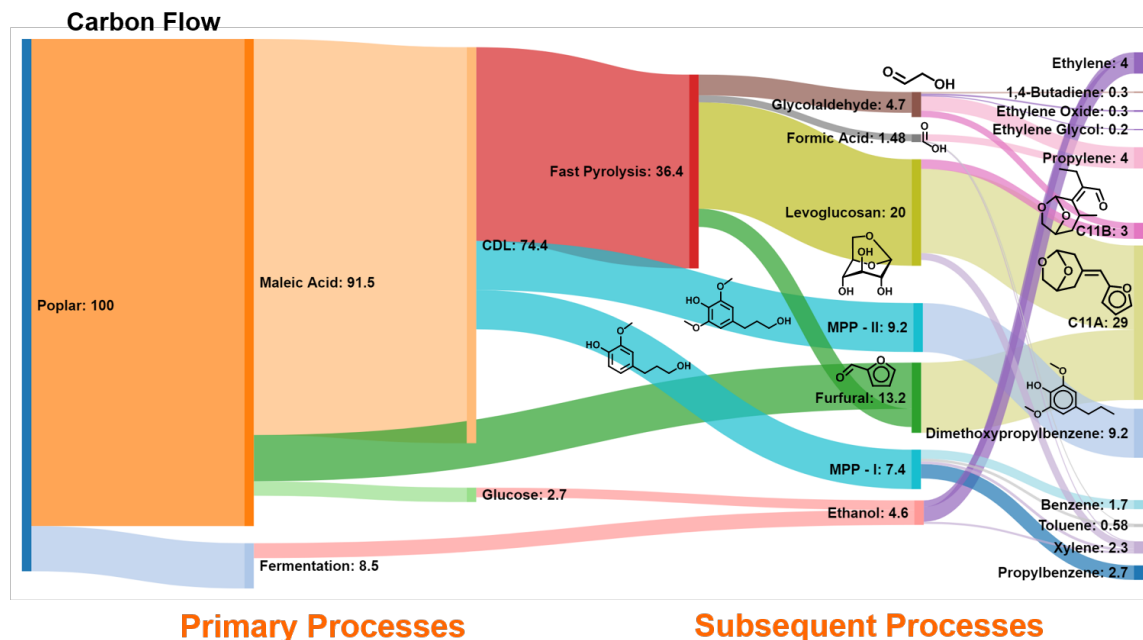
Figure 4.9.: Biomass-derived molecules allocations toward target products in biorefinery with the maximum achievable carbon efficiency subject to US production demands.

Only glycolaldehyde is employed toward fulfilling production of fuels in considerable abundance.

Heavy oxygenates, such as levoglucosan, furfural, 5-HMF, and dihydroeugenol, are mainly channeled toward fulfilling diesel and jet fuel production. These molecules generate C11 oxygenates which can be directly hydrodeoxygenated or further carbon-coupled with itself or other C11 to form heavier oxygenates before undergoing hydrodeoxygenation.

At best, the maximum potential carbon recovery of an integrated biorefinery based on C3Bio processes is estimated to be 60%, which suggests that current potential of sustainably available biomass can only sustain either diesel and jet fuel, commodity chemicals, or supplying one demand while leaving the other at a shortage. Given that current sustainably available biomass potential production ranges from 505 - 709 million tons per year and an achievable carbon efficiency of 60% for a biorefinery

system that co-produces diesel and commodity chemicals, at best case scenario, at which we consider the upper bound for the potential production of sustainably available biomass, only 75% of the US diesel and commodity chemical production can be met.

4.8   Sustaining Organic Commodity Chemical Production Using Poplar

As emerging electric vehicle technologies can potentially replace diesel and gasoline need, it is also worth considering a scenario where SA biomass is needed for only commodity chemical production. It is pertinent to identify the minimum amount of SA biomass that is needed to sustain the current commodity chemical production in United States. Therefore, another optimization problem can be posed in order to identify the optimal biorefinery configuration that is capable of delivering all commodity chemical needs in the United States efficiently. Therefore, we propose the following objective function:

$$min \ \dot{n}_{poplar}^{in,o} \tag{4.7}$$

In addition to this objective function, we also impose the following target production constraints:

$$\sum_{i \in I^{ProductSet_k}} \dot{n}_i^{out} \geq \dot{n}_k^{target} \ \ \forall \, k \tag{4.8}$$

where, $\dot{n}_k^{target}$, is the total annual molar flow rate of target product set, k. With this objective function and target production constraints, no constraint limits the number of active reactions. In order to limit the number of reactions selected, we impose the following constraint:

$$\sum_j a_j \leq NRL \tag{4.9}$$

where, NRL, is an upper bound on the number of active reactions. Here, NRL is set at 40 based on the optimal biorefinery configuration for co-production of diesel, jet

fuel, and chemicals. After posing and solving this optimization problem, the results are shown in Table 4.7.

Table 4.7.: Minimization of poplar feedstock in order to sustain the United States organic commodity chemical production.

Cases	SA Poplar (Million tons/year)	η_{Carbon}	Number of Reactions
Biorefinery with Only Fast Pyrolysis	1,346	7.9	23
Biorefinery with Only Lignocellulosic Fermentation	–	–	–
Optimal Biorefinery	288	36.9	33

Considering that approximately $505 - 709$ million tons of SA biomass are available, the remaining $217 - 421$ million tons/year can be allocated for diesel and jet fuel productions.

4.9 Comparison with Existing Roadmap for Lignocellulosic Biomass Conversion to Chemicals and Fuels

Many research studies proposed various co-production strategies for biomass transformation to fuel and chemicals. There are two key distinguishing features of the proposed biorefinery configurations in this study.

First, utilization of lignin toward fuels and molecules increases the overall carbon efficiency of the process as lignin typically accounts for 35 - 40% of the overall carbon content in intact lignocellulosic biomass. In lignocellulosic fermentation and other biorefinery systems, lignin is often used for heat and power generation instead of toward production of fuels and/or chemicals [41].

Second, selective and individual removal of biomass constituents and their conversion toward various biomass-derived molecules enables their further utilization in subsequent processing through catalytic means. Many proposed biorefinery systems focuses on using single biomass fractionation steps, such as pyrolysis, enzymatic hydrolysis, and lignocellulosic fermentation. These single step processes are usually

designed for removal of only a single biomass constituent and rendering other biomass constituents inaccessible for further subsequent processes.

These key distinctions are the main underlying reasons for this proposed biorefinery system to achieve 63% carbon recovery compared to 60% and 33% carbon recovery of standalone fast pyrolysis and standalone lignocellulosic fermentation, respectively.

4.10   Conclusion

In this work, the potential of sustainably available biomass to substitute traditional refinery through the concept of the biorefinery is assessed. Systems-level molecular mapping is applied to a a set of primary processes. This network is constructed based on six process groups and contains 15 primary processes. These primary processes provide a set of 13 biomass-derived molecules and each process generates them at various abundances.

Using systems-level molecular mapping, carbon efficient biorefinery with minimum number of reactions is identified. This configuration utilized a set of primary process that serially removes biomass constituent removal. In addition, carbon efficient biorefinery with the minimum number of reaction that is capable of producing diesel and commodity chemicals is also proposed. Through combining newly reported primary processes with existing lignocellulosic fermentation processes, both chemicals and diesel can be produced efficiently.

Compared to existing roadmaps proposed in the literature, biorefinery configuration proposed in this work can achieve between 58 - 63% carbon efficiency for both diesel and chemical productions. In a petroleum-deprived future where the transportation sector demand is heavily substituted by electricity, a carbon efficient biorefinery system that is capable of sustaining all commodity chemical production in the United States is proposed. This enables an effective employment of sustainably available lignocellulosic biomass resource in a renewable and sustainable economy.

Indeed, further rigorous process analysis and catalyst development must be undertaken in order to assess the potential of biorefinery configuration proposed here

accurately. Instead of using biomass only as a feedstock substitute for petroleum resource, a true biorefinery should generate molecules that closely resemble biomass-derived molecules or biomass itself and also have niches in today's society. Moreover, if those molecules possess distinct physical properties than those of petrochemicals, then this current society itself may have to evolve as it once did when petroleum resource was discovered. Nevertheless, this modeling and optimization approach has enabled identification of new process configurations and also provide a roadmap for productive employment of lignocellulosic biomass for diesel, jet fuel, and commodity chemical productions.

5. ELUCIDATION OF CHAR FORMATION DURING FAST PYROLYSIS OF CELLULOSE

5.1 Introduction

Char accounts for up to 34% of carbon loss during fast pyrolysis of intact lignocellulosic biomass [30, 31]. There are several research studies on which biomass constituents lead to char. It has been hypothesized that hemicellulose and lignin contribute significantly to char formation and cellulose tends not to form char [30, 79]. Inorganic presence in biomass has also been proposed to contribute toward char formation. Heat transfer during pyrolysis has also been shown to have an impact on char formation.

Recent advances in mass spectroscopy allowed analysis of primary products of pyrolysis. Mass spectrometry (MS) can provide detailed information on the structures of individual compounds in complex mixtures. However, the very complex structure of biochar and its poor solubility in the solvents used in mass spectrometric analysis hinder these efforts. In order to avoid the problems having to do with solubilization of char, char samples have been subjected to fast pyrolysis and the pyrolysis products have been detected by gas chromatography coupled with mass spectrometry (GC/MS). Jiang et al. proposed a total of 52 structures for the unknown compounds in cellulose char sample by employing multiple analytical methods to obtain structural features of the biochar sample formed during fast pyrolysis of cellulose.

It remains unclear as to how these proposed structures may form during fast pyrolysis. Understanding the mechanism behind the formation of these char precursors may offer new research guidance in the effort of reducing char formation during pyrolysis. Here, using the systems-level molecular mapping approach described in chapter 3, we seek to identify potential pathways for the formation of the proposed char

precursors. Ultimately, this knowledge can facilitate material and process synthesis of pyrolytic systems to minimize char formation.

5.2   Char-precursor from Fast Pyrolysis of Cellulose

Jiang et al. proposed 52 structures for the unknown compounds in cellulose char. These proposed molecules can be categorized into four groups based on their molecular backbone, shown in Figure 5.1. Note that the molecules in group I share a cyclic ether five-carbon ring jointed with a four-carbon unsaturated ring. There are several side chains attached to the two-ring carbon backbone. Molecules in group II share a twelve-carbon backbone consists of a central furan ring and two adjacent four-carbon unsaturated on each side. Similar to group II, molecules in group III are polycyclic aromatics hydrocarbons. The structure of group III is what has been generally reported in the literature to be the structure of cellulose char **I**nsert reference. Lastly, molecules in group IV all are all polysubstituted benzene with various alkyl and oxygen-containing side chains.
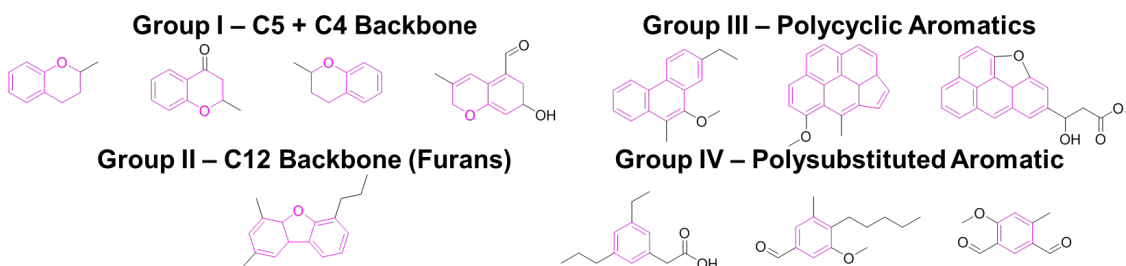
Figure 5.1.: Four categories of char-precursors determined by Jiang et. al.

In our analysis, the focus is on identifying potential pathways for the formation of these backbones that are present in each group. As these structures are proposed, the absolute location of the side alkyl chains is not critical. In the later section, we describe as to how these side chains may form. Prior to identifying the pathway, the particular system at which char may form must be clearly defined.

5.3 Potential Char Formation System during Pyrolysis

In order to discover potential pathways that lead to the formation of these char-derived molecules, it is pertinent to identify the system under which these molecules might form. Considering fast pyrolysis of cellulose, shown in Figure 5.2, these char precursors might form in the gas phase or the melt phase of cellulose through inter- and intramolecular reactions. Intermolecular reactions refer to the potential reactions between the primary products of cellulose, such as levoglucosan and furfural, while intramolecular reactions include reactions that may occur within the cellulose polymer itself. It is also possible that both intermolecular and intramolecular reactions lead to char formation, which would involve the cellulose polymer and primary products of fast pyrolysis. Given the phases at which these reactions may occur, it is unlikely that intramolecular reaction occurs in the gas phase as the cellulose would not undergo a phase change. Similarly, due to the presence of an enormous diluent, such as nitrogen, helium, and hydrogen, char precursors that form due to intermolecular reactions in the gas phase are unlikely to condense out of the gas phase due to their low partial pressures. Therefore, it is likely that the char precursors are forming on the melt phase of the cellulose, indicated in Figure5.2.
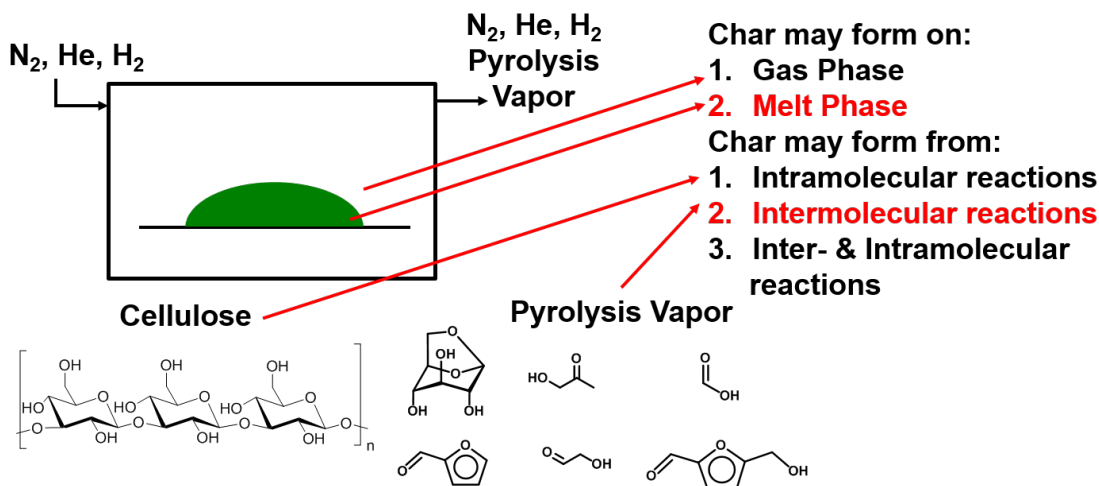
Figure 5.2.: Char formation system considered in this study.

Due to the relatively large structure of cellulose, it is difficult to exhaustively define all potential intramolecular reactions, let alone, potential intermolecular reactions with its primary products during fast pyrolysis. Therefore, we focus on the intermolecular reactions of primary products of fast pyrolysis of cellulose in the melt phase of the cellulose sample.

Here, we only consider that char precursors form in the melt phase of cellulose through intermolecular reactions between the primary products of fast pyrolysis of cellulose. Among the primary product of fast pyrolysis, we only consider levoglucosan and furan. As the primary objective is to understand the formation of the carbon backbone in each group, in our analysis, only levoglucosan and furan are considered as the starting molecules for the char formation. Here, furan is used as an analog for 5-HMF and furfural. We describe in the later section as to how the side chains in 5-HMF and furfural may fit into the formation of the proposed char precursor structures and of char itself.

5.4   Pathway Elucidation

To consider all chemistries relevant to biomass-derived molecules, we utilize Rule Input Network Generator (RING) that is described by Rangarajan et al. while including a set of reaction rules that are defined by Taufik et al. [14, 22]. Using this tool, we found potential pathways to cyclic molecules that contain 10 carbon atoms and 16 carbon atoms from levoglucosan and furan as shown in Figures 5.3 and 5.4. In addition, we also found pathways that generate molecules that fall under all four categories we defined earlier.

5.5   Results and Discussions

5.5.1   Group I, III, and IV Potential Reaction Pathway

As shown in Figure 5.3, levoglucosan first undergoes dehydration, followed by tautomerization of enol which generates water and a ketone group on the cyclic ether

carbon backbone. Next, the cyclic ether on six-membered carbon ring hydrolyzes and forms the corresponding ring-opened product. Lastly, one of the remaining hydroxyls dehydrates to form a dienophile for a Diels-Alder reaction. Furan then serves as the conjugated diene in this Diels-Alder reaction. This cycloaddition reaction forms the molecular backbone that exists in group I molecules. A ketone group is also present in the cyclic ether carbon backbone, which forms by tautomerization during the initial dehydration of levoglucosan. The newly formed ring dehydrates to form a benzene, as reported in the literature [90].
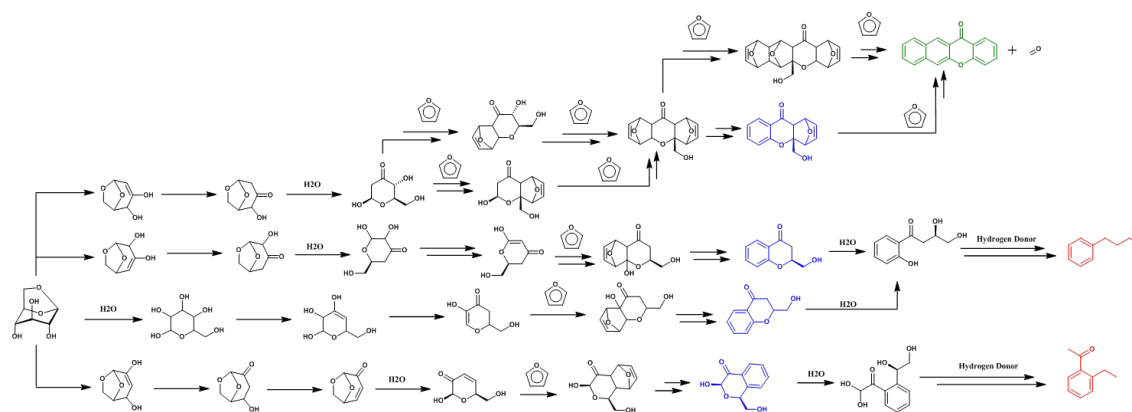
Figure 5.3.: Potential pathways for the formation of Group I, III, and IV molecules from levoglucosan and furan.

Group I molecules can also undergo further hydrolysis of cyclic ether and ring open to form precursors to Group IV molecules. The resulting molecules are substituted benzene with a side chain containing five carbon atoms. Due to the lack of hydrogen in the melt phase, hydrogenation of the side chain is likely to occur through hydrogen donor molecules, such as formic acid or acetic acid, which has been reported in the literature [91, 92].

Based on potential pathways for Group I and IV molecules, it is likely that group II molecules form from consecutive Diels-Alder reactions between furan molecules as shown in Figure 5.4. Self-condensation of furan through Diels-Alder has been described in literature [93, 94]. Reaction sequence proposed for group II can be extended to

furfural and 5-HMF and the presence of those highly reactive carbonyl side chains can ultimately grow to longer side alkyl chains.

5.5.2 Group II Potential Reaction Pathway

Lastly, polycyclic aromatics can also form through further Diels-Alder of Group I molecules with furan. Prior to undergoing dehydration, furan can act as a conjugated diene for further Diels-Alder reactions. The resulting polycyclic aromatics have a linear polycyclic aromatic structure whereas the proposed structures for Group IV possess clusters of aromatic molecules. Ketone attached in these linear polycyclic aromatics can undergo acylation with other linear polycyclic aromatics to generate non-linear polycyclic aromatics and these reactions have been described in the literature [89].
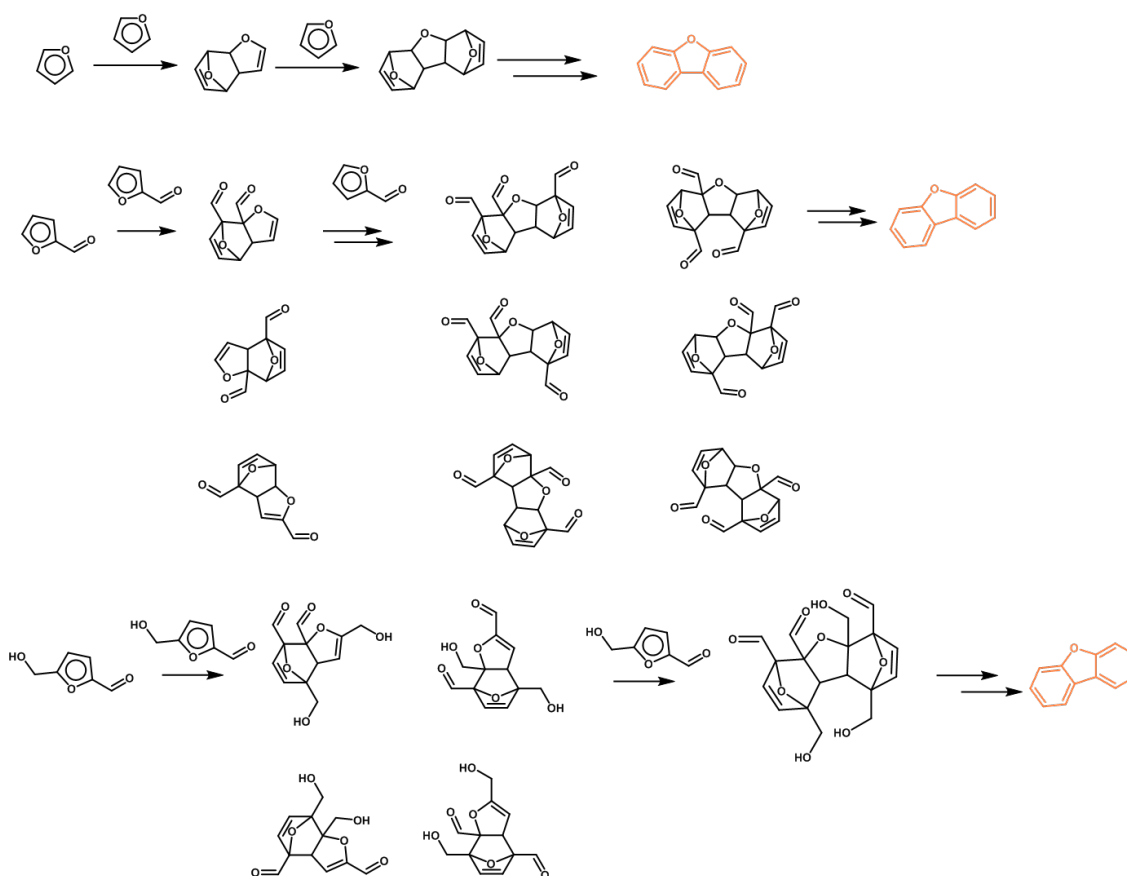
Figure 5.4.: Potential pathways for the formation of group II molecules from furan.

5.5.3   General Reaction Sequence for Char Pre-Cursor Formation during Fast-Pyrolysis

Based on all the potential pathways we found, the general pathway for transformation of levoglucosan and furan toward char-derived molecules starts with dehydration of levoglucosan followed by ring opening of the cyclic ether and further dehydration before undergoing Diels-Alder reactions with furanic molecules. Furthermore, many of these described reactions have also been reported in the literature to occur catalytically at a temperature below 300°C [90–92]. Therefore, it is likely that the energy barriers for these reactions can be sufficiently overcome at the pyrolysis temperature of 500°C .

5.6   Conclusion

Advances in mass spectroscopy and employment of multiple analytic chemistry tools allowed identification of char precursor during fast pyrolysis of cellulose. Jiang et al. proposed a set of 52 molecules that can be categorized into four groups of molecules. Insights into their potential pathways can provide an initial starting point to guide experimental research. Here, using the systems-level molecular mapping approach described in chapter 3, several potential pathways for all the groups are proposed.

A series of dehydration and tautomerization followed by Diels-Alder reactions can potentially lead to the formation of these char precursors starting from cellulose. This general reaction sequence can generate the carbon backbones that exist in many proposed molecules. The substituted alkyl groups that are present in the proposed pathways are also highly reactive, consisting of carbonyl groups.

Although the pathways presented here have not been verified, it offers insights into additional potential contributors toward char formation during pyrolysis. As these char precursors have not been identified before, these pathways offer an initial point in elucidating their formation. As further experiments and analysis are conducted on these pathways, the systems-level molecular mapping can be employed again in order to screen other potential pathways or provide deeper analysis of the pathways presented in this work.

6. VALORIZATION OF SHALE GAS CONDENSATE THROUGH CATALYTIC DEHYDROGENATION AND OLIGOMERIZATION

6.1 Introduction

In order to meet the energy demands of the twenty-first century, engineers and scientists are working to develop new methods to discover, extract, and refine fossil resources including oil, coal, natural gas, shale oil, and shale gas. Recent advances in hydraulic fracturing and horizontal drilling have led to a surge in shale resource production. Similar to natural gas, methane concentration in shale gas ranges from 50% to 90%, which sets it as the major component [27, 28]. However, unlike natural gas, shale gas contains higher concentrations of hydrocarbons other than methane, such as ethane, propane, butane, isobutane, and pentane. These hydrocarbons are known as condensate or natural gas liquids (NGLs), and their concentrations vary from 0% to 50% [29].

From 2006 to 2016, United States NGL production doubled from 635 million barrels to 1284 million barrels. However, not all the produced NGL can be transported to gas processing or upgrading facilities. As shown in Figure 6.1a–c, natural gas and hydrocarbon gas liquid (HGL) pipeline infrastructure which is used to transport NGL, and gas processing plant infrastructure are not extensive in several remote shale gas basins compared to basins that are located in historically gas producing or consuming regions such as the Gulf Coast. These remote shale gas basins constitute a large portion of United States shale resource production, shown in Figure 6.1d.

When the gas processing and distribution infrastructure is limited or non-existent, gas associated with shale oil is often deemed as stranded gas and is mostly flared (40% in Bakken field) [29, 98]. In addition, in several remote basins, such as Marcellus, the local spot price of natural gas can be cheaper by 40% compared to the Henry hub spot

(a)

(b)

(c)

(d)

(e)
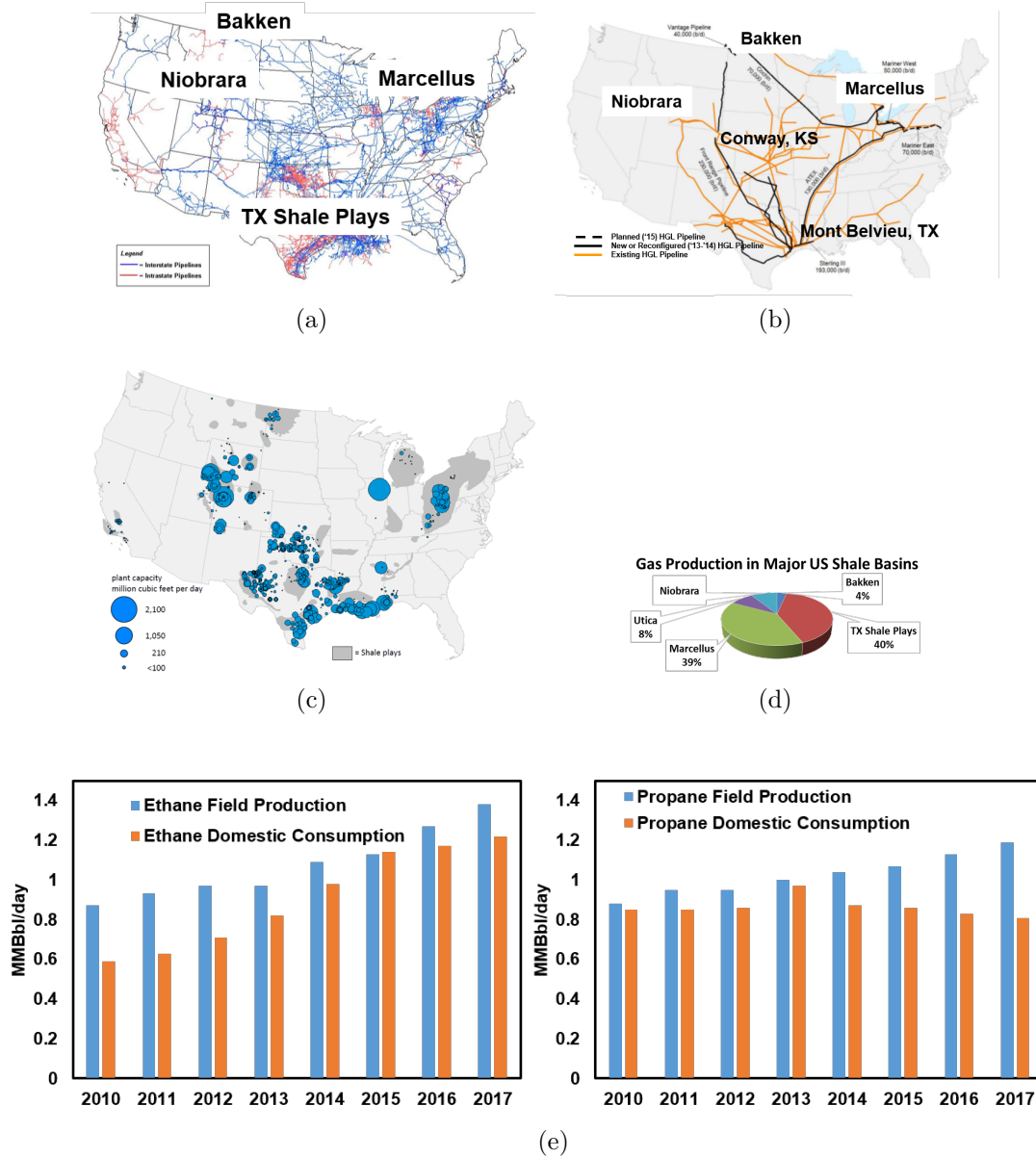
Figure 6.1.: (**a**) United States gas transportation systems network. TX Shale Plays include Barnett, Eagle Ford, and Permian basins. Adapted from the Energy Information Agency (EIA) [33]. (**b**) Existing United States hydrocarbon gas liquid (HGL) pipeline network. Adapted from the EIA [95, 96]. (**c**) Existing United States gas processing capacity. Adapted from the EIA [95, 96]. (**d**) Distribution of shale gas production in the United States based on the shale basins. TX Shale Plays include Barnett, Eagle Ford, and Permian basins [33]. (**e**) United States propane and ethane production and consumption from 2010 to 2017 [97].

price, due to the abundance of shale gas. These circumstances provide an opportunity to exploit the NGL produced in these remote shale basins.

Currently, a substantial quantity of NGL is fed into the chemical industries. Ethane is almost exclusively used for ethylene production through steam cracking, which ultimately turns into plastics. Propane and butane are also partially used for chemical feedstocks [99].

He et al. proposed several integrated processes between gas treatment, steam cracking, and catalytic dehydrogenation, and showed the economic potential of producing ethylene and propylene from shale gas [28, 100]. However, ethane crackers are highly capital-intensive facilities and take several years to build [101].

Furthermore, as shown in Figure 6.1e, the consumption of ethane and propane, which is mainly as feedstocks for ethylene and propylene production in the United States, is lower than their current production [97, 102]. Thus, olefins such as ethylene and propylene are not reasonable target products for wellhead NGL conversion.

The United States' transportation sector is still dominated by traditional petroleum resources [103, 104]. Despite increases in renewable energy and natural gas resources and advances and projected increase in light duty electric and hybrid vehicles, petroleum resources in the United States are expected to play a major role in the future, with gasoline accounting for 35% of the global transportation fuel consumption in 2040 [76, 105]. Synfuel International Inc. proposed a new ethane-to-gasoline process consisting of a pyrolysis reactor followed by an ethylene reactor and oligomerization reactor to produce liquid hydrocarbons [106]. The conventional method for the gas-to-liquid (GTL) process involves the partial oxidation of natural gas to obtain synthetic gas composed of CO and H_2, followed by chain growing processes such as Fischer–Tropsch [107, 108]. Another alternative to consider is the catalytic dehydrogenation of light alkanes followed by oligomerization of the olefins to form fuel range hydrocarbons.

The catalytic dehydrogenation of light alkanes has been widely studied as an alternative process for producing olefins [109–115]. However, for olefins production, there are only a few reports on process synthesis and design for the production of

olefins through the oxidative and non-oxidative catalytic dehydrogenation of light alkanes [112, 114, 115]. UOP Oleflex is a commercially proven technology for the catalytic conversion of propane to propylene using a PtSn alloy catalyst [56]. The catalytic dehydrogenation of light alkanes can be preferred over conventional technology such as steam cracking, as it has the potential of mitigating the formation of by-products and reducing energy consumption [109, 112, 116]. Despite these advantages, coking is known as a major problem, which causes rapid catalyst deactivation [111]. According to our knowledge, there is a lack of use of catalytic dehydrogenation of light alkanes in the context of overall process synthesis for the transformation of NGLs to liquid hydrocarbons.

We propose a process that can upgrade shale condensate into liquid hydrocarbons via catalytic dehydrogenation followed by catalytic oligomerization. In this work, we only focus on converting ethane, propane, and butane in shale condensate into liquid fuel, and we do not consider the coupling of methane.

6.1.1 Thermodynamic Analysis of the NGL-to-Liquid Pathways

As mentioned earlier, apart from catalytic dehydrogenation followed by oligomerization, there are other routes to upgrade NGL to liquid fuel feedstocks. Alkenes or syngas are common intermediates for these routes. Taking ethane as an example, ethane can be converted to either ethylene or syngas and then upgraded to liquid fuel. Now for a comparison of different synthetic routes from NGL to liquid fuel, the energy demands of different pathways of ethane conversion are evaluated. For our current analysis, we only consider ethane to octane conversion. Figure 6.2 below summarizes the different pathways for the thermodynamic analysis that will be discussed.

For the "ethane–ethylene–octane" route, we consider two different dehydrogenation methods: catalytic dehydrogenation and steam cracking. For catalytic dehydrogenation, the ethane is assumed to be converted to ethylene with 100% selectivity and the conversion of ethane is 45% according to reported experimental results; for steam cracking, the conversion of ethane is 67% and selectivity towards ethylene is 81% [20, 110].

The catalytic dehydrogenation reactor and steam cracker are both operated at 900 K and 3.5 bar. The dehydrogenation unit is followed by the oligomerization reactor, in which ethylene is coupled to produce octane. The oligomerization reactors are operated at 600 K. Although the coupling reaction is exothermic, the generated heat cannot be recovered to provide heat for the dehydrogenation due to the lower oligomerization operating temperature. Therefore, to compare the energy consumption, we only consider the dehydrogenation units. Through Aspen Plus simulation, with pure ethane feed, the heat duties are 65 MJ/kmol of ethane reacted and 144 MJ/kmol of ethylene produced for the catalytic dehydrogenation reactor and 103 MJ/kmol of ethane reacted and 190 MJ/kmol of ethylene produced for the steam cracker, respectively. The actual ethane dehydrogenation reactions within the two dehydrogenation reactors are similar, and the difference in heat duty comes from the different conversion and the generation of byproducts in steam cracking. Furthermore, if we consider that the generation of high-temperature steam also demands energy input, catalytic dehydrogenation is a less-energy-intensive route for ethane conversion.
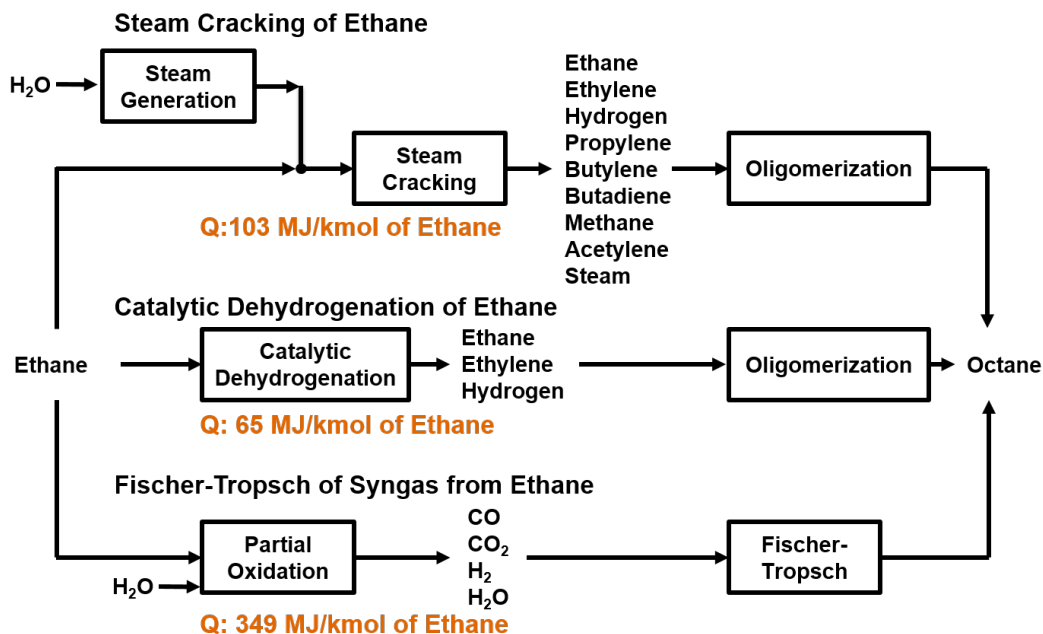
Figure 6.2.: Three potential pathways for converting ethane to octane.

Another possible route from ethane to liquid fuel is via syngas. Ethane can be partially oxidized to syngas either by oxygen or steam and followed by a Fischer–Tropsch reactor for fuel synthesis. Considering the energy demand for air separation, we only consider ethane partial oxidation by steam. At 1000 K and 3.5 bar (the same condition as dehydrogenation), ethane and steam are reacted to produce syngas. The REQUIL reactor model in Aspen Plus was used to model the reformer or oxidation reactor. In this process, the reformer reactor consumes 349 MJ/kmol of ethane, which is higher than that of the dehydrogenation reactor. In addition, this process is counterproductive, as ethane is decomposed to carbon monoxide and hydrogen which are then later recombined to form long carbon chain molecules through Fischer–Tropsch or methanol-to-gasoline technology. Furthermore, in this process, high-temperature steam has to be generated, and the gas product from the oxidation reactor has to be compressed in order to go through the Fischer–Tropsch process. Once again, the large amount of heat generated in the Fischer–Tropsch process is at a much lower temperature than the reformer temperature, leading to a substantial degradation in the quality of heat. Therefore, among the three routes discussed, catalytic dehydrogenation followed by oligomerization is the most energy efficient method of light alkane upgrading.

6.2   Problem Statement

Given a shale gas condensate stream from a remote reservoir, it is desired to synthesize, simulate, and integrate a NGL-to-liquid hydrocarbons (NTL) process using catalytic dehydrogenation and oligomerization reactions and to carry out economic analysis to answer the following questions:

- What is the necessary pretreatment of shale gas?

- What is the correct flow sheet to achieve the NTL conversion?

- What separation technologies are required for the process?

- What are the economic criteria of the process and how do they compare with existing processes?

- What is the cost differential between this process and existing GTL processes?

The following assumptions, basis, and data were used in all processes considered here:

The Bakken field is located in a remote part of North Dakota. Currently, the pipeline infrastructure is already at its full capacity, and the state's natural gas consumption is well below its shale gas production [117]. Considering the variability and decay of shale resource production, installing infrastructure for NGL distribution may not be attractive, as the payback period can easily exceed the well production lifetime [29]. Therefore, it is desirable to convert the NGL locally into liquid fuel components, as it can be refined and marketed locally and nationally through various distribution channels. A 96 million standard cubic feet per day (MMSCFD) basis feed flow rate was selected because a typical single wellhead production rate in the Bakken field ranges from 1 to 4.8 MMSCFD, and this flow rate represents a medium-scale facility that processes outputs from between 20 and 100 wells [29]. The composition of this stream is shown in Table X in Appendix C. Additional process assumptions shown in Table 6.1 are also considered.

Table 6.1.: General Process Assumptions

Assumptions
Bakken Field Shale Feed Rate: 96 MMSCFD
On-stream Factor: 0.92
Flash Tank Pressure Drop: 0.21 bar
Heat Exchanger Pressure Drop: 0.21 bar
Ambient Temperature: 308 K
No pressure drop across the reactors
Compressor Efficiency: 0.7

6.3   Process Description

Shale gas requires the same conventional gas treatment as natural gas. As gas treatment is a well-known technology and UOP-ThomasRussell has an operating modular field-erected gas treatment plant with a current proven size of 200 MMSCFD, we begin with conventional shale gas treatment which consists of acid gas and water removal [105]. Depending on the nitrogen content of the raw shale gas, nitrogen removal may be necessary to meet the typical natural gas pipeline specifications, which is ≤ 4 mol % for nitrogen. In the case of the Bakken field, nitrogen removal may not be required because the region is known to produce both nitrogen-rich and nitrogen-deficient shale gas streams, and the two types of streams can be easily mixed in order to meet the pipeline specification.

Both acid gas and water removal processes are well-established and understood. Depending on the content of acid gas and water, there are various process options. Methyl diethyl amine (MDEA) absorption and triethylene glycol (TEG) absorption are the most common processes for acid gas and water removal, respectively. These processes are capable of reducing the acid gas content down to 4 ppm and the water content to 100 ppm [118]. After the shale gas is treated, it is termed dry, sweet shale gas, which can then undergo further downstream processing.

Catalytic dehydrogenation is the next step and, in this unit operation, ethane, propane, and butane undergo dehydrogenation with a catalyst that reduces selectivities toward undesirable byproducts. The dehydrogenation of ethane is an endothermic reaction, and in order to achieve a reasonable equilibrium conversion, the reaction must be performed at moderately high temperature (900–1100 K).

Hydrogen generated during dehydrogenation may need to be removed prior to the oligomerization reaction, as it can re-saturate olefins. If the oligomerization catalyst has a high hydrogen tolerance such that selectivity toward hydrogenation products is low, then hydrogen can remain in the mixture. Otherwise, hydrogen must be

removed, and this separation task can be accomplished using cryogenic distillation or gas membrane separation.

After selectively dehydrogenating ethane, propane, and butane at moderately high temperature, the resulting olefins can be converted to higher molecular weight hydrocarbons through an oligomerization reaction. Catalysts for oligomerization are available, and have been used for similar applications in the past [56,119]. The product of the oligomerization reaction is a mixture of high molecular weight hydrocarbons and unconverted light alkenes. Due to a large difference in their boiling points, high molecular weight hydrocarbons can be recovered through condensation by cooling the mixture. Then, the remaining vapor, which contains unconverted light alkenes, is recycled to the inlet of the catalytic dehydrogenation reactor.

6.4 Process Modeling

6.4.1 Gas Treatment

As stated earlier, acid gas treatment and water removal are well-known processes, and the selection of the specific process depends highly on the concentration of the acid gas and water in the shale gas stream. Based on the literature, MDEA sweetening and TEG dehydration processes are suitable for the Bakken field shale gas [118]. In MDEA amine sweetening, MDEA solution is contacted with the shale gas, and carbon dioxide and hydrogen sulfide react with the amine solution. Then, the amine solution is regenerated in a stripper by releasing the acid gas from the solution. For water removal, TEG (triethylene glycol) solution is contacted with the sweet gas shale, where the water is ionically bonded with the TEG solution. The TEG solution is then recovered in a boiler by vaporizing the water. In this work, the economics and energy input of these processes are not considered as in other GTL processes. A treated natural gas stream is assumed as the feed.

6.4.2   Demethanizer

After gas treatment, NGL must be separated from the shale gas stream (Figure 6.3: 102; Figure 6.4: 204). As methane is not converted to liquid hydrocarbons, a high concentration of residual methane in the NGL stream from the demethanizer can possibly lead to large accumulation in downstream recycle loop. Conventionally, cryogenic distillation is used for the demethanizer. Due to the potential of relatively small-scale application of this process, membrane separation is also considered for NGL separation, which has proven to be a viable and practical option in NGL recovery from natural gas [120, 121]. Considering the limitations of existing CH_4-NGL separation processes, we propose two process designs based on methane recovery of 86% and 96% in the demethanizer section, and they are labeled Process I and Process II, shown in Figures 6.3 and 6.4. For the 96% recovery demethanizer, a turbo-expander process scheme with a distillation column modeled using RadFrac in Aspen Plus was used [122]. For 85% recovery, cascade gas membrane separation was used, and cost calculation for this unit operation was based on a well-mixed membrane model. Note that the turbo-expander process scheme can also be employed for the 85% recovery, and the cascade membrane here was selected to illustrate the deployment of other separation technologies apart from distillation. The detailed schemes for these unit operations can be found in the Supplementary Information. The membrane was assumed to have a permeability of 120 barrer for C_{2+} and permselectivity of 12 for CH_4/CH_{2+} [123]. The capital cost of the membrane module was assumed to be $50/m^2$.

6.4.3   Dehydrogenation

Ethane, propane, and butane can be transformed to its corresponding mono-olefins through catalytic dehydrogenation. The dehydrogenation reaction can be generalized as follows:

$$C_nH_{2n+2} \Rightarrow C_nH_{2n} + H_2. \tag{6.1}$$

The reaction is endothermic, and for light hydrocarbons, the equilibrium conversion is reasonable at high temperature ranging between 800 K and 1100 K [124]. Based on Le Chatelier's principle, lower pressure shifts the chemical equilibrium toward the product side. Hence, the reaction should be operated at low pressure. Currently, the industrial catalytic dehydrogenation of light hydrocarbons is limited to only propane and butane. Honeywell Oleflex is an example of the industrial implementation of catalytic dehydrogenation which entails the dehydrogenation of propane to propylene [56]. Using $PtSn/Al_2O_3$ catalyst, propane is dehydrogenated at 1.4 barg and 873 K. The dehydrogenation of ethane is usually achieved through steam cracking [56]. Ethane conversion of 45% with selectivity of 99% toward ethylene has been reported at 873 K using $PtZn/SiO_2$ catalyst [110].

Here, we assumed that through catalyst development, 95% of equilibrium conversion of ethane, propane, and butane dehydrogenation at 1073 K and 6.58 bar can be reached. Note that for dehydrogenation, 95% of the true equilibrium conversion was considered in order to account for the fact that dehydrogenation is a highly endothermic reaction and heat transfer is the rate-limiting step. In Figure 6.3, R101 represents the catalytic dehydrogenation reactor and 103 is the inlet stream to R101. The REQUIL reactor model in Aspen Plus was used. Three reactions (dehydrogenation of ethane, propane, and butane), and their respective temperature approaches were specified in order to adjust the equilibrium conversion. No competing reactions (e.g., hydrogenolysis of alkanes) were considered. The same modeling details for the dehydrogenation reactor were applied for Process II in Figure 6.4.

6.4.4 Hydrogen Recovery

The product stream (Figure 6.3, 104; Figure 6.4, 205) from the dehydrogenation reactor which contains mono-olefins, hydrogen, and unconverted light alkanes is then cooled down to 500 K. Using membrane separation, hydrogen will be partially recovered. Some retained hydrogen in the retenate stream is desirable to ensure the stability of the dehydrogenation and oligomerization catalyst [110]. In Aspen Plus,

the membrane was simulated using a separator and calculator block. Within the calculator block, the material balance and design equation for a well-mixed membrane were employed and the output from this block was used in the separator block to determine the purity and flow rate of the permeate and retenate streams. For sizing and economics calculation, a well-mixed membrane system and $50/m^2 capital cost for a spiral wound membrane module were assumed [?]. The hydrogen membrane used in this work was assumed to have permeability of 250 barrer for hydrogen and selectivity of 590 and 125 for hydrogen/ethylene and hydrogen/methane, respectively [121, 125]. The gas membrane was modeled as a well-mixed membrane system with a binary feed, and a polyimide membrane was used. In addition, it was assumed that the feed was a binary mixture of hydrogen and pseudo component of C_{1+}. The permselectivity of H_2/C_{1+} for this membrane here was taken to be 483. The gas membrane was designed to achieve a target of 15% mole of hydrogen in the retenate stream in order to stabilize the catalysts used in this process. The permeate purity was 83.87% mole of hydrogen. The net recovery of hydrogen through the membrane was 0.105 kmol of H_2/m^2 h. Using a single membrane configuration and setting the pressure of the permeate side at 1 bar, the hydrogen removal in the permeate was 54% and ethane slip to the permeate stream was 16%. This resulted in 15% mole of hydrogen in the retenate stream according to our simulation results.

6.4.5 Oligomerization

The retentate stream (Figure 6.3, 105) from the hydrogen membrane unit was heated to 573 K and then fed to the oligomerization reactor. In this reactor, olefins couple together to form higher molecular weight olefins. For the oligomerization of olefins , the reaction can be generalized as follows:

$$C_mH_{2m} + C_nH_{2n} \Rightarrow C_{m+n}H_{2(m+n)}. \tag{6.2}$$
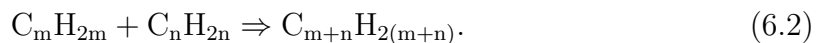
The oligomerization reaction is exothermic and generally runs at low temperature [56]. This reaction is carried out at 573 K and 5.47 bar [56] H-ZSM-5 is commonly used for the olefin oligomerization reaction [119]. It has been reported that 90 wt % conversion to liquid has been observed from propene at 500 K and 24 bar with 88% of the liquid being C_{9+} hydrocarbons [126]. Similarly, ethylene fed with nitrogen at 773 K obtained a yield of 54.2% toward C_{5+} hydrocarbons on H-ZSM-5 [127]. Toch et al. also reported 99% ethylene conversion with 25% and 55% selectivities toward propene and gasoline, which is hydrocarbon with a carbon number ranging from five to eight, using Ni-beta zeolite at 500 K and 1.0 MPa [60, 128].

In this work, we assumed that this chemical system achieves thermodynamic equilibrium at 600 K and 5.47 bar and only alkene coupling that produces a larger alkene occurs. Therefore, we only considered the C_4–C_{12} alkene oligomerization products. The selectivity to various high molecular weight alkenes are defined based on equilibrium. In Figure 6.3, R102 represents the oligomerization reactor. The RGIBBS reactor model in Aspen Plus was used to estimate the equilibrium composition. In addition, all paraffin molecules, methane, and hydrogen were set to be inert, indicating that they do not participate in the minimization of Gibbs free energy calculation. Note that in these coupling reactions, it is very likely for the olefins to also form both cyclic and branched molecules, but this was not considered in this study.

6.4.6   Liquid Hydrocarbon Recovery

After the oligomerization reactor, the final step is to recover liquid hydrocarbons and recycle the unconverted C_2 and C_3 into either of the reactors depending on whether they are olefinic or aliphatic light hydrocarbons. First, the product stream (Figure 6.3, 106) from the oligomerization reactor is cooled down to 275 K to condense liquid hydrocarbons. This temperature was selected because C_{9+} hydrocarbons may form into waxes and solids below 275 K. The downstream processing of the vapor stream is a crucial step in the overall separation process. This vapor stream mainly contains unconverted olefinic and aliphatic light hydrocarbons. If this vapor stream

is directly recycled to the fresh feed stream of the dehydrogenation reactor and the methane recovery in the upstream CH_4/C_{2+} separator is not very high, this necessitates a very large recycle ratio. With a large recycle ratio, the feed stream entering the dehydrogenation reactor may be compositionally worse than the shale gas composition. There are several separation and recycle process configuration options to avoid a large recycle ratio, and here we consider the two following configurations:

In the first configuration, labeled Process I, the vapor stream coming out of the condenser (Figure 6.3, V101) after the oligomerization reactor is directly recycled to the fresh NGL stream entering the dehydrogenation reactor R101 (Process I, Figure 6.3). In order to avoid a large accumulation of methane, the CH_4/C_{2+} separation step must recover a large percentage of methane. For 86% and 96% methane recovery, the recycle ratios are 4.8 and 1.4, respectively, for Process I. Membrane separation can achieve 86% recovery, but it is difficult to achieve 96% recovery, which may require refrigeration and/or a multiple-stage cascade membrane system [129, 130] . Thus, for Process I, the CH_4/C_{2+} separation step was designed to recover 96% of the methane in the feed.

The second configuration, labeled Process II, entails multiple recycle loops (Process II, Figure 6.4). By compressing and cooling the vapor stream (Figure 6.4, 210) to 275 K, a liquid stream containing up to 30% mono olefins of C_2, C_3, and C_4 and 40% of C_2, C_3, and C_4 alkanes is obtained, and combining this liquid stream with the feed to the oligomerization reaction results in the two recycle loops shown in Figure 6.4. This results in smaller recycle ratios compared to those of Process I, as the light alkenes are reacted in the oligomerization reactor. The vapor stream (Figure 6.4, 211) from the second condenser (Figure 6.4, 211) contains up to 20% methane. After compressing the vapor to 30 bar, the vapor is combined with the incoming shale gas stream (Figure 6.4, 202). This setup results in two loops. Each loop has a recycle ratio of less than two.

We proposed and simulated two different process designs for NGL-to-liquid fuel using Aspen Plus. The stream-data results of processes I and II are shown in Tables 6.2 and 6.3, respectively. These data were used to perform the techno-economic analysis.
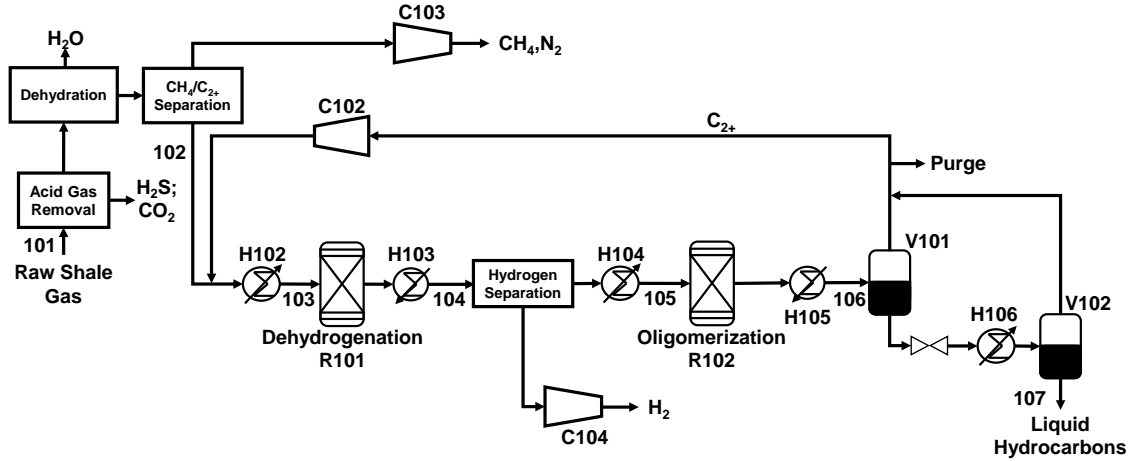
Figure 6.3.: Process flow sheet for ERC Process I.
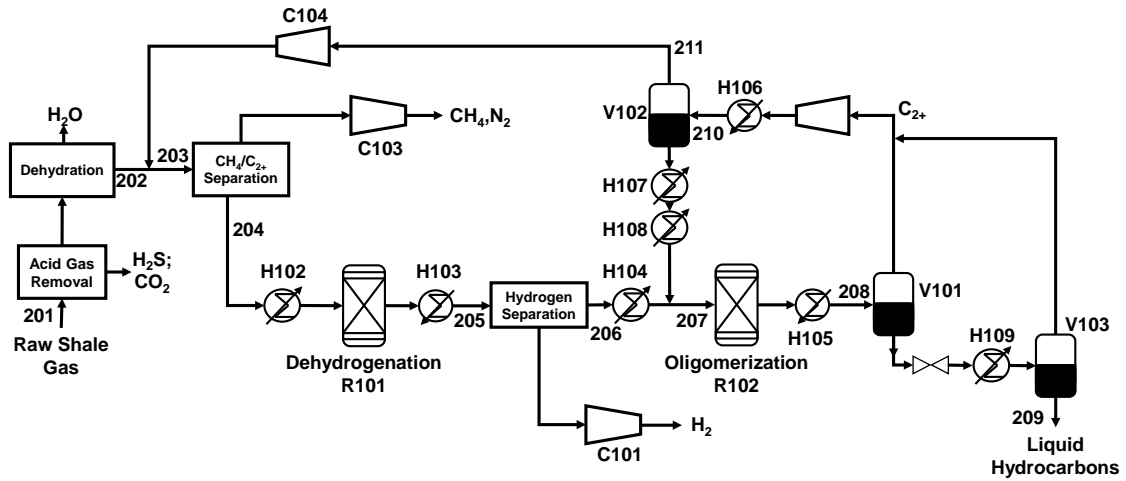
Figure 6.4.: Process flow sheet for ERC Process II.

6.5   Results and Discussion

As mentioned earlier, REQUIL and RGIBBS reactor models were used to model catalytic dehydrogenation and oligomerization reactions, respectively. For dehydro-

Table 6.2.: Key stream data for Process I. NGL: natural gas liquid.

Stream Name	Raw Shale Gas	Fresh NGL	Dehydrogenation Feed	Hydrogen Membrane Feed	Oligomerization Feed	Per Pass Product	Fuel-Grade Hydrocarbons	Hydrogen Rich Outlet
Stream Number	101	102	103	104	105	106	107	108
Components (Mole %)								
H_2	-	-	14.21	28.69	15.17	17.20	-	83.59
CO_2	0.57	-	-	-	-	-	-	-
CH_4	57.55	8.11	20.72	17.23	19.81	22.46	0.01	6.72
C_2H_6	19.89	46.92	29.54	15.80	18.18	20.61	0.45	6.16
C_2H_4	-	-	0.36	9.05	10.41	0.43	-	3.53
C_3H_8	11.30	30.92	12.11	3.39	4.22	4.79	1.27	-
C_3H_6	-	-	6.69	12.24	15.25	8.28	1.65	-
$n-C_4H_{10}$	2.82	7.84	3.35	1.34	1.67	1.90	3.33	-
$i-C_4H_{10}$	0.96	2.65	4.70	3.91	4.87	5.52	6.08	-
$n-C_5H_{12}$	0.55	1.53	0.72	0.60	0.75	0.85	4.13	-
$i-C_5H_{12}$	0.38	1.05	0.59	0.49	0.61	0.69	2.82	-
C_6H_{14}	0.22	0.61	0.20	0.16	0.20	0.23	1.68	-
C_7H_{16}	0.09	0.25	0.07	0.06	0.07	0.08	0.69	-
C_8H_{18}	0.04	0.11	0.03	0.03	0.03	0.04	0.31	-
N_2	5.20	-	-	-	-	-	-	-
H_2S	0.29	-	-	-	-	-	-	-
H_2O	0.15	-	-	-	-	-	-	-
C_4H_8	-	-	4.38	5.09	6.34	6.32	8.94	-
C_5H_{10}	-	-	1.75	1.46	1.82	4.24	18.63	-
C_6H_{12}	-	-	0.45	0.37	0.47	2.68	18.83	-
C_7H_{14}	-	-	0.10	0.08	0.10	1.83	15.08	-
C_8H_{16}	-	-	-	-	-	0.56	4.85	-
C_9H_{18}	-	-	-	-	-	0.59	5.21	-
$C_{10}H_{20}$	-	-	-	-	-	0.15	1.28	-
$C_{11}H_{22}$	-	-	-	-	-	0.30	2.64	-
$C_{12}H_{24}$	-	-	-	-	-	0.24	2.13	-
Total Flow (kmol/h)	4834	1733	6475	7789	6251	5514	626	1539
Temperature (K)	308	1073	1073	473	573	275	295	473
Pressure (bar)	30	7	6	6	5	5	1	1

genation, the conversions of ethane, propane, and butane per pass were 37.76%, 65.63%, and 50.16%, respectively, for Process I and Process II. In steam cracking, the molar conversion of ethane to ethylene is approximately 70% and the main by-product

Table 6.3.: Key stream data for Process II.

Stream Name	Raw Shale Gas	Fresh Demethanizer Feed	Demethanizer Feed	Dehydrogenation Feed	Hydrogen Membrane Feed	Fresh Oligomerization Feed	Oligomerization Feed	Per Pass Product	Fuel-Grade Hydrocarbons	Off-Gas	Recycle Gas
Stream Number	201	202	203	204	205	206	207	208	209	210	211
Components (Mole %)											
H_2	-	-	8.49	-	25.72	15.31	13.43	15.81	-	18.65	22.47
CO_2	0.57	-	-	-	-	-	-	-	-	-	-
CH_4	57.55	58.14	41.40	12.08	8.98	9.40	8.30	9.77	-	11.52	13.80
C_2H_6	19.89	20.09	22.51	41.17	17.26	18.08	16.63	19.57	0.30	23.03	26.48
C_2H_4	-	-	0.30	0.55	13.72	14.38	12.62	0.58	-	0.68	0.79
C_3H_8	11.30	11.42	9.36	18.22	3.38	4.22	4.43	5.22	0.98	5.98	5.98
C_3H_6	-	-	5.01	9.16	16.96	21.16	19.90	11.14	1.56	12.85	13.26
$n-C_4H_{10}$	2.82	2.85	2.30	4.47	1.07	1.34	1.87	2.20	2.65	2.12	1.39
$i-C_4H_{10}$	0.96	0.97	3.54	6.90	5.12	6.39	8.22	9.68	7.35	10.10	7.79
$n-C_5H_{12}$	0.55	0.55	0.42	0.82	0.61	0.76	1.06	1.25	4.21	0.72	0.20
$i-C_5H_{12}$	0.38	0.38	0.33	0.65	0.48	0.60	0.88	1.04	2.91	0.70	0.25
C_6H_{14}	0.22	0.22	0.14	0.27	0.20	0.25	0.27	0.32	1.68	0.08	0.01
C_7H_{16}	0.09	0.09	0.06	0.11	0.08	0.10	0.10	0.11	0.69	0.01	-
C_8H_{18}	0.04	0.04	0.03	0.05	0.04	0.05	0.04	0.05	0.31	-	-
N_2	5.20	5.25	3.27	-	-	-	-	-	-	-	-
H_2S	0.29	-	-	-	-	-	-	-	-	-	-
H_2O	0.15	-	-	-	-	-	-	-	-	-	-
C_4H_8	-	-	2.35	4.56	5.64	7.04	8.67	8.58	8.33	8.62	6.21
C_5H_{10}	-	-	0.46	0.90	0.67	0.83	2.65	5.80	17.67	3.68	1.22
C_6H_{12}	-	-	0.04	0.08	0.06	0.08	0.73	3.71	18.71	1.02	0.11
C_7H_{14}	-	-	-	0.01	-	-	0.17	2.56	15.49	0.23	0.01
C_8H_{16}	-	-	-	-	-	-	0.02	0.79	5.07	0.02	-
C_9H_{18}	-	-	-	-	-	-	0.01	0.85	5.52	0.01	-
$C_{10}H_{20}$	-	-	-	-	-	-	-	0.21	1.37	-	-
$C_{11}H_{22}$	-	-	-	-	-	-	-	0.43	2.85	-	-
$C_{12}H_{24}$	-	-	-	-	-	-	-	0.35	2.33	-	-
Total Flow (kmol/h)	4834	4785	7689	3951	5319	4262	4861	4130	629	3502	2903
Temperature (K)	308	323	325	1073	473	573	573	573	294	278	274
Pressure (bar)	30	29	29	5	5	4	4	4	1	1	5

is a hydrogen-rich off gas [20]. Clearly, the catalytic molar conversion of ethane to ethylene is lower, but reported catalyst for the dehydrogenation of ethylene has shown

to have high selectivity toward the dehydrogenation of ethane and to suppress the hydrogenolysis of ethane to methane. One of the performance metrics is the overall amount of C_{2+} being converted to C_{4+}. Equation (3) defines this metric as follows:

$$Conversion_{C_{2+}} = \frac{\sum_{i=2}^{4} C_{i,in} - C_{i,out}}{\sum_{i=2}^{4} C_{i,in}},\tag{6.3}$$

where $C_{i,in}$ is the molar flow rate of hydrocarbons with carbon number i in the dry and sweet shale gas stream and $C_{i,out}$ is the molar flow rate of the hydrocarbons with carbon number i in the final liquid hydrocarbon, hydrogen-rich, and methane-rich streams (Figure 6.3: liquid hydrocarbons; H_2; CH_4, N_2). The overall C_{2+} conversion was calculated to be 76% and 72% for Processes I and II, respectively. The loss of reactants is due to the purge streams and gas membrane separation. These conversions translate to 139 and 141 BPD of liquid hydrocarbons per MMSCFD of shale gas from the Bakken field used in our simulation. Existing GTL plants using natural gas yield approximately 134 BPD per MMSCFD [131]. Both Processes I and II achieve similar yields. It is estimated that the hydrocarbon yield from syngas followed by Fischer–Tropsch is 135 bbl/MMSCF of ethane, and gasoline yield from syngas followed by methanol synthesis and methanol-to-gasoline is 111 bbl/MMSCF of ethane. The main distinctions between the two proposed processes are the process complexity, the degree of methane recovery, and their economics. Process I only possesses one recycle loop and fewer unit operations compared to Process II, which has two recycle loops and more unit operations. Demethanization in Process I cannot be achieved using existing membrane technology, while in Process II, gas membrane separation is viable for methane removal.

6.5.1   Energy Integration

Each process design has several process cooling and heating duties. Within the recycle loop, the recycle stream is heated to 1073 K from ambient temperature (308 K) after being combined with the fresh feed stream. The final liquid hydrocarbon stream is

brought back to ambient temperature and pressure. Additionally, the dehydrogenation and olefin coupling reactions are endothermic and exothermic, respectively. Operating costs include cooling and heating duties. Integrating these duties can reduce the overall operating cost, since identifying one heat integration results in two operating cost savings, heating and cooling duties. Thermal pinch analysis can be used to determine the best heat integration in a process. The Aspen Energy Analyzer was used to determine the minimum heating and cooling duties for the two process designs considered here.

(a)   (b)
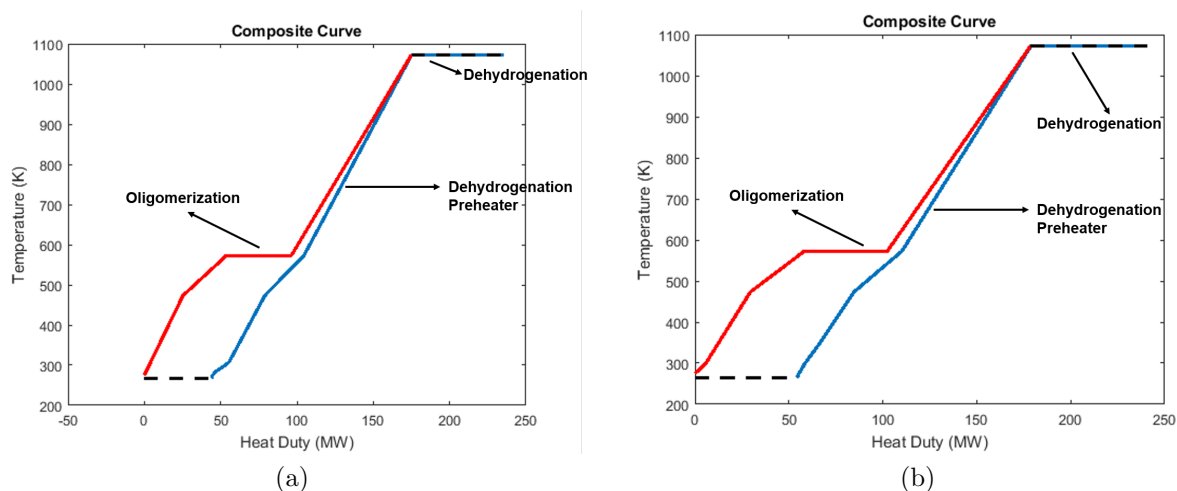
Figure 6.5.: (**a**) Composite curve for Process I. (**b**) Composite curve for Process II.

As shown in Figures 6.5a and 6.5b, the minimum heat duty is the horizontal gap between the cooling (blue line) and the heating curve (red line). For Process I, it was 64 MW, which is the heat of reaction for dehydrogenation. Thermal pinch results also indicated that the heat duty requirement could be reduced by 72%. For Process II, it was 65 MW, which is approximately the heat of reaction for dehydrogenation. Both minimum heat duties are equivalent to the heat of the reaction in dehydrogenation. Hence, the heat flows within the loops were being integrated except for the dehydrogenation, as it demands heat at 1073 K and no other unit

operation generates heat at that temperature. The minimum cooling duty can further reduce the electricity consumption through the means of co-generation [46, 132].

Using the heating and cooling utilities prior to heat integration, the process thermal efficiency was calculated and shown in Table 6.4. For the efficiency calculation, the energy inputs were set on the basis of primary energy and the products were taken to be only liquid hydrocarbons. Hydrogen and pipeline quality gas are considered.The equation below describes this efficiency:

$$\eta = \frac{\dot{m}_{LiquidHydrocarbons}LHV_{LiquidHydrocarbons} + \dot{m}_{HydrogenRich}LHV_{HydrogenRich} + \dot{m}_{MethaneRich}LHV_{MethaneRich}}{\dot{m}_{ShaleGas}LHV_{ShaleGas} + Q_{Heat} + Q_{Electricity}},$$

$$(6.4)$$

where $\dot{m}_i$ is the mass flow rate of stream i, LHV_i is the lower heating value of stream i, Q_{Heat} is the total heat consumption from heat exchangers and reactors, and $Q_{Electricity}$ is the total heat consumption for electricity. These efficiencies are higher compared to GTL-FT (Fischer–Tropsch) and GTL-MTG (methanol-to-gasoline) efficiencies of 56% and 41%, respectively. Of course, GTL-FT releases a large amount of heat from the Fischer–Tropsch reactor that could be used for co-generation to improve that process efficiency. The catalytic dehydrogenation of light alkanes followed by oligomerization has the potential to be more efficient than existing technologies.

Table 6.4.: Thermal efficiency for the proposed processes and existing technologies. FT: Fischer–Tropsch; GTL: gas-to-liquid; MTG: methanol-to-gasoline.

	Thermal Efficiency
Process I	0.83
Process II	0.88
GTL-FT	0.56
GTL-MTG	0.41

6.5.2   Economics

In order to measure the economic performance of the processes proposed in this study, an economic analysis was performed to estimate the total capital investment (TCI) and return-on-investment (ROI). Standard procedures were used to assess those economic parameters [46]. Table 6.5 summarizes the cost parameters that were assumed and the operating costs of both processes. Note that here we are only considering the NGL from shale gas and the resulting liquid hydrocarbon product. Hence, we are not considering the capital cost for methane gas treatment and revenue gained from methane. As shown in Table 6.5, the main difference between the operating costs of Process I and Process II lies in the electricity consumption.

Table 6.5.: Key economic parameters and operating costs for Process I and II. MM-SCFD: million standard cubic feet per day.

Item	Unit Cost	Process I (MMUSD)	Process II (MMUSD)
NGL in Shale Gas	$2.5/MMSCFD	32.7	32.7
Heating Utility	$4/MMBtu	6.2	6.3
Cooling Utility	$2/MMBtu	2.7	2.8
Electricity	$0.045/kWh	6.4	9.7
Liquid Hydrocarbon Sales	$1.19/gal	224	227

6.5.2.1   Total Capital Investment (TCI)

In order to estimate the total capital investment, two techniques were used together to estimate the capital cost of each unit operation. First, standard sizing algorithms and calculation in Aspen Economic Analyzer were used to estimate most of the unit operations. Second, a combination of cost charts, Lang's method, and estimates from various pieces of literature were used to estimate the dehydrogenation reactor and other unit operations [46, 133]. Tables B.1 and B.2 in the Supplementary Information summarize the TCI distribution for these processes and also the technique used for each unit operation. The estimated TCIs for Process I and Process II were $251

million and \$243 million, respectively. For comparison with other existing processes (i.e., GTL-FT and GTL-MTG), to produce the same amount of liquid hydrocarbons, GTL–FT costs between 300 to 525 million USD [107, 108] and GTL–MTG costs approximately 1.5 billion USD [20, 134]. SynFuels International Inc.'s GTL process is estimated to have TCI of \$135 MMUSD for 20 MMSCFD. Using the sixth-tenth rule, the estimated capital cost for a 90 MMSCFD plant is \$332 MMUSD. Figure 6.6 highlights the comparison of the processes in this work with other existing technologies. The TCI for the processes proposed here was at least 17% less than the alternate technologies.
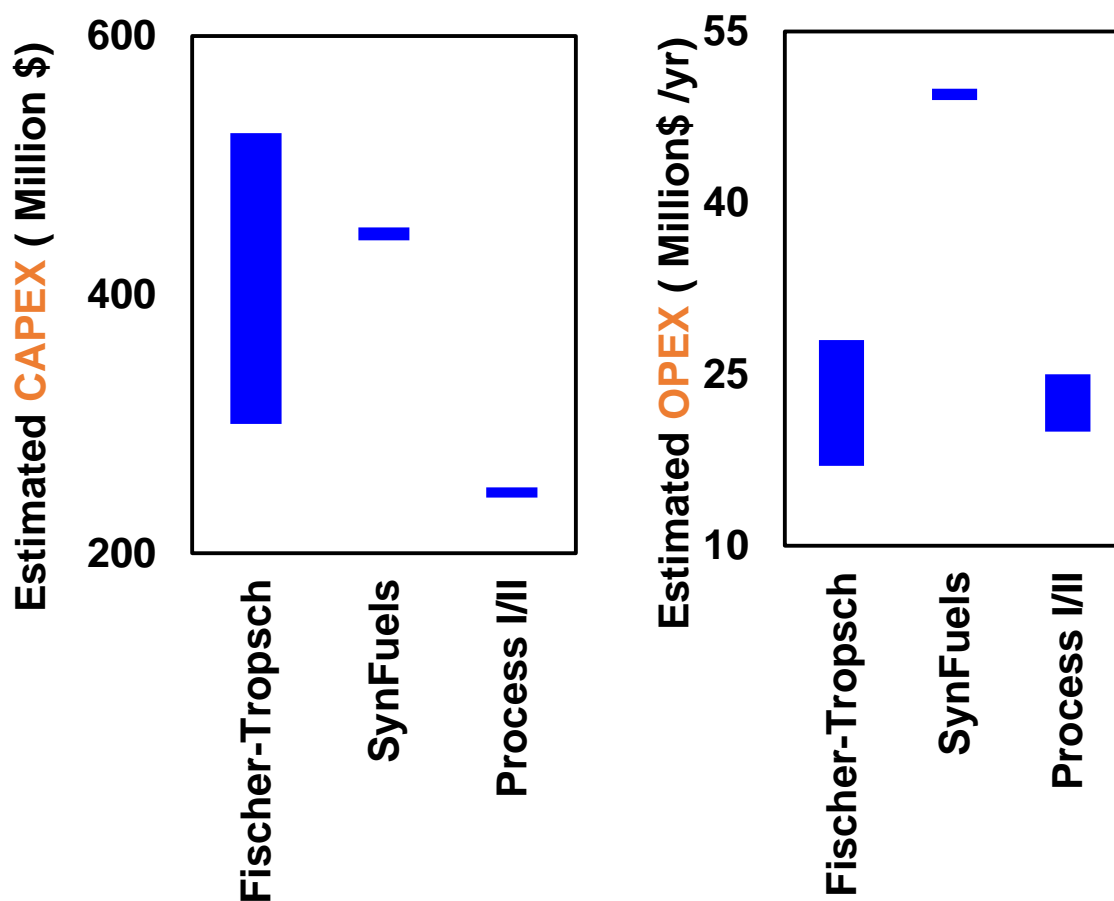

Figure 6.6.: Comparison of total capital and operating costs from this study with the capital and operating costs of other existing technologies.

6.5.2.2 ROI and Payback Period

Besides the TCI, ROI is generally used to determine the economic feasibility of a plant. In order to calculate these values, the following assumptions are made: (1) linear depreciation model of five year period with 10% salvage value at the end of the period; (2) tax rate is 30% and the discount rate is 10%. Further details on the ROI evaluation can be found in the Supplementary Information. The ROI is calculated to be 0.52 and 0.54 for Processes I and II, respectively. A process with an ROI of 0.15 or higher is considered to be lucrative. The slight difference in ROI of Processes I and II is due to the difference in the TCI of the two processes. Although Process II has a higher operating cost and a lower C2 and C3 recovery. The annual net income for this process is higher because of the lower depreciation. Therefore, this results a slightly higher ROI compared to Process I. Despite Process II having a slightly higher ROI, Process I involves a demethanizer with 95% methane recovery, which can be difficult to achieve using membrane separation technology. Note that a gas membrane system is generally deployed for gas plants of size less than 100 MMSCFD and the size of the plant considered here is 96 MMSCFD. Therefore, the ROI difference between these two processes may widen at smaller plant sizes.

The ROI values can be directly translated into payback period. The payback periods for Processes I and II are 1.9 years and 1.8 years, respectively. Considering the decline of well productivity, which can be up to 75% within three years, the payback periods of these processes are well within the lifetime of these wells [135].

6.6 Potential of the Proposed Processes for Modularization

Considering the economic opportunity presented by either stranded shale gas or associated shale gas, the proposed process can be deployed at modular scales. In a modular plant, the process equipment and its supporting components are mounted within a structural metal framework and each module is a self-contained process [136]. There are many factors that determine whether a process is amenable to modularization,

and process complexity is one of the main factors. As stated previously, many of the existing technologies for thes conversion of natural gas liquid to liquid fuel have only been implemented at large scale. Steam cracking plants generally process up to 1500 MM lbs/year. The smallest proved GTL plant using Fischer–Tropsch process that has been proven is 14,700 bbl/day. These GTL processes mainly consist of syngas generation followed by Fischer–Tropsch or methanol synthesis with methanol-to-gasoline (MTG).

Each process described in this study is amenable to process modularization. However, the proposed process has been shown to be potentially more economically lucrative assuming high selectivity of catalytic dehydrogenation and considering the large boiling point difference between liquid hydrocarbons and light hydrocarbons. Steam cracking requires either downstream upgrading and/or separation in order to hydrogenate acetylene or remove methane. Fischer–Tropsch synthesis produces a liquid product that requires hydrogenation and hydrocracking. Therefore, the existing NTL processes clearly require more unit operations than the proposed NTL process. Although the economics of modular NTL proposed in this work have not been evaluated, this NTL process has the potential to be more economically modularized compared to other existing technologies.

6.7   Conclusions

Shale gas is projected to be one of the dominant forces in the future of the United States energy landscape. With a projected supply for more than one hundred years, fitting the shale gas into the United States energy landscape requires processes that can convert shale gas into different forms of energy. Shale gas utilization can vary widely from electricity production to chemical production. However, existing infrastructure and market saturation do not allow for some of its common utilizations, particularly as chemical feedstock for olefin plants. However, converting shale gas to liquid fuel can overcome limitations from existing infrastructure, as liquid fuel is transportable and easily marketed. Several large shale gas fields are located in historically non-gas-

producing regions (e.g., Bakken and Niobrara basins), where infrastructure for gas distribution is limited or non-existent. Liquid hydrocarbons can be easily transported through different channels such as railways and trucks for further refining. In addition to this, the liquid fuel market is widely distributed with minimal time-variant demand. Herein, we proposed a process for the transformation of shale gas that converts the NGL in shale gas into liquids using a catalytic system that differs from the existing technologies.

There were two processes proposed in this study depending on the separation technology that is considered. Both processes entail dehydrogenation and oligomerization reactions. The main distinctions between the two processes are the separation technology used for the demethanizer and the recycle loop configurations. In terms of energy consumption, both processes have similar minimum heating and cooling duties and product yield. The main difference in energy consumption between these two processes is the electricity consumption. Based on the evaluated economic indicators, Process II is more economically attractive than Process I. In addition, it is not clear whether the demethanizer separation target in Process I can be achieved using membrane technology solely and whether Process I is amenable to modularization for wellhead applications.

Existing GTL-FT and GTL-MTG processes are estimated to be economically less attractive than the proposed processes. The total capital costs of Processes I and II are estimated to be at least 17% lower than that of the conventional GTL processes. The payback periods of Processes I and II are about two years. Clearly, the proposed processes are expected to be much more lucrative than existing technologies.

This study only considered regional or gathering scale facilities. Varying the scale of this proposed process can impact not only its economics, but also the economics and supply chain of NGL, liquid fuels, and other end-use products, especially when the entire chemical manufacturing industry is considered. It is worth assessing how this process fits into the current United States chemical manufacturing industry.

7. CONCLUSIONS AND OUTLOOK

7.1 Overview

This dissertation has identified various carbon efficient and novel reaction networks and process configurations for transforming biomass carbon into fuels and chemicals. These findings come from the implementation and construction of systems-level molecular mapping, which is an optimization-based approach that enables the identification of reaction sequences for the transformation of biomass to target molecules. These efforts have been complemented by analysis of optimal utilization of biomass constituents in lignocellulosic biomass toward various target molecules, such as diesel and commodity chemicals.

In addition to this, circumstances associated with the geographical distribution of shale gas presented an opportunity to valorize this shale resource. In this dissertation, a catalytic shale gas upgrading process to liquid hydrocarbon is synthesized and proposed. Preliminary thermodynamic analysis and thermal efficiencies evaluation indicated that this process concept has the potential to be economically competitive and lucrative.

Below is a summary of the key findings, along with recommendations for future work.

7.2 Basic Guideline for Biomass Carbon Transformation toward Fuels and Chemicals

Analysis of various biomass transformation processes in this dissertation have revealed the following points for carbon-efficient conversion of biomass:

- Light oxygenates that are not directly susceptible toward carbon coupling reactions are likely to be highly oxidized and resembles light commodity chemicals

that are employed today. Therefore, they should be channeled toward light chemical production.

- Heavy oxygenates should be mainly channeled toward fulfilling diesel and jet fuel production. These molecules generate C10+ oxygenates which can be directly hydrodeoxygenated or further carbon-coupled with itself or other C10+ to form heavier oxygenates before undergoing hydrodeoxygenation.

- Assuming 100% carbon efficiency, there is a sufficient amount of carbon in lignin to sustain the current and future production of commodity chemicals. The use of lignin as pre-cursor to commodity chemicals has been demonstrated through propylbenzene, which serves as a platform toward all major aromatic-based commodity chemicals. Therefore, the carbon in lignin should not be employed for power and heat generation if a carbon efficient conversion system is desired.

- Levoglucosan, which is a significant product during fast pyrolysis, can be activated in several options for carbon coupling reaction. These include a reduction to levoglucosenone, further reduction to 5-HMF, and oxidation to gluconic acid. Among these options, reduction to levoglucosenone holds the most promise as its formation and subsequent carbon coupling can occur consecutively within a reducing environment. Coupling of gluconic acid leads to carbon loss and generation of gluconic acid from levoglucosan requires an oxidation environment. Combining this system with hydrodeoxygenation can be cumbersome as a reducing environment is needed.

7.3 Process Design of CDL and H2Bioil Process

Process design of H2Bioil and catalytic depolymerization using in-house experimental data determines the potential of these thermochemical processes.

Existing H2Bioil process generates up to 34.1% of biomass carbon as char using a poplar feed. As SA biomass itself is limited, carbon flow to any non-liquid hydrocarbon must be minimized. Lignin had been suggested as a major contributor to char

formation. By first removing lignin using catalytic depolymerization of lignin, a lignin-poor residue and substituted propylphenols are recovered. Preliminary analysis indicates that an integrated CDL H2Bioil process has the potential to improve carbon efficiency by 28% which results in an overall carbon efficiency of 53.9%. The process synthesis of the process integration must be carefully analyzed

7.4   Upgrading Fast Pyrolysis Vapor toward Higher Molecular Weight Products

Fast-Hydropyrolysis vapor of cellulose generates a mixture of oxygenated molecules with levoglucosan and glycolaldehyde as the two most abundant products. Although HDO catalyst can substantially convert these molecules to hydrocarbons, the resulting hydrocarbons have relatively low carbon number (less than six). Glycolaldehyde is known to undergo aldol condensation readily, but it is unclear whether levoglucosan can undergo aldol condensation or aldol condensation itself is the optimal carbon coupling reaction for this mixture. The known reaction sequence for coupling levoglucosan involves oxidation followed by ketonization. This reaction sequence, however, requires both oxidation and reduction environments which can be difficult to couple in a gas-phase reactor. Our approach identified another reaction sequence. This reaction sequence is preferred because all reactions are all under reducing condition and also co-generates an aldol condensation reaction site.

Several light oxygenates, such as methanol and acetic acid, are not susceptible to carbon coupling in the three-bed catalytic systems. Unless these molecules are intercepted, they ultimately become light hydrocarbons which are unsuitable as liquid fuel and, under current circumstances, undesirable. Therefore, we envision a co-production of chemicals and liquid fuel from fast-hydropyrolysis vapor of cellulose. This is also true for fast-hydropyrolysis of poplar as experimental results indicate that hemicellulose and lignin vapor from pyrolysis mainly contains furans and aromatics, respectively. Therefore, light oxygenates derived from cellulose should be still directed toward chemical production.

7.5 Biorefinery: A Roadmap toward Sustainable Production of Fuels and Chemicals from Lignocellulosic Biomass

Integrated biorefinery has the potential to achieve 63% carbon recovery compared to 33% and 60% carbon recovery of standalone fast pyrolysis and standalone lignocellulosic fermentation, respectively. Other reported biorefinery systems achieve 25-60% carbon recovery.

In the integrated biorefinery case, it is evident that selective removal of each constituents using C3Bio processes results in higher carbon recovery than direct employment of C3Bio processes toward intact lignocellulosic biomass.

The use of lignin as pre-cursor to commodity chemicals has been demonstrated as propylbenzene serves as a platform toward all major aromatic-based commodity chemicals. In addition, there is sufficient carbon in lignin to sustain the current and future production of commodity chemicals.

Light oxygenates are utilized as precursors toward commodity chemicals, ligands for chemical and diesel production. Heavy oxygenates are mainly channeled toward fulfilling diesel and jet fuel production. These molecules generate C11+ oxygenates which can be directly hydrodeoxygenated or further carbon-coupled with itself or other C11+ to form heavier oxygenates prior to undergoing hydrodeoxygenation.

At best, the maximum potential carbon recovery of an integrated biorefinery based on new primary processes is estimated to be 58%, which suggests that current potential of sustainably available biomass can only sustain either diesel and jet fuel, commodity chemicals, or supplying one demand while leaving the other at a deficit.

One underlying assumption regarding this approach is ideal separation following the reactor. This idealization was made to reduce the complexity of the problem. It is established that separation can incur large energy requirement. Therefore, it is imperative to account for separations during the synthesis of biorefinery configuration.

7.6 Valorization of Shale Gas Condensate through Catalytic Dehydrogenation and Oligomerization

There are two processes proposed in this study depending on the separation technology that is considered. Both processes entail dehydrogenation and oligomerization reactions. The main distinctions between the two processes are the separation technology used for demethanizer and recycle loop configurations. In terms of energy consumption, both processes have similar minimum heating and cooling duties and yield of the products. The main difference in energy consumption between these two processes is electricity consumption. Based on the evaluated economic indicators, Process II is more economically attractive than Process I. In addition, it is not clear whether the demethanizer separation target in Process I can be achieved using membrane technology solely and whether Process I is amenable to modularization for wellhead applications.

Existing GTL-FT and GTL-MTG processes are estimated to be economically less attractive than the proposed processes. The total capital costs of Process I and II are estimated to be at least 17% lower than that of the conventional GTL processes. Process I and II payback periods are about two years. Clearly, the proposed processes are expected to be much more lucrative than existing technologies.

This study has only considered regional or gathering scale facility. Varying the scale of this proposed process can impact not only its economics, but also the economics and supply chain of NGL, liquid fuels, and other end-use products, especially when the entire chemical manufacturing industry is considered. It is worth assessing how this process fits into the current United States chemical manufacturing industry.

7.7 Concluding Remarks

Sustainably available biomass has the potential to replace petroleum resources in a petroleum-deprived future. Biorefinery concept is particularly promising as it envisions the transformation of lignocellulosic biomass into target molecules that are needed

today. As sustainably available biomass is limited, it is crucial to identify high carbon efficient biorefinery configuration. In this dissertation, several process configurations are identified and they hold the potential to be more carbon efficient than existing reported biorefinery system. They can produce not only fuel-type molecules, but also commodity chemical molecules ranging from light chemicals, such as ethylene and propylene, to heavy chemicals, such as aromatics.

Despite efforts in finding reaction sequences and efforts to convert lignocellulosic biomass into today's commodity chemicals and fuel, it is crucial to understand the optimal utilization of biomass from its true natural structure. Current fuel and chemical landscapes are based on fossil resource and, although biomass and fossil resource are made up of similar atoms, their compositions and structures are very distinct. Chemicals derived from petroleum today did not inherit their utilization in our society today; instead, extensive research studies characterized their properties and identified proper utilization. Therefore, similarly, biomass-derived molecules need not be converted to chemicals derived from petroleum. Instead, their properties and potential must be thoroughly defined and investigated. Therefore, instead of using biomass as a feedstock substitute for petroleum resource, the entire portfolio of commodity chemicals might also be altered to effectively use biomass resource as a feedstock for commodity chemical production. This, in effect, might require the current society to evolve as it once did after the discovery of fossil resources.

In order to properly place lignocellulosic biomass into renewable energy, we must understand the properties and potential uses of hemicellulose-, lignin-, and cellulose-derived molecules. Thus, enabling the current society to reach beyond the paradigm of a fossil-based economy.

As the transition toward a sustainable economy is gradual, there is a need to switch toward cleaner and more sustainable fossil resources. Recent shale gas boom in the United States has opened up an ample supply of shale gas reserves. Along with electricity generation and residential heating, the excess amount of shale gas and its

scattered presence in the United States have brought an opportunity to valorize its natural gas liquids to liquid hydrocarbons and chemicals.

Employment of shale resources can vary from region to region and it is imperative to consider the spatial variation of shale gas availability and local demands for certain blend stocks or fuel requirements. Therefore, it is imperative to synthesize process flow sheets capable of handling several major regions containing shale resources and also their subregions.

REFERENCES

REFERENCES

[1] Lee R. Lynd, Charles Wyman, M. Laser, D. Johnson, and R. Landucci. Strategic biorefinery analysis: analysis of biorefineries. *National Renewable Energy Laboratory, Golden, CO, Technical Report No. NREL/SR-510-35578*, 2005.

[2] Elizabeth Kemf and United Nations Environment Programme. *GCO–Global Chemicals Outlook: towards sound management of chemicals.* 2013. OCLC: 919008518.

[3] History of energy consumption in the United States, 1775 - 2009. *U.S. Energy Information Administration.*

[4] International Energy Outlook 2009. Technical report, U.S. Energy Information Administration, 2009.

[5] Alan W Weimer. Solarthermal chemical processing challenges and commercial path forward. *Current Opinion in Chemical Engineering*, 1(3):211–217, August 2012.

[6] Rakesh Agrawal and Navneet R. Singh. Synergistic routes to liquid fuel for a petroleum-deprived future. *AIChE Journal*, 55(7):1898–1905, July 2009.

[7] Rakesh Agrawal, Navneet R. Singh, Fabio H. Ribeiro, and W. Nicholas Delgass. Sustainable fuel for the transportation sector. *Proceedings of the National Academy of Sciences*, 104(12):4828–4833, March 2007.

[8] Onur Onel, Alexander M Niziolek, and Christodoulos A Floudas. Integrated biomass and fossil fuel systems towards the production of fuels and chemicals: state of the art approaches and future challenges. *Current Opinion in Chemical Engineering*, 9:66–74, August 2015.

[9] Susanne B. Jones, Corinne Valkenburg, Christie W. Walton, Douglas C. Elliott, Johnathan E. Holladay, Don J. Stevens, Christopher Kinchin, and Stefan Czernik. Production of gasoline and diesel from biomass via fast pyrolysis, hydrotreating and hydrocracking: a design case. *Pacific Northwest National Laboratory: Richland, WA*, 2009.

[10] Jesse Q. Bond, Aniruddha A. Upadhye, Hakan Olcay, Geoffrey A. Tompsett, Jungho Jae, Rong Xing, David Martin Alonso, Dong Wang, Taiying Zhang, Rajeev Kumar, Andrew Foster, S. Murat Sen, Christos T. Maravelias, Robert Malina, Steven R. H. Barrett, Raul Lobo, Charles E. Wyman, James A. Dumesic, and George W. Huber. Production of renewable jet fuel range alkanes and commodity chemicals from integrated catalytic processing of biomass. *Energy and Environmental Science*, 7(4):1500–1523, 2014.

[11] Michiel Dusselier, Mark Mascal, and Bert F. Sels. Top chemical opportunities from carbohydrate biomass: a chemist's view of the Biorefinery. *Topics in Current Chemistry*, 353:1–40, 2014.

[12] Lik Yin Ng, Viknesh Andiappan, Nishanth G. Chemmangattuvalappil, and Denny K. S. Ng. A systematic methodology for optimal mixture design in an integrated biorefinery. *Computers & Chemical Engineering*, 81:288–309, October 2015.

[13] Ethanol Biorefinery Locations, May 2015.

[14] Srinivas Rangarajan, Aditya Bhan, and Prodromos Daoutidis. Rule-based generation of thermochemical routes to biomass conversion. *Industrial & Engineering Chemistry Research*, 49(21):10459–10470, 2010.

[15] Adam J. Kelloway. *Biorefinery systems engineering: From facility location to process synthesis and design.* PhD thesis, UNIVERSITY OF MINNESOTA, 2015.

[16] Jeehoon Han, S. Murat Sen, Jeremy S. Luterbacher, David Martin Alonso, James A. Dumesic, and Christos T. Maravelias. Process systems engineering studies for the synthesis of catalytic biomass-to-fuels strategies. *Computers & Chemical Engineering*, 81:57–69, October 2015.

[17] Daniel J. Garcia and Fengqi You. Multiobjective optimization of product and process networks. *AICHE Journal*, 61(2):530–554, February 2015.

[18] DennyKS Ng, Viet Pham, MahmoudM El-Halwagi, Arturo Jimnez-Gutirrez, and HDennis Spriggs. A Hierarchical Approach to the Synthesis and Analysis of Integrated Biorefineries. In *Design for Energy and the Environment*, pages 425–432. CRC Press, June 2009.

[19] Pascual Eduardo Murillo-Alvarado, Jos Mara Ponce-Ortega, Medardo Serna-Gonzlez, Agustn Jaime Castro-Montoya, and Mahmoud M. El-Halwagi. Optimization of Pathways for Biorefineries Involving the Selection of Feedstocks, Products, and Processing Steps. *Industrial & Engineering Chemistry Research*, 52(14):5177–5190, April 2013.

[20] Mohamed M. B. Noureldin and Mahmoud M. El-Halwagi. Synthesis of C-H-O Symbiosis Networks. *AIChE Journal*, 61(4):1242–1262, April 2015.

[21] A. Voll and W. Marquardt. Reaction network flux analysis: Optimization-based evaluation of reaction pathways for biorenewables processing. *AIChE Journal*, 58(6):1788–1801, June 2012.

[22] W. Alex Marvin, Srinivas Rangarajan, and Prodromos Daoutidis. Automated Generation and Optimal Selection of Biofuel-Gasoline Blends and Their Synthesis Routes. *Energy & Fuels*, 27(6):3585–3594, June 2013.

[23] Manuel Hechinger, Anna Voll, and Wolfgang Marquardt. Towards an integrated design of biofuels and their production pathways. *Computers & Chemical Engineering*, 34(12):1909–1918, 2010.

[24] Kirsten Ulonska, Mirko Skiborowski, Alexander Mitsos, and Jorn Viell. Early-stage evaluation of biorefinery processing pathways using process network flux analysis. *AIChE Journal*, pages n/a–n/a, May 2016.

[25] Kirsten Ulonska, Anna Voll, and Wolfgang Marquardt. Screening Pathways for the Production of Next Generation Biofuels. *Energy & Fuels*, 30(1):445–456, January 2016.

[26] Jeffrey J. Siirola. The impact of shale gas in the chemical industry. *AIChE Journal*, 60(3):810–819, March 2014.

[27] Victoria M. Ehlinger, Kerron J. Gabriel, Mohamed M. B. Noureldin, and Mahmoud M. El-Halwagi. Process Design and Integration of Shale Gas to Methanol. *ACS Sustainable Chemistry & Engineering*, 2(1):30–37, January 2014.

[28] Chang He and Fengqi You. Shale Gas Processing Integrated with Ethylene Production: Novel Process Designs, Exergy Analysis, and Techno-Economic Analysis. *Industrial & Engineering Chemistry Research*, 53(28):11442–11459, July 2014.

[29] Bulba Ka and Krouskop Pe. Compositional variety complicates processing plans for US shale gas. *Oil & Gas Journal*, 107(10):50–55, 2009.

[30] Vinod Kumar Venkatakrishnan, W. Nicholas Delgass, Fabio H. Ribeiro, and Rakesh Agrawal. Oxygen removal from intact biomass to produce liquid fuel range hydrocarbons via fast-hydropyrolysis and vapor-phase catalytic hydrodeoxygenation. *Green Chemistry*, 17(1):178–183, 2015.

[31] Vinod Kumar Venkatakrishnan, John C. Degenstein, Andrew D. Smeltz, W. Nicholas Delgass, Rakesh Agrawal, and Fabio H. Ribeiro. High-pressure fast-pyrolysis, fast-hydropyrolysis and catalytic hydrodeoxygenation of cellulose: production of liquid fuel from biomass. *Green Chemistry*, 16(2):792–802, 2014.

[32] Matthew S. Mettler, Alex D. Paulsen, Dionisios G. Vlachos, and Paul J. Dauenhauer. Pyrolytic conversion of cellulose to fuels: levoglucosan deoxygenation via elimination and cyclization within molten biomass. *Energy & Environmental Science*, 5(7):7864, 2012.

[33] EIA - Natural Gas Pipeline Network - Transporting Natural Gas in the United States.

[34] M. H. Langholtz, B. J. Stokes, and L. M. Eaton. 2016 Billion-ton report: Advancing domestic resources for a thriving bioeconomy, Volume 1: Economic availability of feedstock. 2016.

[35] Rakesh Agrawal. Novel process for producing liquid hydrocarbon by pyrolysis of biomass in …, March 2009.

[36] Rakesh Agrawal. Novel integrated gasification - pyrolysis process, April 2009.

[37] Dharik S. Mallapragada, Mohit Tawarmalani, and Rakesh Agrawal. Synthesis of augmented biofuel processes using solar energy. *AIChE Journal*, 60(7):2533–2545, July 2014.

[38] Pushkaraj R. Patwardhan, Robert C. Brown, and Brent H. Shanks. Understanding the Fast Pyrolysis of Lignin. *ChemSusChem*, 4(11):1629–1636, November 2011.

[39] Trenton Parsell, Sara Yohe, John Degenstein, Tiffany Jarrell, Ian Klein, Emre Gencer, Barron Hewetson, Matt Hurt, Jeong ImKim, Harshavardhan Choudhari, Basudeb Saha, Richard Meilan, Nathan Mosier, Fabio Ribeiro, W. NicholasDelgass, Clint Chapple, Hilkka I.Kenttmaa, Rakesh Agrawal, and Mahdi M.Abu-Omar. A synergistic biorefinery based on catalytic conversion of lignin prior to cellulose starting from lignocellulosic biomass. *Green Chemistry*, 17(3):1492–1499, 2015.

[40] Hao Luo, Ian M. Klein, Yuan Jiang, Hanyu Zhu, Baoyuan Liu, Hilkka I. Kenttmaa, and Mahdi M. Abu-Omar. Total Utilization of Miscanthus Biomass, Lignin and Carbohydrates, Using Earth Abundant Nickel Catalyst. *ACS Sustainable Chemistry & Engineering*, 4(4):2316–2322, April 2016.

[41] Kefeng Huang, Wangyun Won, Kevin J. Barnett, Zachary J. Brentzel, David M. Alonso, George W. Huber, James A. Dumesic, and Christos T. Maravelias. Improving economics of lignocellulosic biofuels: An integrated strategy for coproducing 1,5-pentanediol and ethanol. *Applied Energy*, November 2017.

[42] R.F. Probstein and R.E. Hicks. *Synthetic Fuels*. 2006.

[43] Emre Gencer, D. S. Mallapragada, Mohit Tawarmalani, and Rakesh Agrawal. Synergistic biomass and natural gas conversion to liquid fuel with reduced CO 2 emissions. In *8th International Conference on Foundations of Computer-Aided Process Design, Elsevier, Cle Elum, WA*, pages 525–530, 2014.

[44] Terry L. Marker, Larry G. Felix, Martin B. Linck, Michael J. Roberts, Pedro Ortiz-Toral, and Jim Wangerow. Integrated hydropyrolysis and hydroconversion (IH2) for the direct production of gasoline and diesel fuels or blending components from biomass, Part 2: continuous testing. *Environmental Progress & Sustainable Energy*, 33(3):762–768, 2014.

[45] Cynthia B. Tarun, Eric Croiset, Peter L. Douglas, Murlidhar Gupta, and Mohammad H. M. Chowdhury. Techno-economic study of CO2 capture from natural gas based hydrogen plants. *International Journal of Greenhouse Gas Control*, 2007.

[46] Mahmoud M. El-Halwagi. *Sustainable Design Through Process Integration: Fundamentals and Applications to Industrial Pollution Prevention, Resource Conservation, and Profitability Enhancement*. Butterworth-Heinemann, Amsterdam ; Boston, 1st edition edition, 2011.

[47] AJJE Eerhart, W. J. J. Huijgen, R. J. H. Grisel, J. C. Van Der Waal, E. De Jong, A. de Sousa Dias, A. P. C. Faaij, and Martin Kumar Patel. Fuels and plastics from lignocellulosic biomass via the furan pathway; a technical analysis. *Rsc Advances*, 4(7):3536–3549, 2014.

[48] Dhairya D Mehta. Kinetic studies of model reactions to transform biomass into fuels. *Theses and Dissertations Available from ProQuest*, pages 1–186, January 2014.

[49] William Alexander Marvin. Optimal supply chain and product design of biofuels. August 2013.

[50] Srinivas Rangarajan, Aditya Bhan, and Prodromos Daoutidis. Identification and analysis of synthesis routes in complex catalytic reaction networks for biomass upgrading. *Applied Catalysis B: Environmental*, 145:149–160, 2014.

[51] Srinivas Rangarajan, Ted Kaminski, Eric Van Wyk, Aditya Bhan, and Prodromos Daoutidis. Language-oriented rule-based reaction network generation and analysis: Algorithms of RING. *Computers & Chemical Engineering*, 64:124–137, May 2014.

[52] Srinivas Rangarajan, Aditya Bhan, and Prodromos Daoutidis. Language-oriented rule-based reaction network generation and analysis: Description of RING. *Computers & Chemical Engineering*, 45:114–123, 2012.

[53] Srinivas Rangarajan, Aditya Bhan, and Prodromos Daoutidis. Language-oriented rule-based reaction network generation and analysis: Applications of RING. *Computers & Chemical Engineering*, 46:141–152, 2012.

[54] William H. Green. Automated Discovery of New Chemical Reactions and Accurate Calculation of Their Rates. Technical report, DTIC Document, 2015.

[55] Sidney W. Benson and Jerry H. Buss. Additivity Rules for the Estimation of Molecular Properties. Thermodynamic Properties. *The Journal of Chemical Physics*, 29(3):546–572, September 1958.

[56] Robert A. Meyers. *Handbook of Petroleum Refining Processes, Fourth Edition*. McGraw-Hill Education, New York, NY, 4 edition edition, July 2016.

[57] Janice Smith. *Organic Chemistry*. McGraw-Hill Education, New York, NY, 4 edition edition, January 2013.

[58] Qiang Lu, Xiao-ning Ye, Zhi-bo Zhang, Chang-qing Dong, and Ying Zhang. Catalytic fast pyrolysis of cellulose and biomass to produce levoglucosenone using magnetic SO42-/TiO2-Fe3o4. *Bioresource Technology*, 171:10–15, November 2014.

[59] Ehud. Keinan and Noam. Greenspoon. Highly chemoselective palladium-catalyzed conjugate reduction of .alpha.,.beta.-unsaturated carbonyl compounds with silicon hydrides and zinc chloride cocatalyst. *Journal of the American Chemical Society*, 108(23):7314–7325, November 1986.

[60] K. Toch, J.W. Thybaut, and G.B. Marin. Ethene oligomerization on Ni-SiO2-Al2o3: Experimental investigation and Single-Event MicroKinetic modeling. *Applied Catalysis A: General*, 489:292–304, January 2015.

[61] Y. Halpern, R. Riffer, and A. Broido. Levoglucosenone (1,6-anhydro-3,4-dideoxy-.DELTA.3-.beta.-D-pyranosen-2-one). Major product of the acid-catalyzed pyrolysis of cellulose and related carbohydrates. *The Journal of Organic Chemistry*, 38(2):204–209, January 1973.

[62] Alan Allgeier, Namal Desilva, Ekaterini Korovessi, Carl Menning, Joachim Ritter, Sourav Sengupta, and Christina Stauffer. Process for Preparing 1, 6-Hexanediol, July 2013. CIB: B01J23/44; C07C29/94; C07C31/20.

[63] Shengcheng Luo and John L. Falconer. Acetone and Acetaldehyde Oligomerization on TiO2 Surfaces. *Journal of Catalysis*, 185(2):393–407, July 1999.

[64] Shengcheng Luo and John L. Falconer. Aldol condensation of acetaldehyde to form high molecular weight compounds on TiO2. *Catalysis Letters*, 57:89–93, February 1999.

[65] Shuai Wang, Konstantinos Goulas, and Enrique Iglesia. Condensation and esterification reactions of alkanals, alkanones, and alkanols on TiO 2 : Elementary steps, site requirements, and synergistic effects of bifunctional strategies. *Journal of Catalysis*, 340:302–320, August 2016.

[66] H. Idriss, K. S. Kim, and M. A. Barteau. CarbonCarbon Bond Formation via Aldolization of Acetaldehyde on Single Crystal and Polycrystalline TiO2 Surfaces. *Journal of Catalysis*, 139(1):119–133, January 1993.

[67] James E. Rekoske and Mark A. Barteau. Kinetics, Selectivity, and Deactivation in the Aldol Condensation of Acetaldehyde on Anatase Titanium Dioxide. *Industrial & Engineering Chemistry Research*, 50(1):41–51, January 2011.

[68] James E. Rekoske and Mark A. Barteau. Competition between Acetaldehyde and Crotonaldehyde during Adsorption and Reaction on Anatase and Rutile Titanium Dioxide. *Langmuir*, 15(6):2061–2070, March 1999.

[69] Yong Liu, Lungang Chen, Tiejun Wang, Qi Zhang, Chenguang Wang, Jinyue Yan, and Longlong Ma. One-Pot Catalytic Conversion of Raw Lignocellulosic Biomass into Gasoline Alkanes and Chemicals over LiTaMoO6 and Ru/C in Aqueous Phosphoric Acid. *ACS Sustainable Chemistry & Engineering*, 3(8):1745–1755, August 2015.

[70] Aron Deneyer, Tom Renders, Joost Van Aelst, Sander Van den Bosch, Dries Gabrils, and Bert F Sels. Alkane production from biomass: chemo-, bio- and integrated catalytic approaches. *Current Opinion in Chemical Biology*, 29:40–48, December 2015.

[71] A. Deneyer, T. Ennaert, G. Cavents, J. Dijkmans, J. Vanneste, C. M.Courtin, M. Dusselier, and B. F.Sels. Compositional and structural feedstock requirements of a liquid phase cellulose-to-naphtha process in a carbon- and hydrogen-neutral biorefinery context. *Green Chemistry*, 18(20):5594–5606, 2016.

[72] Michael W.Nolte, Jing Zhang, and Brent H.Shanks. Ex situ hydrodeoxygenation in biomass pyrolysis using molybdenum oxide and low pressure hydrogen. *Green Chemistry*, 18(1):134–138, 2016.

[73] Xuesong Zhang, Hanwu Lei, Lei Zhu, Yi Wei, Yupeng Liu, Gayatri Yadavalli, Di Yan, Joan Wu, and Shulin Chen. Production of renewable jet fuel range alkanes and aromatics via integrated catalytic processes of intact biomass. *Fuel*, 160:375–385, November 2015.

[74] Xuesong Zhang, Hanwu Lei, Lu Wang, Lei Zhu, Yi Wei, Yupeng Liu, Gayatri Yadavalli, and Di Yan. Renewable gasoline-range aromatics and hydrogen-enriched fuel gas from biomass via catalytic microwave-induced pyrolysis. *Green Chemistry*, 17(7):4029–4036, 2015.

[75] W. Alex Marvin, Lanny D. Schmidt, and Prodromos Daoutidis. Biorefinery Location and Technology Selection Through Supply Chain Optimization. *Industrial & Engineering Chemistry Research*, 52(9):3192–3208, March 2013.

[76] The Outlook for Energy: A View to 2040. Technical report, ExxonMobil, 2016.

[77] Use of Oil - Energy Explained, Your Guide To Understanding Energy - Energy Information Administration.

[78] Michael P. Rosynek. Industrial Chemicals, 2012.

[79] Pushkaraj R. Patwardhan, Robert C. Brown, and Brent H. Shanks. Product Distribution from the Fast Pyrolysis of Hemicellulose. *ChemSusChem*, 4(5):636–643, May 2011.

[80] D. Humbird, R. Davis, L. Tao, C. Kinchin, D. Hsu, A. Aden, P. Schoen, J. Lukas, B. Olthof, M. Worley, D. Sexton, and D. Dudgeon. Process Design and Economics for Biochemical Conversion of Lignocellulosic Biomass to Ethanol: Dilute-Acid Pretreatment and Enzymatic Hydrolysis of Corn Stover. Technical Report NREL/TP-5100-47764, 1013269, March 2011.

[81] Eurick S. Kim, Shuo Liu, Mahdi M. Abu-Omar, and Nathan S. Mosier. Selective Conversion of Biomass Hemicellulose to Furfural Using Maleic Acid with Microwave Heating. *Energy & Fuels*, 26(2):1298–1304, February 2012.

[82] Ximing Zhang, Barron B. Hewetson, and Nathan S. Mosier. Kinetics of Maleic Acid and Aluminum Chloride Catalyzed Dehydration and Degradation of Glucose. *Energy & Fuels*, 29(4):2387–2393, April 2015.

[83] Yulin Lu and Nathan S. Mosier. Kinetic modeling analysis of maleic acid-catalyzed hemicellulose hydrolysis in corn stover. *Biotechnology and Bioengineering*, 101(6):1170–1181, December 2008.

[84] I. Agirrezabal-Telleria, Y. Guo, F. Hemmann, P. L.Arias, and E. Kemnitz. Dehydration of xylose and glucose to furan derivatives using bifunctional partially hydroxylated MgF 2 catalysts and N 2 -stripping. *Catalysis Science & Technology*, 4(5):1357–1368, 2014.

[85] Basak Cinlar. Acid catalyzed carbohydrate degradation and dehydration. page 187.

[86] G. Ucar. Pretreatment of poplar by acid and alkali for enzymatic hydrolysis. *Wood Science and Technology*, 24(2):171–180, June 1990.

[87] W. Alex Marvin, Lanny D. Schmidt, Saif Benjaafar, Douglas G. Tiffany, and Prodromos Daoutidis. Economic Optimization of a Lignocellulosic Biomass-to-Ethanol Supply Chain. *Chemical Engineering Science*, 67(1):68–79, January 2012.

[88] James Speight. *Chemical Process and Design Handbook*. McGraw-Hill Professional, New York, 1 edition edition, December 2001.

[89] Jeffrey A. Herron, Tyler Vann, Nhung Duong, Daniel E. Resasco, Steven Crossley, Lance L. Lobban, and Christos T. Maravelias. A Systems-Level Roadmap for Biomass Thermal Fractionation and Catalytic Upgrading Strategies. *Energy Technology*, 5(1):130–150, January 2017.

[90] C. Luke Williams, Chun-Chih Chang, Phuong Do, Nima Nikbin, Stavros Caratzoulas, Dionisios G. Vlachos, Raul F. Lobo, Wei Fan, and Paul J. Dauenhauer. Cycloaddition of biomass-derived furans for catalytic production of renewable p-xylene. *Acs Catalysis*, 2(6):935–939, 2012.

[91] M. Perez, C. B. Caputo, R. Dobrovetsky, and D. W. Stephan. Metal-free transfer hydrogenation of olefins via dehydrocoupling catalysis. *Proceedings of the National Academy of Sciences*, 111(30):10917–10921, July 2014.

[92] Albrecht Berkessel, Thomas J. S. Schubert, and Thomas N. Mller. Hydrogenation without a Transition-Metal Catalyst: On the Mechanism of the Base-Catalyzed Hydrogenation of Ketones. *Journal of the American Chemical Society*, 124(29):8693–8698, July 2002.

[93] S. Vaitheeswaran, Sara K. Green, Paul Dauenhauer, and Scott M. Auerbach. On the Way to Biofuels from Furan: Discriminating DielsAlder and Ring-Opening Mechanisms. *ACS Catalysis*, 3(9):2012–2019, September 2013.

[94] Shoucheng Du, David P. Gamliel, Marcus V. Giotto, Julia A. Valla, and George M. Bollas. Coke formation of model compounds relevant to pyrolysis bio-oil over ZSM-5. *Applied Catalysis A: General*, 513:67–81, March 2016.

[95] Sean Edward DeRosa. *Impact of natural gas and natural gas liquids on chemical manufacturing in the United States*. Thesis, April 2016.

[96] Hydrocarbon Gas Liquids (HGL): Recent Market Trends and Issues. Technical report, U.S. Energy Information Administration, WASHINGTON, D. C., November 2014.

[97] Short-Term Outlook for Hydrocarbon Gas Liquids. Technical report, U.S. Energy Information Administration, March 2016.

[98] ELIZABETH M. WALLACE. *Associated Shale Gasfrom Flares to Rig Power*. PhD thesis, Texas A&M University, 2014.

[99] Chang He, Ming Pan, Bingjian Zhang, Qinglin Chen, Fengqi You, and Jingzheng Ren. Monetizing shale gas to polymers under mixed uncertainty: Stochastic modeling and likelihood analysis. *AIChE Journal*, 64(6):2017–2036, June 2018.

[100] Jian Gong and Fengqi You. A new superstructure optimization paradigm for process synthesis with product distribution optimization: Application to an integrated shale gas processing and chemical manufacturing process. *AIChE Journal*, 64(1):123–143, January 2018.

[101] Growing U.S. HGL production spurs petrochemical industry investment - Today in Energy - U.S. Energy Information Administration (EIA).

[102] Jesse F. Goellner and Booz A. Hamilton. Expanding the Shale Gas Infrastructure. *AIChE Journal*, pages 49–59, August 2012.

[103] Dharik S. Mallapragada, Gang Duan, and Rakesh Agrawal. From shale gas to renewable energy based transportation solutions. *Energy Policy*, 67:499–507, April 2014.

[104] DHARIK S MALLAPRAGADA and RAKESH AGRAWAL. Role of Natural Gas in Americas Energy Future: Focus on Transportation. page 6.

[105] Thomas H. Russell. Changes of Cryogenic, Amine Plant and Standard Plant Concept. *The Gas Processing Experts, Thomas Russell Co.*, pages 1–18, 2011.

[106] Joel Cantrell, Jerry A. Bullin, Gavin McIntyre, Clark Butts, and Bryon Cheatham. Economic Alternative for Remote and Stranded Natural Gas and Ethane in the US.

[107] B Lutz. New Age Gas-to-Liquid Processing. *Hydrocarbon Engineering*, (23), November 2001.

[108] M Senden and M McEwan. The Shell Middle Distillates Synthesis (SMDS) Experience, June 2000.

[109] Zhenwei Wu, Evan C. Wegener, Han-Ting Tseng, James R. Gallagher, James W. Harris, Rosa E. Diaz, Yang Ren, Fabio H. Ribeiro, and Jeffrey T. Miller. PdIn intermetallic alloy nanoparticles: highly selective ethane dehydrogenation catalysts. 6(18):6965–6976, September 2016.

[110] Viktor J. Cybulskis, Brandon C. Bukowski, Han-Ting Tseng, James R. Gallagher, Zhenwei Wu, Evan Wegener, A. Jeremy Kropf, Bruce Ravel, Fabio H. Ribeiro, Jeffrey Greeley, and Jeffrey T. Miller. Zinc Promotion of Platinum for Catalytic Light Alkane Dehydrogenation: Insights into Geometric and Electronic Effects. *ACS Catalysis*, 7(6):4173–4181, June 2017.

[111] Jesper J. H. B. Sattler, Javier Ruiz-Martinez, Eduardo Santillan-Jimenez, and Bert M. Weckhuysen. Catalytic Dehydrogenation of Light Alkanes on Metals and Metal Oxides. *Chemical Reviews*, 114(20):10613–10653, October 2014.

[112] Chinmoy Baroi, Anne M. Gaffney, and Rebecca Fushimi. Process economics and safety considerations for the oxidative dehydrogenation of ethane using the M1 catalyst. *Catalysis Today*, 298:138–144, December 2017.

[113] Kaidong Chen, Alexis T. Bell, and Enrique Iglesia. Kinetics and Mechanism of Oxidative Dehydrogenation of Propane on Vanadium, Molybdenum, and Tungsten Oxides. *The Journal of Physical Chemistry B*, 104(6):1292–1299, February 2000.

[114] D Wolf, N Dropka, Q Smejkal, and O Buyevskaya. Oxidative dehydrogenation of propane for propylene production comparison of catalytic processes. *Chemical Engineering Science*, 56(2):713–719, January 2001.

[115] Tao Ren, Martin Patel, and Kornelis Blok. Olefins from conventional and heavy feedstocks: Energy use in steam cracking and alternative processes. *Energy*, 31(4):425–451, March 2006.

[116] Alain Chauvel and Gilles Lefebvre. *Petrochemical Processes: Technical and Economic Characteristics*. Gulf Publishing Company, 1989. Google-Books-ID: 6sjrAAAAMAAJ.

[117] Michael Ford and Neal Davis. Nonmarketed natural gas in North Dakota still rising due to higher total production - Today in Energy - U.S. Energy Information Administration (EIA), March 2014.

[118] Dollahon PR. Gas Processors Suppliers Association.

[119] A Bhan, S Hsu, G Blau, J Caruthers, V Venkatasubramanian, and W Delgass. Microkinetic modeling of propane aromatization over HZSM-5. *Journal of Catalysis*, 235(1):35–51, October 2005.

[120] Field Demonstration of A Membrane Process to Recover Heavy Hydrocarbons and to Remove Water from Natural Gas. Technical Report DE-FC26-99FT40723, National Energy Technology Laboratory (NETL), August 2007.

[121] Richard W. Baker. Future Directions of Membrane Gas Separation Technology. *Industrial & Engineering Chemistry Research*, 41(6):1393–1411, March 2002.

[122] Mesfin Getu, Shuhaimi Mahadzir, Nguyen Van Duc Long, and Moonyong Lee. Techno-economic analysis of potential natural gas liquid (NGL) recovery processes under variations of feed compositions. *Chemical Engineering Research and Design*, 91(7):1272–1283, July 2013.

[123] O.M. Ilinitch, G.L. Semin, M.V. Chertova, and K.I. Zamaraev. Novel polymeric membranes for separation of hydrocarbons. *Journal of Membrane Science*, 66(1):1–8, February 1992.

[124] Heinz Zimmermann and Roland Walzl. *Ullmann's Encyclopedia of Industrial Chemistry*. Wiley-VCH Verlag GmbH & Co. KGaA, Weinheim, Germany, April 2009.

[125] A.A. Al-Rabiah, K.D. Timmerhaus, and R.D. Noble. Membrane Technology for Hydrogen Separation in Ethylene Plants. Melbourne, Australia, September 2001.

[126] K. G. Wilshier, P. Smart, R. Western, T. Mole, and T. Behrsing. Oligomerization of propene over H-ZSM-5 zeolite. *Applied Catalysis*, 31(2):339–359, June 1987.

[127] Dbora S. Fernandes, Cludia O. Veloso, and Cristiane A. Henriques. Modified HZSM-5 zeolites for the conversion of ethylene into propylene and aromatics.

[128] K. Toch, J. W. Thybaut, M. A. Arribas, A. Martnez, and G. B. Marin. Steering linear 1-alkene, propene or gasoline yields in ethene oligomerization via the interplay between nickel and acid sites. *Chemical Engineering Science*, 173:49–59, December 2017.

[129] Jianguo Xu and Rakesh Agrawal. Membrane separation process analysis and design strategies based on thermodynamic efficiency of permeation. *Chemical Engineering Science*, 51(3):365–385, February 1996.

[130] Max Peters, Klaus Timmerhaus, Ronald West, and Max Peters. *Plant Design and Economics for Chemical Engineers*. McGraw-Hill Education, New York, 5 edition edition, December 2002.

[131] Gas to liquids (GTL), June 2015.

[132] Easa I. Al-musleh, Dharik S. Mallapragada, and Rakesh Agrawal. Continuous power supply from a baseload renewable power plant. *Applied Energy*, 122:83–93, June 2014.

[133] Abdulsalam Hussain Qassim and Ajay Kumar Mathur. Optimized CAPEX and OPEX for Acid Gas Removal Units: Design AGR without Sulphur Recovery Processes. Society of Petroleum Engineers, 2012.

[134] Terry Helton and Mitch Hindman. Methanol to Gasoline: An Alternative for Liquid Fuel Production, July 2014.

[135] Enno Peters. Visualizing US Shale Oil Production.

[136] Minbo Yang and Fengqi You. Modular methanol manufacturing from shale gas: Techno-economic and environmental analyses of conventional large-scale production versus small-scale distributed, modular processing. *AIChE Journal*, 64(2):495–510, February 2018.
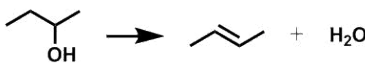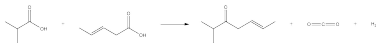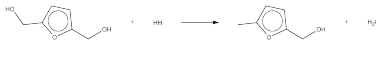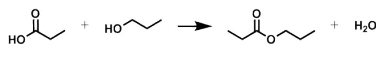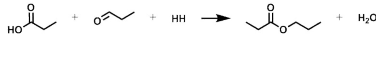
APPENDICES
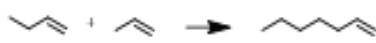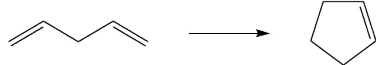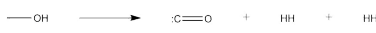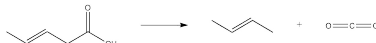
A. APPENDIX A
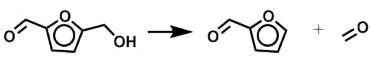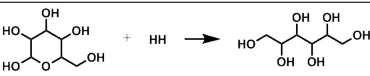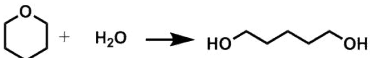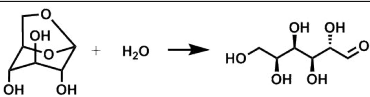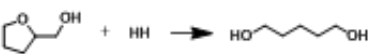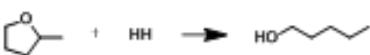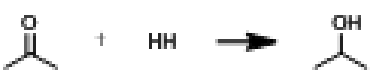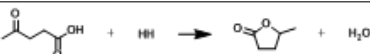
A.1 Reaction Rules
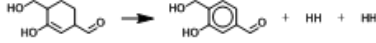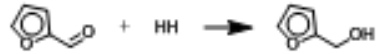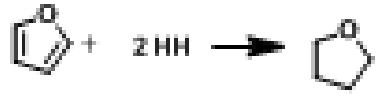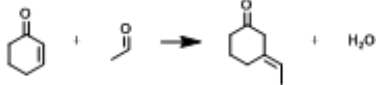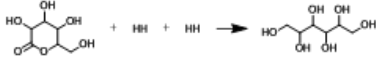
Table A.1 below summarizes all reaction rules included for systems-level molecular mapping in this dissertation. Each example illustrates what transformation the reaction rule performs.
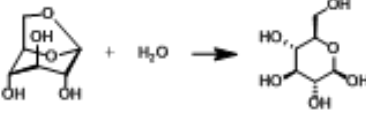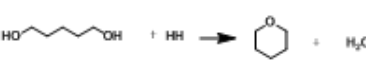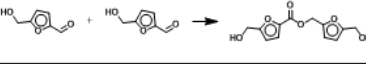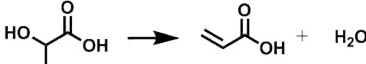
Table A.1.: List of reaction rules considered in chapter 3.

No.	Name	Example	Source
1	1,2 Alcohol Dehydration		Smith, J.G. Organic Chemistry. Third Edition. McGrawHill. 2011. Kochloefl, The dehydration of alcohols on alumina: XIV. Reactivity and mechanism. Journal of Catalysis, 24, 57 68, 1972
2	Ketonization		Dumesic, et. al. IECR 2010, 49, 6027 6033. J Cat. 2009, 266, 71
3	Hydrogenolysis of Alcohol		Neurock, Davis, and Dumesic, JACS 2011, 133, 12675 - 12689
4	Hydrogenolysis of Aromatic Alcohol		Resasco et al. Journal of Catalysis 2011, 277, 1-13
5	Ester formation (Carboxylic Acid + Alcohol)		J. Bedard, H. Chiang, and A. Bhan, Kinetics and mechanism of acetic acid esterification with ethanol on zeolites, Journal of Catalysis, vol. 290, pp. 210219, Jun. 2012.
6	Ester formation (Aldehyde + Alcohol)		S. Wang, K. Goulas, and E. Iglesia, Condensation and esterification reactions of alkanals, alkanones, and alkanols on TiO2: Elementary steps, site requirements, and synergistic effects of bifunctional strategies, Journal of Catalysis, vol. 340, pp. 302320, Aug. 2016.
7	Lactone to Diol		Smith, J.G. Organic Chemistry. Third Edition. McGrawHill. 2011. Hermann, U; Emig, G. , Liquid Phase Hydrogenation of Maleic Anhydride and Intermediates on Copper-Based and Noble Metal Catalysts. IECR 1997, 36 (8), 2885 2896. Hermann, U; Emig, G., Liquid Phase Hydrogenation of Maleic Anhydride and Intermediates on Copper-Based and Noble Metal Catalysts. IECR 1997, 36 (8), 2885 2896.

8	Acid Hydrogenolysis		Smith, J.G. Organic Chemistry. Third Edition. McGrawHill. 2011. P. Claus, M. Lucas, B. Lcke, T. Berndt, and P. Birke, Selective hydrogenolysis of methyl and ethyl acetate in the gas phase on copper and supported Group VIII metal catalysts, Applied Catalysis A: General, vol. 79, no. 1, pp. 118, Nov. 1991.
9	Ester Hydrogenolysis		P. Claus et. al., App Cat A: General, 79, 1991, 1-18
10	Oligomerization of Alkenes		M. G. Musolino, F. Mauriello, C. Busacca, and R. Pietropaolo, Aromatic Alcohols as Model Molecules for Studying Hydrogenolysis Reactions Promoted by Palladium Catalysts, Top Catal, vol. 58, no. 1417, pp. 10771084, Aug. 2015. [1]M. Chia, Y. J. Pagn-Torres, D. Hibbitts, Q. Tan, H. N. Pham, A. K. Datye, M. Neurock, R. J. Davis, and J. A. Dumesic, Selective Hydrogenolysis of Polyols and Cyclic Ethers over Bifunctional Surface Sites on RhodiumRhenium Catalysts, Journal of the American Chemical Society, vol. 133, no. 32, pp. 1267512689, Aug. 2011.
11	Cyclization		Smith, J.G. Organic Chemistry. Third Edition. McGrawHill. 2011
12	Glycerol Decomposition		Smith, J.G. Organic Chemistry. Third Edition. McGrawHill. 2011
13	Ethylene Glycol Decomposition		Dumesic and Mavrikakis, JPCC 2011, 115, 961- 971
14	Methanol Decomposition		Mavrikakis and Dumesic, Topics in Catalysis 2006, 37, 1, 17-28
15	Formic Acid Decomposition	$CO + H2O$	Iglesia. Angewandte Chemie Int. Ed. 48, 4800 4803, 2009
16	Lactic Acid Decomposition	$3CO + 3H2$	Iglesia. Angewandte Chemie Int. Ed. 48, 4800 4803, 2009
17	Eneoic Acid Decarboxylation		Dumesic et al., Journal of Catalysis 2011, 281, 290-299
18	Hydrogenationolysis of Anhydride to Lactone		Emig, IECR 1997, 36 (8), 2885 2896
19	Diacid Dehydration to Cyclic Anhydride		Smith, J.G. Organic Chemistry. Third Edition. McGrawHill. 2011

20	Formaldehyde Removal from HMF		Weingarten, Conner, Huber, Energy & Environmental Sciences ,2012
21	Water Gas Shift	$CO + H_2O \Rightarrow CO_2 + H_2$	Speight, Chemical Process and Design Handbook, McGraw-Hill, 2002
22	Hydrogenation of Glucose		Smith, J.G. Organic Chemistry. Third Edition. Mc-GrawHill. 2011
23	Cleavage of Ether		Smith, J.G. Organic Chemistry. Third Edition. Mc-GrawHill. 2011
24	Hydrolysis of Acetal		Smith, J.G. Organic Chemistry. Third Edition. Mc-GrawHill. 2011
25	Tautomerization of Enol		Smith, J.G. Organic Chemistry. Third Edition. Mc-GrawHill. 2011
26	Cyclic Ether Hydrogenolysis with hydroxymethyl at alpha carbon		M. Chia, Y. J. Pagn-Torres, D. Hibbitts, Q. Tan, H. N. Pham, A. K. Datye, M. Neurock, R. J. Davis, and J. A. Dumesic, Selective Hydrogenolysis of Polyols and Cyclic Ethers over Bifunctional Surface Sites on RhodiumRhenium Catalysts, Journal of the American Chemical Society, vol. 133, no. 32, pp. 1267512689, Aug. 2011.
27	Cyclic Ether Hydrogenolysis with methyl at alpha carbon		M. Chia, Y. J. Pagn-Torres, D. Hibbitts, Q. Tan, H. N. Pham, A. K. Datye, M. Neurock, R. J. Davis, and J. A. Dumesic, Selective Hydrogenolysis of Polyols and Cyclic Ethers over Bifunctional Surface Sites on RhodiumRhenium Catalysts, Journal of the American Chemical Society, vol. 133, no. 32, pp. 1267512689, Aug. 2011.
28	C=O Hydrogenation		Smith, J.G. Organic Chemistry. Third Edition. Mc-GrawHill. 2011. R. M. Rioux and M. A. Vannice, Hydrogenation/dehydrogenation reactions: isopropanol dehydrogenation over copper catalysts, Journal of Catalysis, vol. 216, no. 12, pp. 362376, May 2003.
29	CHOH Dehydrogenation		Smith, J.G. Organic Chemistry. Third Edition. Mc-GrawHill. 2011. R. M. Rioux and M. A. Vannice, Hydrogenation/dehydrogenation reactions: isopropanol dehydrogenation over copper catalysts, Journal of Catalysis, vol. 216, no. 12, pp. 362376, May 2003.
30	Keto-Acid Hydrocyclization		Smith, J.G. Organic Chemistry. Third Edition. Mc-GrawHill. 2011.

31	Naphthenes Dehydrogenation		Froment, App Cat, 24, 53 68, 1986,
32	Aromatic C=O Hydrogenation		Smith, J.G. Organic Chemistry. Third Edition. Mc-GrawHill. 2011. S. Sitthisa, T. Sooknoi, Y. Ma, P. B. Balbuena, and D. E. Resasco, Kinetics and mechanism of hydrogenation of furfural on Cu/SiO2 catalysts, Journal of Catalysis, vol. 277, no. 1, pp. 113, Jan. 2011.
33	C=C Hydrogenation		Smith, J.G. Organic Chemistry. Third Edition. Mc-GrawHill. 2011. R. D. Cortright, P. E. Levin, and J. A. Dumesic, Kinetic studies of isobutane dehydrogenation and isobutene hydrogenation over Pt/Sn-based catalysts, Industrial & engineering chemistry research, vol. 37, no. 5, pp. 17171723, 1998.
34	Furan Hydrogenation		N. Merat, C. Godawa, and A. Gasand, Hydrogenation selective de lalcool furfurylique en alcool tetrahydrofurfurylique, Journal of Molecular Catalysis, vol. 57, no. 3, pp. 397415, Jan. 1990.
35	Aldol Condensation		Kunkes, E.L.; Gurbuz, E.I.; Dumesic, J.A. J Cat 2009, 266, 236-249. Smith, J.G. Organic Chemistry. Third Edition. McGrawHill. 2011.
36	Michael Addition		Smith, J.G. Organic Chemistry. Third Edition. Mc-GrawHill. 2011.
37	Paraffin Isomerization		F. J. M. M. de Gauw, J. van Grondelle, and R. A. van Santen, The Intrinsic Kinetics of n-Hexane Hydroisomerization Catalyzed by Platinum-Loaded Solid-Acid Catalysts, Journal of Catalysis, vol. 206, no. 2, pp. 295304, Mar. 2002.
38	Ring Expansion		Smith, J.G. Organic Chemistry. Third Edition. Mc-GrawHill. 2011.
39	Lactone to Eneoic Acid		R. Gmez-Bombarelli, E. Calle, and J. Casado, Mechanisms of Lactone Hydrolysis in Acidic Conditions, The Journal of Organic Chemistry, vol. 78, no. 14, pp. 68806889, Jul. 2013. J. Q. Bond, D. Wang, D. M. Alonso, and J. A. Dumesic, Interconversion between -valerolactone and pentenoic acid combined with decarboxylation to form butene over silica/alumina, Journal of Catalysis, vol. 281, no. 2, pp. 290299, Jul. 2011.

40	Levoglucosenone Dehydration to 5-HMF		F. Cao, T. J.Schwartz, D. J.McClelland, S. H.Krishna, J. A.Dumesic, and G. W.Huber, Dehydration of cellulose to levoglucosenone using polar aprotic solvents, Energy & Environmental Science, vol. 8, no. 6, pp. 18081815, 2015.
41	LVG hydrolysis		X. Hu et al., Mediating acid-catalyzed conversion of levoglucosan into platform chemicals with various solvents, Green Chemistry, vol. 14, no. 11, p. 3087, 2012.
42	Diol to Cyclic Ether		Smith, J.G. Organic Chemistry. Third Edition. McGrawHill. 2011. Saeed Sahaebdelfar, Evaluation of Zeolites in Production of Tetrahydrofuran from 1,4-Butanediol: Performance Tests and Kinetic Investigations. IECR 2007. 46. 726-733.
43	Diels Alder		Smith, J.G. Organic Chemistry. Third Edition. McGrawHill. 2011.
44	Tishchenko Reaction		Smith, J.G. Organic Chemistry. Third Edition. McGrawHill. 2011.
45	Lactic Acid Dehydration		Smith, J.G. Organic Chemistry. Third Edition. McGrawHill. 2011.

A.2 Potential Pathways to Hydrocarbons

In case of transformation of the oxygenated intermediates to hydrocarbon molecules, the approach identified alternative optimal solutions for each intermediates. The main difference between these solutions is the order at which oxygen atoms are removed from a molecule. Considering that these oxygenates have at least five oxygen atoms per mole of molecule, there are many permutations of oxygen removal. Below are several potential pathways that were identified:
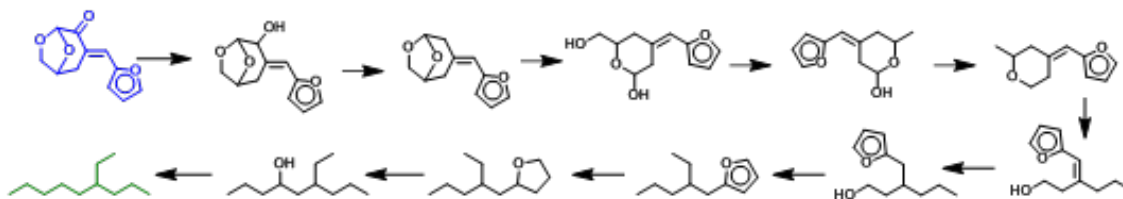
Figure A.1.: Potential pathway with the minimum number of steps to hydrodeoxygenate the starting intermediate I.
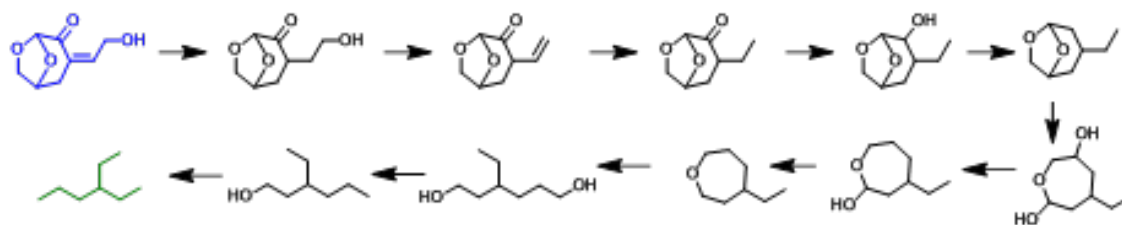
Figure A.2.: Potential pathway with the minimum number of steps to hydrodeoxygenate the starting intermediate II.
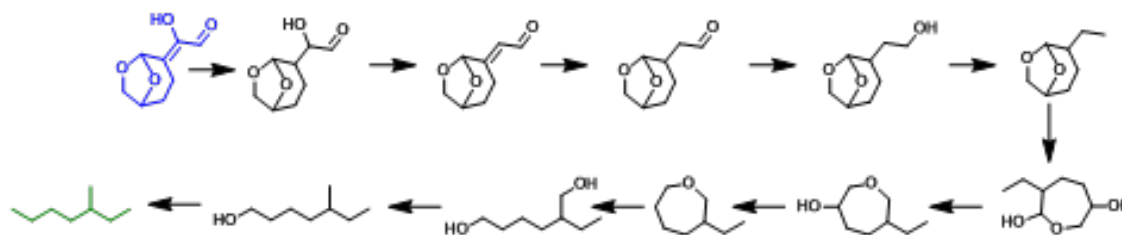
Figure A.3.: Potential pathway with the minimum number of steps to hydrodeoxygenate the starting intermediate III.
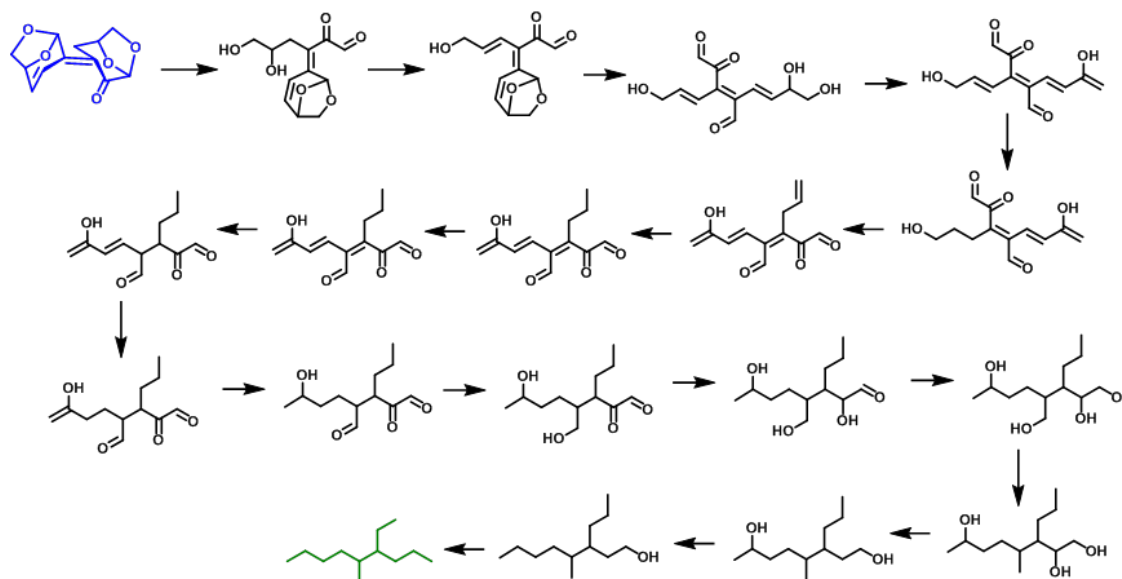
Figure A.4.: Potential pathway with the minimum number of steps to hydrodeoxygenate the starting intermediate IV.

For a complete list of all alternative solutions, refer to Appendix A. The table below summarizes the number of reactions that is in each set of alternative optimal solutions.

Table A.2.: Number of reactions in all set of alternative optimal solutions for each intermediate.

Intermediate	Number of Reactions
I	39
II	101
III	256
IV	314

A.3   Breadth-first Traversal Algorithm for Identification of Side Reactions

To identify side reactions within certain catalytic and operating condition, breadth-first search is employed along with the following two parameters for the filters:

1. Reaction Rule Chemistry

2. Estimated Gibbs Free Energy of Reaction at a temperature of interest.

In this implementation of breadth-first search, an edge, i.e. a reaction, can only be traversed if the following criteria are simultaneously satisfied:

1. The reaction belongs to a reaction rule family that has a matching chemistry with the specified catalytic chemistry.

2. The estimated Gibbs free energy of the reaction at 573 K is less than or equal to 0.

Details regarding Breadth-first traversal algorithm can be found in several literatures. The algorithm that is employed in this breadth-first search is shown below:

Using NetworkX, the terminal nodes are then identified by querying nodes with in degree ≥ 1 and out degree of zero. In the traversed network, the terminal nodes represent molecules that may form under this catalytic and operating condition.

FindSideReactions (**Initial Molecules M$_o$, Temperature, Catalytic Condition**)

ReactionStack ← {} Stack of Traversed Reactions

MoleculeQueue ← {**M$_o$**} Stack of Queued Molecules

MoleculeVisited ←{} Stack of Traversed Molecules

While !MoleculeQueue.empty() do

      M=MoleculeQueue.pop(0)

      if M not in MoleculeVisited

            MoleculeVisited.add(M)

            AdjacentMolecules contains all molecules that are connected from M

            for Molecule in AdjacentMolecules do

                  Edge=Reaction that generates Molecule from M

                  if (**Catalytic Condition** = ReactionRule of Edge) AND (GibbsFreeEnergy(**Temperature**) of Edge <= 0)

                        Continue

                        Store Edge in ReactionStack

                        Add Molecule to MoleculeQueue and MoleculeVisited

                Else:

                    Disregard this Edge and Molecule

Return All Traversed Reactions and Molecule, MoleculeVisited &ReactionStack

Figure A.5.: Pseudocode describing the breadth-first search algorithm with filters.

A.4 Reaction Rule Chemistry

Each reaction rule usually require a catalytic environment at which the reaction can occur favorably. Table A.3 below summarizes the catalytic environment in which each rule can occur.

Table A.3.: Valid catalyst functions for each reaction rule [57].

Reaction Rule	Acid	Base	Metal
1,2 Alcohol Dehydration	X	X	X
Ester formation (Carboxylic Acid + Alcohol)	X		X
Ester formation (Aldehyde + Alcohol)	X	X	X
Lactone to Diol	X	X	X
Ester Hydrogenolysis			X
Oligomerization of Alkenes			X
Cyclic Ether Hydrogenolysis w hydroxymethyl at alpha carbon			X
Cyclic Ether Hydrogenolysis w methyl at alpha carbon			X
C=O Hydrogenation			X
CHOH Dehydrogenation			X
Keto-Acid Hydrocyclization			X
Naphthenes Dehydrogenation			X
Aromatic C=O Hydrogenation			X
C=C Hydrogenation			X
Furan Hydrogenation			X
Aldol Condensation	X	X	
Michael Addition	X	X	
Paraffin Isomerization	X		
Ring Expansion	X		
Lactone to Eneoic Acid	X	X	
Eneoic Acid Decarboxylation	X	X	
Lactic Acid Dehydration	X		
Levoglucosan Dehydration to 5-HMF	X		
Levulinic and Formic Acid from 5-HMF	X		

LVG hydrolysis	X	X	
Diol to Cyclic Ether	X	X	
Diels Alder	X	X	X
Glycerol Decomposition			X
Ethylene Glycol Decomposition			X
Methanol Decomposition			X
Formic Acid Decomposition			X
Lactic Acid Decomposition			X
Tautomerization of Enol	X	X	X
Tishchenko Reaction		X	
Ether Cleavage	X		
Hydrolysis of Levoglucosan		X	
Levoglucosenone to HMF	X		
Oligomerization			X
Lactic Acid Dehydration	X		
Dehydrogenation of Naphthenes			X
Water Gas Shift			X
Hydrogenation of Glucose			X
Hydrolysis of Acetal	X		
Hydrogenationolysis of Anhydride to Lactone			X
Diacid Dehydration to Cyclic Anhydride	X		-

A.5 Side Reaction Networks

Two side reaction networks are derived using the breadth-first traversal algorithm based on the optimal reaction sequence. The first network begins with levoglucosan as the seed node and only acid catalyzed reaction rules are allowed. This network

consists of 140 reactions. The complete network is shown in Appendix B. Note that here aldol condensation and Michael addition are not considered as acid site for dehydration reaction is not suitable for these carbon coupling reactions. The second network is obtained with four intermediates highlighted in Figure 1-4 as the seed nodes and metal-acid catalyzed reaction rules are allowed. This network consists of 2,332 reactions. This is shown in Appendix B.

A.6 Aldol Condensation and Hydrodeoxygenation Reactions with Levoglucosenone and Glycolaldehyde to Hydrocarbons - Micro-Scale Pulse Reactor

The experimental setup described below was developed by Richard Caulkins and Abhijit T. Talpade from Charles D. Davidson School of Chemical Engineering. In addition, they also conducted the experiments described in Chapter 3.

A.6.1 Catalyt Preparation

The Cu/TiO2 catalyst was synthesized via electrostatic adsorption of copper onto titania. Degussa P-25 TiO2 (Aeroxide) was first densified by adding excess Millipore water to form a paste. This paste was dried at 120C overnight and ground and sieved to a particle size of less than 250 m. Copper (II) nitrate hydrate (99.999%, Alfa Aesar) was dissolved in Millipore water. Ammonium hydroxide was added to this solution until a deep blue solution was formed. TiO2 and the copper solution were combined in Millipore water and filtered. The solid was dried at room temperature and at 120C, calcined at 300C for two hours, and sieved to a particle size between 125 m and 250 m. The copper content of the catalyst was determined to be 2 wt% using a PerkinElmer 300 AAnalyst atomic absorption spectrometer.

The procedure used to synthesize PtMo/MWCNTs has been previously described [66]. It is synthesized through the incipient wetness impregnation of multiwalled carbon nanotubes (MWCNTs) (Cheap Tubes, Inc.) of Pt(NH3)4(NO3)2 (99.995%, Sigma Aldrich) and (NH4)6-Mo7O244H2O (99.98%, Sigma Aldrich). Platinum and molybdenum are in a 1:1 ratio to form the 5% PtMo catalyst. The catalyst is dried

overnight and calcined for 2 hours at 450C, then reduced at 450C in H2 for two hours. As with the Cu/TiO2 catalyst, the PtMo catalyst was sieved to a particle size between 125 m and 250 m.

A.6.2   Reactants

Levoglucosenone (95%, Carbosynth) was dissolved in water as a 48 wt% solution. Glycolaldehyde dimer (Sigma Aldrich) was dissolved in water as a 19 wt% solution. A levoglucosenone-glycolaldehyde solution was synthesized using these same materials as a 10 wt% glycolaldehyde, 42 wt% levoglucosenone solution in water, giving a levoglucosenone/glycolaldehyde molar ratio of 1.9. The glycolaldehyde dimer is known to decompose into monomer units at 100C [68].

A.6.3   Pulsed Micro-Reactor: Pyroprobe

A pulse micro-reactor was used to study aldol condensation plus hydrodeoxygenation of levoglucosenone and glycolaldehyde solutions. A CDS 5200 Pyroprobe was used to vaporize samples. 1 L droplets were deposited inside quartz tubes and heated to 300C at a rate of 1000C/s and holding at 300C for 10s. The resulting vapors were passed through a reactor containing first a bed of 2% Cu/TiO2, then a bed of 5% PtMo/MWCNTs, both held at a temperature of 300C. The catalyst beds were separated by quartz wool and a stainless steel frit. Both the vaporization and the upgrading reactions were carried out in 100 mL/min flow of H2 (99.999%, Praxair) at 40 psi. The resulting products were identified by electron ionization mass spectrometry and quantified by gas chromatography using a flame ionization detector. A J&W GS-GasPro column of length 6.2 m was used to separate products.

A.7   Finding Reaction Routes through Other Carbon Coupling Reactions

Number of reactions in a reaction sequence does not determine whether this sequence is kinetically favorable or a major reaction pathway. However, reaction

sequence with least number of reactions is likely to be attractive as the overall carbon efficiency is higher than that of reaction sequence with more reactions assuming there is a constant carbon loss in each step. Noting this observation, reaction sequences with more reactions than that of the optimal sequence are worth observing. To identify these sequences, we shut off key reactions in the previous reaction sequence, which is the formation of carbonyl group on levoglucosan.

In the case study, through this approach, we found the following sequences:
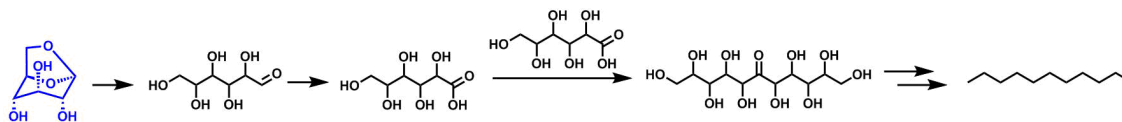
Figure A.6.: Alternate pathway for levoglucosenone self-coupling through oxidation followed by ketoniztion and this requires higher number of reactions.
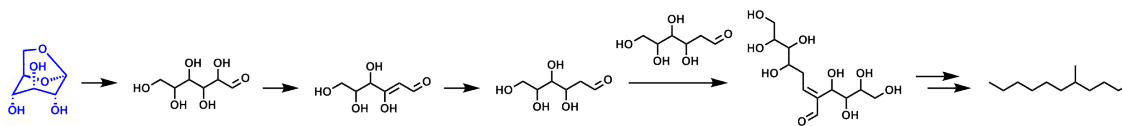
Figure A.7.: Alternate pathway for levoglucosenone self-coupling through ring opening followed by aldol condensation and this requires higher number of reactions.

From the sequence above, the first step involved ring opening of levoglucosan which requires a strong hydrogenation function. This hydrogenation function, however, can reduces the carbonyl groups, which are crucial for carbon coupling reactions, such as aldol condensation, in other molecules. Following ring opening, either oxidation or reduction is required to generate the proper site for carbon coupling reaction.

B. APPENDIX B

B.1   Economic Analysis

In this work, the economic analysis was performed to evaluate the total capital investment, operating cost, return-on-investment, and break even price for crude oil. For the total capital cost investment, a combination of standard procedure from Aspen Economic Analyzer and estimates from literature along with Lang's method is used to obtain the total capital cost for each unit operation. Table B.1 and B.2 summarize the capital or the installed cost for each unit operation and their methodology. The summation of all unit operation costs listed in the tables below alone does not give the total capital cost. Aspen Plus Economic Analyzer only provides the installed cost for each unit operations and the values obtained using Aspen Plus Economic Analyzer in the tables below are the installed costs.

Table B.1.: Equipment cost for Unit Operations in Process I.

Unit Operation	MMUSD	Method
Demethanizer Distillation Column System	1.9	Aspen Economic Analyzer
Hydrogen Membrane	1.8	Well-mixed membrane system and $50/m^2
HEX-101	0.018	Aspen Economic Analyzer
HEX-102	4.8	Aspen Economic Analyzer
HEX-103	1.37	Aspen Economic Analyzer
HEX-104	0.43	Aspen Economic Analyzer
HEX-105	0.14	Aspen Economic Analyzer
Dehydrogenation Reactor	4.6	Aspen Economic Analyzer
Oligomerization Reactor	1.8	Aspen Economic Analyzer
COMP-102	5.2	Aspen Economic Analyzer
COMP-103	0.99	Aspen Economic Analyzer
COMP-104	11.2	Aspen Economic Analyzer
V-101	0.18	Aspen Economic Analyzer
V-102	0.16	Aspen Economic Analyzer
Refrigeration	14	Aspen Economic Analyzer

Table B.2.: Equipment cost for Unit Operations in Process II

Unit Operation	MMUSD	Method
Demethanizer Membrane System	7.3	Well-mixed membrane system and $50/m^2
Hydrogen Membrane	1.0	Well-mixed membrane system and $50/m^2
HEX-102	4.6	Aspen Economic Analyzer
HEX-103	1.3	Aspen Economic Analyzer
HEX-104	0.42	Aspen Economic Analyzer
HEX-105	0.11	Aspen Economic Analyzer
HEX-106	0.03	Aspen Economic Analyzer
HEX-107	0.02	Aspen Economic Analyzer
HEX-108	0.05	Aspen Economic Analyzer
HEX-109	0.02	Aspen Economic Analyzer
Dehydrogenation Reactor	4.7	Six Tenth Rule
Oligomerization Reactor	1.8	Aspen Economic Analyzer
COMP-101	11.2	Aspen Economic Analyzer
COMP-102	5.2	Aspen Economic Analyzer
COMP-103	0.74	Aspen Economic Analyzer
COMP-104	1.73	Aspen Economic Analyzer
Refrigeration	14	Aspen Economic Analyzer
V-101	0.18	Aspen Economic Analyzer
V-102	0.16	Aspen Economic Analyzer
V-103	0.16	Aspen Economic Analyzer

For the standard procedure from Aspen Economic Analyzer, details can be found from the manual. Several of the unit operations such as the dehydrogenation reactor, oligomerization reactor, and membranes, are estimated using literature values along with Lang's method.

B.2 Economic Parameters Calculation

B.2.0.1 Return-on-Investment

The equation for ROI is the following:

$$ROI = \frac{Annual\ Net\ Income (After\ Tax\ Profit)}{TCI} \tag{B.1}$$

The total capital investment is the sum of all unit operations total capital costs. The total capital investment can be calculated by summing all the values in Table 5 and 6, respectively, and multiplying it by the Lang's factor. The second value needed to calculate the ROI is the annual net (After Tax profit) cash flow. To calculate the Annual Net (After Tax Profit) cash flow, the following equation is used

$$AnnualNetIncome(AfterTaxProfit) = (TAR - AOC - AFC - Deprec)(1 - TaxRate) + Deprec$$

$$(B.2)$$

where, TAR is the total annual revenue, AOC is the annual operating cost, AFC is the annual feedstock cost, and $Deprec$ is the depreciation. Note that the assumed selling prices for all outlet streams and feedstock costs for all raw materials are listed in Table 6.5. Linear depreciation model with recovery period five years is used to calculate the depreciation, which is given by the following

$$Deprec = \frac{TCI - 0.1TCI}{Recovery\ Period}$$

$$(B.3)$$

Here, the recovery period is assumed to be five years and the salvage value is 10% of the TCI. The payback period can be calculated by taking the inverse of the return on investment.

B.3 CH_4-N_2/C_{2+} Separation

B.3.1 Demethanizer

In this process configuration, turboexpander and Joule-Thompson valve are used to provide the refrigeration needed to liquefy the natural gas stream. Figure B.1 below describes the industry standard turboexpander process employed in Process I.

B.3.2 Cascade Gas Membrane Scheme

In this cascade gas membrane configuration, the pressure on the permeate side is atmospheric pressure and it is assumed that the pressure drop between the feed and

Figure B.1.: Turbo-Expander Demethanizer Scheme.

retenate streams is negligible. The outlet pressure from every compressor is 10 bar. In order to achieve the desired 85% methane recovery, stage cuts for membrane I, II, and II are set as 1.3%, 53.4%, and 74.8%, respectively. In addition, the most permeable component, in this case methane, mole fraction in the retenate for membrane I, II, and III are 0.15, 0.15, and 0.39, respectively. Figure B.2 describes the cascade gas membrane configuration that is employed in Process II.

Figure B.2.: Cascade Gas Membrane Demethanizer Scheme.

B.4 Shale Gas Composition

Table B.3.: Composition of shale gas from the Bakken field in the United States [28].

Component	Mole Percentage - Bakken
CO_2	0.57
H_2S	0.29
H_2O	0.15
N_2	5.20
CH_4	57.55
C_2H_6	19.89
C_3H_8	11.30
n-C_4H_{10}	2.82
i-C_4H_{10}	0.96
n-C_5H_{12}	0.55
i-C_5H_{12}	0.38
C_6H_{14}	0.22
C_7H_{16}	0.09
C_8H_{18}	0.04

C. APPENDIX C

C.1 Chemical Demands in the United States

Table C.1.: United States annual production of major organic commodity chemicals adjusted based on 2010.

Name	Carbon Number	Production Volume 2016 (Million tonnes)
Ethylene	2	24
Propylene	3	18
Xylenes	8	4
Benzene	6	8
Toluene	7	3
Ethylene Glycol	2	2
Ethylene Oxide	2	2
Styrene	8	4
Cumene	9	2
Phenol	6	2
Ethylbenzene	8	4
Benzoic Acid	6	0.1
Propylene Oxide	3	2
1,3 - Butadiene	4	2

C.2 Methoxy-Substituted Propylphenol Reaction Network based on toward Aromatic-Based Chemicals

Figure C.1 below highlights the reaction network included in analysis in Chapter 4, which consists of existing commercial technologies in the aromatic-type chemicals supply chain.
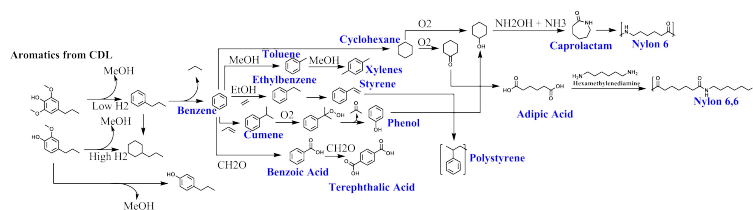
Figure C.1.: Reaction set relevant to upgrading methoxy-substituted propylphenol groups.

C.3   Additional Reaction Rules Considered in Chapter 4

The reaction rules below are used in addition to the set of reaction rules listed in Appendix A to generate the reaction set used in Chapter 4.

Table C.2.: Additional of reaction rules considered in chapter 4.

No.	Name	Example	Source
1	Oxidation of Aldehyde to Acid		Smith, J.G. Organic Chemistry. Third Edition. McGrawHill. 2011.
2	Oxidation of Primary Alcohol to Acid		Smith, J.G. Organic Chemistry. Third Edition. McGrawHill. 2011.
3	Alkylation of Aromatic Rings		Herron et al., Energy Technol. 2017, 5, 130.
4	Acylation of Aromatic Rings		Herron et al., Energy Technol. 2017, 5, 130.
5	Hydroxyalkylation of Aromatic Rings		Herron et al., Energy Technol. 2017, 5, 130.

C.4   Primary Processes Yield Data

Tables below highlight yields for primary processes described in Chapter 4. Note that for yield of residues and feeds that go into primary processes are represented on a carbon mole basis. Unrecoverable and unusable components, such as humins, are not reported in the tables below.

Table C.3.: Fast Pyrolysis Yield for Cellulose and Poplar

Compound	Carbon Yield (mol/ C mol of feed)	
	Cellulose	Poplar
Carbon Monoxide	0.025	0.012
Carbon Dioxide	0.024	0.011
Methane	0.004	0.002
Levoglucosan	0.092	0.043
Glycolaldehyde	0.053	0.025
Formic Acid	0.041	0.019
Water	0.226	0.401
5-HMF	0.0004	0.001
Furfural	0.019	0.008
Hydroxyacetone	0.009	0.004
Acetic Acid	0.014	0.006
Dihydroeugenol	-	0.013
Dimethoxypropylphenol	-	0.01
Methanol	0.006	-
Char	0.075	0.345

Table C.4.: Yield for Fermentation of Poplar

Compound	Carbon Yield (mol/ C mol of Poplar)
Ethanol	0.16
Carbon Dioxide	0.16

Table C.5.: Yield for Catalytic Depolymerization of Lignin for several feeds.

Compound	Carbon Yield (mol/ C mol of feed)	
	Poplar	Residue from Maleic Acid Pretreatment
Dihydroeugenol	0.009	0.013
Dimethoxypropylphenol	0.006	0.014
Residue	0.48	-
Cellulose	-	0.081

Table C.6.: Yield for Enzymatic Hydrolysis of Poplar

Compound	Carbon Yield (mol/ C mol of Poplar)
Glucose	0.047
Xylose	0.007

Table C.7.: Yield for Maleic Acid Pretreatment for several feeds.

Compound	Carbon Yield (mol/ C mol of feed)				
	Poplar	Residue from CDL	Glucan & Xylan	Cellulose	Cellulose containing Lignin
5-HMF	-	0.011	0.11	0.033	0.033
Furfural	0.019	0.006	0.006	-	-
d-Glucose	0.005	-	-	-	-
Hemicellulose-Poor residue	0.81	-	-	-	-
Levulinic Acid	-	0.06	0.006	0.033	0.033
Formic Acid	-	-	-	0.028	0.028

VITA

VITA

Taufik Ridha was born in Jakarta, Indonesia. He was raised there until the age of 15 and moved to Houston, TX. After graduating from Stratford High School in 2010, he attended Texas A&M University for his Bachelor of Science in Chemical Engineering with a minor with Process Safety Engineering. During his time at Texas A&M University, He pursed both research and industrial internships. He completed several research projects while working with Dr. M. Sam Mannan in the Mary Kay O'Connor Process Safety Center. In addition to this, he participated in several AggiE-Challenge projects with Dr. Mahmoud El-Halwagi and Dr. Choongho Yu. In the summer of 2013, he interned for Honeywell Intl. Inc. in the Process Solution division as a project engineer intern in Safety Center for Excellence group. After graduating summa cum laude from Texas A&M University in 2014, he decided to pursue his doctoral degree in Chemical Engineering at Purdue University under the supervision of Prof. Rakesh Agrawal.

During his PhD program, Taufik focuses his research on process systems engineering applied to energy systems and work on the development of systems-level molecular mapping approach for transformation of biomass into fuels and chemicals. Using this approach, he developed a roadmap toward production of diesel and chemicals from lignocellulosic biomass. He also investigated process concepts for valorization of shale gas condensate into liquid hydrocarbons.

Taufik has published several peer-reviewed research articles and presented his research in DOE Energy Frontier Research Center conference and AIChE Annual Meeting.

In addition, he was nominated for and completed the Applied Management Principles (AMP) 'mini-MBA' certificate program from Krannert School of Management,

Purdue University, in May 2018. Also, he was awarded the best teaching assistant for a senior course in Spring 2017 for his commitment during his teaching assistant assignments.

He is also a food adventurist and enjoys going to music events.

List of Publications

- Ridha, T.; Li, Y.; Gençer, E.; Siirola, J.J.; Miller, J.T.; Ribeiro, F.H.; Agrawal, R. Valorization of Shale Gas Condensate to Liquid Hydrocarbons through Catalytic Dehydrogenation and Oligomerization. Processes 2018, 6, 139.

- Pittman, W.; Ridha, T.; Nayak, S.; Carreto, V.; Mannan, M.S. "Zero-Energy Determination: Confirmation of Vessel and Pipeline Discharge and De-Energizing through Non-Invasive Techniques with Strain Gauges". Process Safety Progress 2014, 33-2, 195-199.